MASTER

NYO-9062

FUEL ELEMENT DEVELOPMENT PROGRAM FOR THE PEBBLE BED REACTOR

Phase II Summary Report [Covering the Period]
November 1, 1959 to October 31, 1960

August 1961
[OTI Issuance Date]

Sanderson and Porter
New York, New York

UNITED STATES ATOMIC ENERGY COMMISSION • OFFICE OF TECHNICAL INFORMATION

LEGAL NOTICE

This report was prepared as an account of Government sponsored work. Neither the United States, nor the Commission, nor any person acting on behalf of the Commission:

A. Makes any warranty or representation, expressed or implied, with respect to the accuracy, completeness, or usefulness of the information contained in this report, or that the use of any information, apparatus, method, or process disclosed in this report may not infringe privately owned rights; or

B. Assumes any liabilities with respect to the use of, or for damages resulting from the use of any information, apparatus, method, or process disclosed in this report.

As used in the above, "person acting on behalf of the Commission" includes any employee or contractor of the Commission, or employee of such contractor, to the extent that such employee or contractor of the Commission, or employee of such contractor prepares, disseminates, or provides access to, any information pursuant to his employment or contract with the Commission, or his employment with such contractor.

This report has been reproduced directly from the best available copy.

Printed in USA. Price $2.75. Available from the Office of Technical Services, Department of Commerce, Washington 25, D. C.

USAEC Office of Technical Information Extension
Oak Ridge, Tennessee

DISCLAIMER

This report was prepared as an account of work sponsored by an agency of the United States Government. Neither the United States Government nor any agency Thereof, nor any of their employees, makes any warranty, express or implied, or assumes any legal liability or responsibility for the accuracy, completeness, or usefulness of any information, apparatus, product, or process disclosed, or represents that its use would not infringe privately owned rights. Reference herein to any specific commercial product, process, or service by trade name, trademark, manufacturer, or otherwise does not necessarily constitute or imply its endorsement, recommendation, or favoring by the United States Government or any agency thereof. The views and opinions of authors expressed herein do not necessarily state or reflect those of the United States Government or any agency thereof.

DISCLAIMER

Portions of this document may be illegible in electronic image products. Images are produced from the best available original document.

NYO 9062

METALS, CERAMICS, AND MATERIALS

FUEL ELEMENT DEVELOPMENT PROGRAM

for the

PEBBLE BED REACTOR

PHASE II SUMMARY REPORT

Nov. 1, 1959 to Oct. 31, 1960

Work Performed Under AEC Contract AT(30-1)-2378

SANDERSON & PORTER

NEW YORK, N. Y.

TABLE OF CONTENTS

Table of Contents continued

Summary & Conclusions

The original concept of the fuel element for the Pebble Bed Reactor was an uncoated sphere of graphite fueled with fissile and/or fertile material. This concept was based on the use of an exceedingly cheap fuel element to offset the increased costs associated with the resulting higher activity levels in the primary coolant stream. In view of the experimental programs which would be required to properly assess the increased primary loop costs (i.e. shielding, maintenance, and hazards), the use of ceramic coatings to retain fission products within the fuel element at high temperature was selected as the major undertaking of the PBR Fuel Element Development Program under Contract AT(30-1)-2378. Two methods of retaining fission products were extensively investigated. These were coatings on the fuel element surface, and coatings on individual fuel particles.

Surface Coated Fuel Elements. To date, a total of ten PBR fuel element specimens with surface coatings have been subjected to varying amounts of high level irradiation in the Capsule Irradiation program. Of this number, cracks or pinholes have been found in six of the coatings. One specimen (FA-8 in Capsule SP-3) was found to have no pinholes or cracks and the condition of three other specimens (one FA-23 and two FA-20 in the static compartment of Capsule SP-5) are presently unknown. The exact causes of the failures are not known precisely, but evidence indicates that the graphite matrix contributed to most of the failures, either through incipient flaws in the graphite or through dimensional changes of matrix under irradiation.

It is unfortunate that the failure statistics to date are so oppressive because at least one of these materials has been found to be an excellent barrier to fission product diffusion, a property heretofore thought to be solely in the realm of metallic claddings. Release factors of the order of 10^{-9} for the Si-SiC coating under high level irradiation existed for a period of about 1 month. Indeed, this fission product retention by the Si-SiC above 1200°F probably would exceed that of many metals if the metals were subjected to similar tests. Previous tests have shown that an Si-SiC coated specimen can meet all the pre-irradiation strength requirements, that the coating is well bonded to the graphite matrix, and that the coating can withstand the internal pressures generated by the fission product gases. This coating will have a temperature limitation

slightly in excess of 2000°F due to migration of the free phase silicon from the coating. Future work would have to include a detailed understanding of the properties of the underlying graphite body that could cause coating failure and a rather large quantity of specimens would have to be fabricated and tested in order to insure statistical confidence with this type of coating.

The pyrolytic carbon coating has shown some promise as a fission product barrier in several neutron activation tests. It has the advantage of overcoming the temperature limitation inherent in the Si-SiC coating. However, it appears that while relatively thick coatings are necessary to achieve good fission product retention, interlayer cracking in these thicker coatings seriously weakens the coating. As with the Si-SiC coating, a better understanding of the graphite matrix and the evaluation of a large quantity of specimens would be required before this type of coating could be utilized.

Alumina Coated UO_2 Particles. Fourteen batches of UO_2 particles have been coated with Al_2O_3 by the vapor deposition process. UO_2 particle sizes ranged from 100 to 400 microns and coating thicknesses ranged from 20 to 150 microns. At the 1800°F deposition temperature used for most of the runs, the UO_2 particles are uniformly coated with a dense impermeable layer of Al_2O_3. Greater than 99% of the particles are found to be adequately coated as shown by a subsequent oxidation test in 1200°F air. Uranium contamination on the coating can be kept below 10^{-6} of the contained uranium by rinsing the particles and the equipment after the first thin layer has been deposited. Successive layers can then be well bonded to each other.

Spherically shaped UO_2 particles have been used in most of the batches to avoid possibility of coating failure at sharp corners. However, it has been noted that irregular fuel particles can still be uniformly coated and there may be an economic incentive to use other than spherical fuel particles. Two batches were made with ThO_2-UO_2 particles and no problem was encountered with the use of thoria. One batch was successfully coated containing a porous inner layer of Al_2O_3 deposited at 1400°F which would be useful as a reservoir for fission product gases. However, some difficulty was encountered when this type of coating was applied to irregularly shaped UO_2 particles.

Some slight uranium contamination of the graphite matrix has been found when it is fueled with Al_2O_3 coated UO_2. Sources of the contamination

can arise from uranium on the particle surfaces, from particles broken during the admixture process, and possibly from contaminated process equipment. The operating temperatures of graphite bodies fueled with Al_2O_3 coated UO_2 will be limited to less than 2500°F in order to avoid reaction between Al_2O_3 and graphite. Short time processing temperatures of 2500°F will be satisfactory but this means that the graphite body cannot be completely graphitized. Thermal expansion tests have shown that the Al_2O_3 coating thickness should exceed about 30% of the UO_2 particle diameter so that the slightly higher expansion coefficient of the UO_2 will not rupture the coating at 2500°F. Fuel particles occupy about 1.7 v/o of the graphite matrix in the reference PBR fuel element and the use of coated fuel particles increases this volume to about 10 v/o depending on the ratio of coating thickness to fuel particle diameter. No loss in strength has been found in both impact and compression testing of graphite spheres fueled with coated particles. However, there is some evidence that thin particle coatings (40 microns or less) can be damaged in these tests. Massive coatings (~250 microns thick) were not found to be damaged.

Fission product retention tests at low burnup levels have shown vapor deposition Al_2O_3 to be an excellent barrier to fission product retention. Typical neutron activation (i.e. post irradiation heating) test results show that only 10^{-6} of the contained Xe 133 is released from a graphite sphere fueled with Al_2O_3 coated UO_2 when the specimen is heated at 2000°F for 4 hours. In a continuous irradiation and sampling test in a low neutron flux (i.e. Furnace Capsule Test), a similar specimen was found to have leakage factors (i.e. release rate/production rate) for the long lived fission product gases of 10^{-6} to 10^{-7} at 300°F which increased to only 10^{-4} to 10^{-5} at 1800°F. From both of these tests, it is concluded that the "leakage" was primarily due to uranium contamination in the specimen rather than diffusion through the Al_2O_3 coatings.

The most significant test of this type specimen was a high level irradiation in Sweep Capsule SP-5. The specimen operated at average conditions of 1.5 KW, 1350°F surface temperature and 1550°F central temperature. A burnup of 6 a/o U235 was achieved in this experiment. Up to about 1.5 a/o, the leakage factors for 10 isotopes ranging in half life from 20.8d I 131 to 1.7s Xe 141 were found to be in the range of 10^{-6} to 10^{-9}. Between 1.5 a/o and 3 a/o the leakage factors for the longer-lived isotopes began to increase indicating that measurable diffusion was starting to occur through the Al_2O_3 as a result of radiation damage. At 6 a/o, the leakage factors ranged from 10^{-2} for Xe 133 to 10^{-6} for the very short lived fission gases and it appeared that some of the coatings may have

cracked. The final analysis of these results must await visual inspection of the specimen during hot cell examination.

Further work with Al_2O_3 coated UO_2 should emphasize extending the low leakage factors obtained at the 1.5 a/o level to at least 6 a/o burnup. The use of porous inner layers in the particle coating to minimize rupture due to fission gas pressure buildup should be explored. A fundamental study of neutron damage to the molecularly deposited Al_2O_3 material should be made to determine whether other process conditions or the use of coating additives will minimize radiation induced porosity. A better understanding of factors which influence the reaction between Al_2O_3 and graphite should be obtained. These factors may include the type of filler and binder used in the graphite matrix, the final bakeout cycle, and the impurity levels in the matrix. An optimum particle size should be established since it appears that large particles, of about 400 micron UO_2 with a 200 micron Al_2O_3 coating, would be desirable to minimize both physical damage to the coating and fission product leakage.

Pyrolytic Carbon Coated UC_2 Particles. The interest in this type of coated particle stems from the absence of a temperature limitation due to reaction between the particle coating and the graphite matrix. Also, this type of coating does not effectively displace moderator atoms. The coatings are deposited on the fuel particles by the pyrolysis of hydrocarbon gases. Two batches were prepared at 1900°F, two at 2450°F, and two at 3600°F and test data is available for the first four batches. UC_2 particle sizes ranged from 150 to 250 microns and coating thicknesses ranged from 17 to 160 microns.

Leach tests of as-fabricated particles in hot nitric acid showed that greater than 99% of the particles were adequately coated. The exposed uranium was found to be of the order of 10^{-6} of the contained uranium. Thermal cycle tests have shown a definite tendency for the coatings to rupture when heated above their deposition temperature due to the higher expansion coefficient of the UC_2. One attempt to fabricate a batch of particles into a spherical graphite matrix resulted in the fracture of many of the particle coatings. These failures are believed to have occured during the mixing process because of the irregularly shaped UC_2 particles used in this batch.

The only fission product retention tests on these particles were neutron activation tests of several of the batches. Typical results were 10^{-6} of the contained Xe 133 released in a 1 hr. heating period at

temperatures not exceeding the coating deposition temperatures (1900°F and 2450°F). These results are comparable to the data obtained for Al_2O_3 coated UO_2.

Future work on pyrolytic carbon coated UC_2 should include the effects of radiation damage on coating permeability; the determination of the optimum coating deposition temperature based on strength, permeability, and thermal cycle rupture; and problems associated with incorporation of these coated particles into a graphite matrix.

In other materials developments, a study of the preparation of graphite blanket elements loaded with ThO_2 by the thorium nitrate infiltration process was conducted. It was found that graphite densities below 1.45 g/cc and more than 5 infiltration steps were required to achieve the desired ThO_2 loading. A variety of subsurface coating materials for graphite spheres were studied. It was found that best results would be obtained if a hot-pressing technique were used so that the coating material located beneath an unfueled graphite shell was in a molten phase during fabrication. High density spheres were made with natural graphite filler materials. Densities of 2.0 g/cc were achieved but the spheres did not have adequate strength at the low binder contents needed to achieve the high density.

Future Work. The basic design of the PBR Fuel Element which has evolved from the work to date consists of a molded graphite sphere containing a dispersion of coated fuel particles. No significant deterioration of the structural properties of the graphite matrix was found after irradiation to about 6000 KWH which is the present design objective of the 125 eMW Pebble Bed Reactor. The final choice of the coated fuel particle cannot be made at present. Pyrolytic carbon coated UC_2 particles are favored because they offer an all carbon system with temperature limits above 3000°F. However, there is no information on radiation damage effects on this material. Al_2O_3 coated UO_2 has shown good fission product retention up to at least 1.5 a/o burnup. If future work shows that metal oxide coatings such as Al_2O_3 can be developed to maintain coating integrity to higher burnups, it will be possible to utilize these coatings in Pebble Bed Reactors by limiting top fuel temperatures to about 2500°F.

Some method will be needed to prevent damage or loss of coated fuel particles at the surface of the fuel element. This would include either an unfueled graphite shell or a surface coating such as pyrolytic carbon or siliconized silicon carbide. Since oxidation protection may be required on PBR fuel elements, the surface coatings may serve a dual function. Two

types of possible attack are of concern: the mass transfer of carbon by reaction with trace impurities of CO_2 or H_2O in the helium coolant and the sudden oxidation by the admission of air in the event of a rupture in the primary loop. Si-SiC coatings can prevent these types of attack, however the effects of pinholes and cracks in the coating should be assessed. Al_2O_3 coated UO_2 could not be used in this type of fuel element since 3600°F fabrication temperatures are needed to apply the Si-SiC coating. The resistance of pyrolytic carbon, known to be less reactive than graphite, to this type of attack should be determined.

All of the materials studied in the present program have been made only in laboratory quantities at high unit costs. Manufacturing cost studies were not included in the scope of the present program. However, now that a basic design has evolved, sufficient work should be done to permit realistic fuel element cost estimates to be made.

1.0 Introduction

The basic objective of the Pebble Bed Reactor Fuel Element Development Program is to develop and/or evaluate fuel elements which would be suitable for the economic operation of a large scale Pebble Bed Reactor. The characteristics of a reference design fuel element have been based on design studies of a 125 eMW Pebble Bed Reactor Steam Power Plant (1, 2). This reactor is a high temperature, all-ceramic, helium cooled reactor, consisting of a randomly packed static bed of fueled graphite spheres. Fuel element characteristics have been completely described in the Phase I Report on the PBR Fuel Element Development Program (3) and are summarized below.

1. The fuel element is a 1 1/2 inch diameter sphere of fueled graphite.
2. Fuel loading is 4.75 gms of uranium in the form of either the oxide or the carbide.
3. The maximum power density is 3 KW per sphere. Maximum surface and center temperatures are 1800°F and 2100°F respectively. The design burnup is 5500 KWH per sphere which is equivalent to 6 a/o of total uranium or 40,000 MWD/metric ton of uranium.
4. Fission product retention should be such that the external activity level is $<10^{-6}$ of the activity which would result from the complete release of all isotope chains containing volatile fission products.
5. The spheres shall withstand a 2.0 ft-lb. impact load and a 500 lb. compressive load.
6. Other pertinent features are that adjacent fuel elements should not self weld, fuel element coatings should withstand internal pressure buildup of gaseous fission products, and fuel element surfaces should not dust, abrade, or erode.

The PBR Fuel Element Development Program has been arranged to evaluate these various characteristics. Figure 1-1 is a schematic outline of the evaluation program. In general, fuel element specimens are subjected to pre-irradiation testing, followed by irradiation tests to measure fission product retention characteristics and/or the effects of irradiation on physical properties. Final steps in the program include high level/capsule irradiation and operation of an in-pile loop to simulate problems in the primary loop of a Pebble Bed Reactor. The test apparatus used in this program has been described in ref (3). All phases of the evaluation program up to and including the capsule irradiations are being conducted at the Battelle Memorial Institute. The in-pile program is being conducted by the Nuclear Science and Engineering Corp.

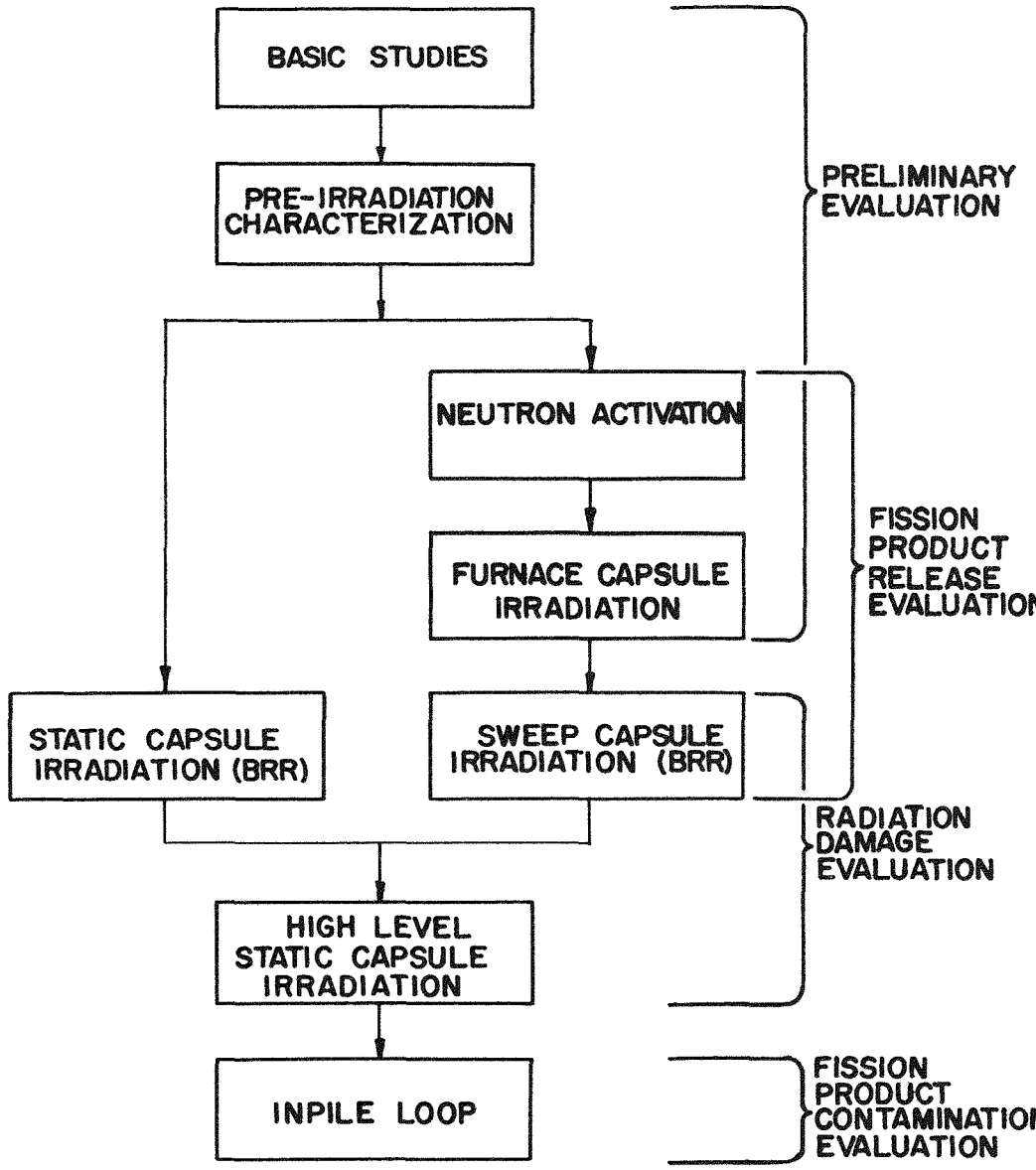

FIG. 1-1 PBR FUEL ELEMENT DEVELOPMENT PROCEDURE

The present report describes the results during Phase II of the PBR Fuel Element Development Program. Phase II covers the period from November 1959 through October 1960 which is the middle 12 month period of a 24 month program. Other reports issued during Phases I and II, exclusive of Monthly Progress Reports, are listed in Table 1-1.

TABLE 1-1

Reports on PBR Fuel Element Development Program

NYO 2706	Phase I Report, May 1, 1959 to Oct. 31, 1959.
NYO 9057	Quarterly Report, Nov. 1, 1959 to Jan. 31, 1960.
NYO 9058	Quarterly Report, Feb. 1, 1960 to Apr. 30, 1960.
NYO 9061	Quarterly Report May 1, 1960 to July 31, 1960.
NYO 9059	Thorium Oxide Infiltration of Graphite Spheres; Speer Carbon Co; June 15, 1960.
NYO 9060	Subsurface Coatings for Fueled Graphite Spheres; June 30, 1960.

2.0 Materials Development

Graphite was initially selected as the matrix material for PBR fuel elements because it is a low cost material which has good strength at high temperatures. Three methods of fueling the graphite matrix have been considered: (1) admixture of ceramic fuel particles with graphite, (2) infiltration of the graphite sphere with a uranyl nitrate solution, and (3) lumping of a ceramic fuel pellet within a graphite shell. The major emphasis has been the retention of fission products in these fueled graphite spheres by means of high temperature ceramic coatings.

Three locations for fission product coatings have been considered:

1. A coating can be applied to the outside surface of the fueled graphite sphere. A surface coating can be applied to any of the three types of fueled graphite spheres and a surface coating is relatively easy to apply. However, the coating is subject to stresses arising from both external loads (i.e. impact, compression) and possible differential expansion with the graphite sphere due to temperature cycling or radiation damage effects.

2. A coating can be located beneath the surface of the graphite sphere, with the fueled region being inside the coating. The coating is not subjected directly to external loads applied to the fuel element but the manufacturing process is somewhat more complex.

3. Coatings can be applied to the individual fuel particles in an admixtured type fuel element. The ceramic coatings can be used in large thickness to diameter ratios which are more stable and individual coating failures would expose only a very small portion of the fuel. However, the fuel particle coatings are subjected to fission fragment recoil damage and rupture due to fission gas pressure buildup which could limit the useful life of the coating.

The ceramic materials which were investigated for these applications differ from ordinary ceramic materials which generally have rather high permeabilities. Materials used in this program such as siliconized silicon carbide, pyrolytic carbon and vapor-deposited alumina have been found to be low permeability materials, of the order of that found for many metals. Indeed, the permeabilities of these special ceramics remain low at temperatures which are beyond the safe limits for many metals. Section 3.0 summarizes all the work on siliconized silicon carbide and pyrolytic carbon

surface coatings. Coated fuel particles are discussed in Section 4.0 (Alumina) and Section 5.0 (Pyrolytic carbon). Subsurface coatings are described in Section 6.2.

In addition to the work on coatings, there were several other programs in the area of materials development. The thorium oxide loadings which can be achieved in graphite by infiltration with thorium nitrate is described in Section 6.1. The use of natural graphite in preparing a high density matrix material is described in Section 6.3. A special capsule irradiation to test the ability of uranium graphite spheres to withstand high burnup is described in Section 7.0.

The most probable application of the Pebble Bed Reactor will be as a high temperature breeder reactor employing a uranium-thorium loading in the core and a thorium loading in the blanket. For purposes of the experimental program, the thorium is replaced with an equivalent weight of uranium Normal enrichment uranium is used in specimens for pre-irradiation tests and certain low level fission product diffusion tests. The use of fully enriched uranium in capsule irradiations greatly accelerates irradiation damage tests such that anticipated burnups in Pebble Bed Reactors can be readily achieved in lower flux research reactors.

Table 2-1 has been prepared to summarize the various types of fuel element specimens evaluated during Phase II. The manufacturer and pertinent characteristics of the fuel elements are listed. Each type of specimen has been assigned a type number. The letters FA and FI refer to the method of fueling the graphite (i. e. admixture and infiltration). In the case of unfueled specimens, the designation FX is used. Numbers are assigned serially within each group, and have no special significance. Occasionally, when it is desired to identify a particular sphere within a group, an additional identification number in parentheses will be added to the type number. Throughout this report, specimens are referred to only by type number. Consequently, the specimens have been listed numerically in Table 2-1 to permit rapid identification.

TABLE 2-1

SUMMARY OF FUEL ELEMENT TYPES

	INFILTRATED	UNFUELED	
Number	FI-1	FX-3	FX-5
Mfgr.	Syl.	Ray.	AMP
FUEL			
Loaded As	UNH	—	—
Final Form	UO_2	—	—
Particle Size, μ	1	—	—
MATRIX			
Reimpreg.	no	—	—
Net Density	1.65	—	—
Shell Thick.	0	—	—
Bake Temp, °F	1470	—	—
COATING			
Material	—	Pyro-G	Pyro-C
Thickness	—	.060"	.0005"

Manufacturers

- AMP - American Metal Products
- BMI - Battelle Memorial Institute
- Carbo - Carborundum
- GLC - Great Lakes Carbon
- 3M - Minnesota Mining and Manufacturing
- NC - National Carbon
- Ray - Raytheon
- Syl - Sylvania-Corning Nuclear

	ADMIXTURED										
Number	FA-1	FA-2	FA-8	FA-10	FA-16	FA-19	FA-20	FA-21	FA-22	FA-23	FA-24
Mfgr.	NC	BMI	Carbo	GLC	3M	NC	NC	Ray	NC(1)	3M	Carbo(1)
FUEL											
Loaded As	UO_2	UO_2	UC_2	UO_2	UO_2	UO_2	UO_2	UO_2	UO_2	UO_2	UC_2
Final Form	UO_2	UO_2	UC_2	UO_2	UC	UC_2	UC_2	UC_2	UO_2	UC	UC_2
Particle Size, μ	100/150	67	100/200	350/420	100/200	100/150	100/150	100/150	100/150	100/200	100/150
MATRIX											
Reimpreg.	no	no	no	yes	yes	no	no	no	no	yes	no
Net Density	1.62	1.49	1.63	1.80	1.75	1.65	1.65	1.65	1.57	1.75	1.55
Shell Thick	0	0	0	0	.060"	0	0	0	0	.125"	0
Bake Temp, °F	2560	2000	3600	2000	3600	4800	4800	4800	2300	3600	2000
COATING											
Location	—	—	Surf.	—	Surf.	—	Surf.	Surf.	Part.	Surf.	Part.
Material	—	—	SiC-Si	—	SiC-Si	—	Pyro-C	Pyro-G	Al_2O_3	SiC-Si	Pyro-C
Thickness	—	—	.030"	—	.003"	—	.002"	.050"	50μ	.003"	40μ

Note (1): Fuel particles coated by Battelle Memorial Institute

3.0 Surface Coated Fuel Elements

One of the earliest approaches to fission product retention was the application of a ceramic coating to the outside surface of the spherical PBR fuel element. A variety of surface coatings had been investigated in the program (3) and work during Phase II centered on two of the most promising types — siliconized silicon carbide (Si-SiC) and pyrolytically deposited carbon. The use of surface coatings presents certain problem areas. The allowable impact load on the fuel element is significantly reduced due to the thin, hard and less resilient nature of the coating compared with the graphite matrix. However, by proper choice of graphite material and coating thickness, fuel elements meeting the 2.0 ft-lb. requirement can be made. Coatings must have adequate adherence to the graphite body and sufficient abrasion resistance to withstand the fuel flow pattern through PBR cores. Coating materials which will self weld and cause the packed bed to freeze up must be avoided. Also, if the coating material reacts with uranium, an unfueled graphite shell must be placed between the fueled graphite core and the coating. These factors, together with the ability of the coating to retain fission products, have formed the basis for the evaluation program.

3.1 Silicon Carbide Surface Coatings

The interest in silicon carbide coatings for Pebble Bed Reactor fuel elements stems from their excellent potential as a barrier to fission product leakage at high temperatures. Actually, this property is due to the presence of a continuous phase of silicon throughout the silicon carbide grains in the coating. This material is referred to as siliconized silicon carbide (Si-SiC). Test results during previous periods had indicated good fission product retention by this material (2). However, due to the potential reaction between free silicon and the fuel particles causing the surface coating to become contaminated with fuel, it has been necessary to include an unfueled graphite shell between the fueled graphite core and the Si-SiC coating. Irradiation of this type of specimen in Capsule SP-3 (3) caused the coating adjacent to incipient flaws in the unfueled shell to fail under the effects of an internal temperature gradient. Another problem area is the potential self-welding between adjacent fuel elements at temperatures approaching the melting point of the free phase silicon in the coating. Work during Phase II consisted primarily of evaluating improved specimens with respect to these problem areas. These specimens include the admixture/shelled types FA-16 and

FA-23 and the admixture type FA-8. These specimens are described in Table 2-1. Figure 3-1 shows an Si-SiC coating similar to the coating on an FA-23 specimen and Fig. 3-2 shows an Si-SiC coating on an FA-8 specimen. In both coatings, the continuous free silicon phase and the excellent bonding to the graphite matrix can be seen.

3.1.1 Physical Evaluation

A total of 15 fueled graphite spheres coated with Si-SiC were received for evaluation during Phase II. The examination of one sphere after high level irradiation in Static Capsule SP-4 is described in this section while fission product retention tests are described in the following section 3.1.2. Pre-irradiation tests performed during Phase II are summarized below.

Abrasion Tests. Abrasion tests were run on 5 specimens. This test consists of tumbling the spheres for a 20 min. period inside a rotating drum which also contains some dummy graphite spheres to enhance the tumbling action. The abrasion test results are summarized in Table 3-1. The specimens with the thickest coatings suffered no noticeable damage except for some weight loss. The thinner coatings developed pin hole leaks. These were most likely thin spots in the coating which were damaged by the tumbling action.

TABLE 3-1

Abrasion Tests on Si-SiC Coated Spheres

Specimen No.	Coating Thickness, in.	Hot Oil Test	Time In Hot Oil, Min.
FA-16(S12)	.004	Several small leaks	10
FA-16(S14)	.004	" "	10
FA-23(E8-1)	.010	No leaks	5
FA-23(E8-2)	.010	"	5
FA-23(E8-6)	.0075	"	5

Compression Tests. Compression tests were run on two of the spheres which had been subjected to the abrasion test. Specimen FA-16(S12) broke at an 825 load after a deflection of 0.068" while FA-23(E8-2) broke at 1445 lbs. and 0.060" deflection. Both of these values are well above the required 500 lb. compressive load.

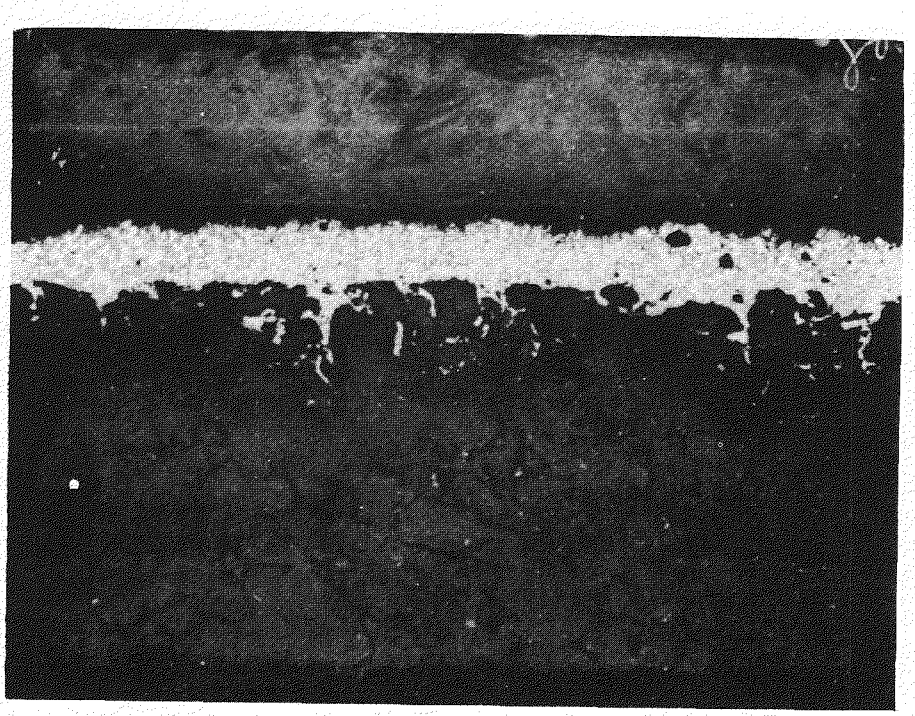

Fig. 3-1. Si-SiC coating similar to coating on an FA-23 specimen (100X)

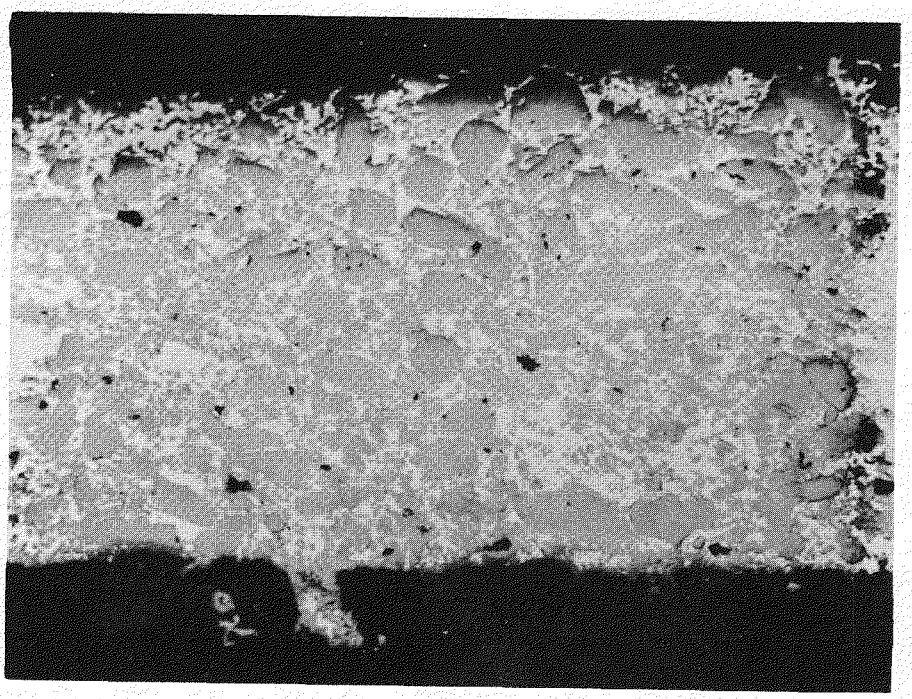

Fig. 3-2. Si-SiC coating on an FA-8 specimen (100X)

Impact Tests. Impact tests were run on two more of the spheres which had been subjected to the abrasion test. The coating on FA-16(S14) developed a pinhole (as indicated by a hot oil test) after an impact load of 0.6 ft-lb. Visual damage to the coating did not appear until after a 1.3 ft-lb. impact. The corresponding impact loads for FA-23(E8-1) were 0.5 ft. lb. to produce a leak and 0.7 ft. lbs to produce visual damage. These values are somewhat below those previously reported for this type of specimen as being in the range of 1.25 to 3.0 ft-lbs. Apparently, the tumbling tests on these specimens weakened the coatings.

1500 1 1/2" diameter unfueled graphite spheres coated with Si-SiC were purchased and used under Contract AT(30-1)-2207 to study pressure drop and thermal expansion characteristics of packed ball beds (12). The acceptance tests for the procurement of the 1500 spheres included a 2 ft-lb. impact load and a 500 lb compressive load applied to each sphere with no evidence of coating failure as indicated by the hot oil leakage test. All of the 1500 spheres passed these tests. However, when the spheres were subsequently used in an oxidizing atmosphere at 1500°F, corrosive attack to the underlying graphite was noted in many of the spheres. From the nature of the damage, it was concluded that the Si-SiC coating had been bruised during the impact tests such that the graphite could be attacked by the highly oxidizing atmosphere through the weakened spots in the coating.

Self Welding. In view of the presence of free phase silicon, having a 2600°F melting point, in the Si-SiC coating, there is some concern about adjacent fuel elements being fused together which would hinder core unloading. Tests were run on unfueled spherical specimens having coatings similar to the FA-16 and FA-23 types. In one test, two spheres were subjected to a 50 lb. compressive load for 66 hours while at 2500°F. A whitish film which appeared on the surface of the specimen due to a reaction with contaminants in the furnace may have accentuated the welding that was observed at the points of contact. The test was repeated with similar specimens at 2300°F and no evidence of self welding was found. Thus, it appears that the permissable surface temperature for this type of specimen will be below 2500°F.

Coating Permeability. A total of 11 specimens of the FA-16 and FA-23 types were immersed in silicone oil at 375°F. One specimen emitted a single very fine bubble stream while all other specimens showed no evidence of pinholes or cracks.

Uranium Contamination. The FA-8 specimen consists of an Si-SiC coating placed directly on a fueled graphite sphere. A detailed alpha assay of this type specimen showed a rather uniform uranium contamination over the entire surface which totalled 0.3% of the uranium inside the sphere. Both the FA-16 and FA-23 specimens have unfueled graphite shells between the fueled core and the Si-SiC coating. A summary of the alpha assay tests on these specimens is given in Table 3-2. Three areas each equal to 1/7 of the total surface area was measured on each sphere. The values reported in Table 3-2 represent the equivalent whole ball contamination. As can be noted, the uranium contamination is slightly higher in the FA-16 specimen which could be due to somewhat greater uranium migration through its thinner unfueled shell during manufacturing.

TABLE 3-2

Surface Uranium Contamination of Si-SiC Coated Specimens

Sphere No.	Position 1	Position 2	Position 3
FA-23(E8-7)	nil	4.0×10^{-7}	2.3×10^{-7}
FA-23(E8-12)	2.3×10^{-7}	2.3×10^{-7}	3.1×10^{-7}
FA-23(E8-1)	1.6×10^{-7}	nil	2.3×10^{-7}
FA-23(SPE-2)	1.1×10^{-6}	1.9×10^{-6}	3.0×10^{-6}
FA-16(E16-4)	8.4×10^{-6}	4.4×10^{-6}	7.0×10^{-6}

Internal Pressure. As fission product gases accumulate inside a coated graphite sphere under irradiation, there is a possibility that gas pressure could cause the coating to rupture. It has been calculated that a pressure of about 300 psi could exist inside such a coated sphere. A special test apparatus was constructed which consisted of a tube fitting gasketed to a coated sphere having a 1/16" diameter hole in the coating. This assembly was mounted in beaker of 375°F silicone oil. An FA-8 specime was tested at 300 psi of argon. The coating did not crack off, indicating that it was securely bonded to the graphite, and no pinhole leaks developed in the coating.

Radiographic Inspection. Some difficulty had been encountered with earlier versions of the FA-16 and FA-23 types in that incipient flaws were detected in the graphite matrix which led to cracking of the Si-SiC coating during capsule irradiation (2). Specimen FA-23(E8-7) which was being considered for irradiation in Capsule SP-5 was subjected to a detailed radiographic inspection. Six radiographs were taken with the specimen

being rotated 60° between shots in order to obtain complete coverage of the unfueled shell. No evidence of cracks or flaws could be noted. This factor together with the direct visual examination of several sectioned specimens which revealed no flaws indicated that this type of specimen was free from internal cracks.

Radiation Effects. An FA-8 specimen had been under irradiation in Static Capsule SP-4 to assess the long-term irradiation effects on an Si-SiC coated specimen, particularly the question of whether radiation induced graphite shrinkage will weaken the specimen. This irradiation started in August 1959 and terminated in March 1960. The design and operating conditions for Capsule SP-4 are described in Section 8.1. Post-irradiation examination of the irradiated specimen was conducted during Phase II. A summary of the irradiation conditions, weight changes, and dimensional changes are given in Table 3-3.

TABLE 3-3

Summary of Irradiation Results for
Si-SiC Coated Specimen FA-8 in Capsule SP-4

Heat Generation Rate	2.2 KW
Measured Graphite Block Temp.	1400°F
Calculated Surface Temp.	1750°F
Calculated Center Temp.	1850°F
Burnup	7400 KWH
Weight, pre-irradiation and change during irradiation	56.2085 gms, + 0.14%
Diameter, pre-irradiation and change during irradiation	1.5009" + 0.43% 1.5683", - 0.16% 1.4908", + 0.65%

Machined flats could not be used for dimensional measurements on this coated specimen as was done for uncoated specimens. Instead, grease.pencil marks were made at the points of measurement. However, it was noted that repeated measurements at the same diameter showed that dimensional changes were very sensitive to micrometer position. Thus, little significance can be placed on the dimensional changes reported in Table 3-3. The gain in weight of the specimen during irradiation is most likely associated with the crack which was subsequently found in the Si-SiC coating. The Si-SiC coating was applied to the graphite sphere at 3600°F in an inert atmosphere which effectively outgasses the graphite matrix before it is coated. Thus, when the coating cracked, it was probable that capsule gas (helium) or atmospheric air (after capsule opening but before weighing) could be readsorbed on the graphite matrix, causing a weight gain.

Visual examination of the FA-8 specimen showed it to be crack-free and otherwise sound. However, upon immersing the sphere in 375°F silicon oil, a line of bubble streams clearly showed a single surface crack about 1/4 inch long. Subsequent macroscopic examination confirmed the presence of the crack. Figure 3-3 is a 34x view of this crack. In view of the importance of trying to determine the cause of this crack, a scheduled impact test on the specimen was omitted. The FA-8 specimen was mounted in plastic so that it could be sectioned and polished to further study the crack. Examination of the polished section actually revealed three cracks through the coating. Two of the cracks were quite large and obviously have been revealed in the hot oil test. It was likely that the cutting and polishing operation caused these cracks. The third crack is shown in Fig. 3-4. There is not conclusive evidence that this is actually the crack previously observed in the hot oil test since in mounting the sphere in plastic, the orientation of the crack may have been lost. However it does not have the large, jagged appearance of the other two cracks and is therefore believed to be the crack of interest. As can be noted in Fig. 3-4, the crack appears to be along the SiC grain boundaries. The crack was probably caused by a stress in the coating which either resulted from the internal temperature gradient in the specimen or from an initial coating flaw in fabrication which did not leak in the pre-irradiation hot oil test but which propagated under the operating conditions. No evidence of coating separation from the graphite matrix can be noted in Fig. 3-4. This is significant because it was thought that radiation induced shrinkage of the graphite matrix might have produced some coating separation. Except for the crack, there is no other visible evidence of a radiation induced change to the Si-SiC material.

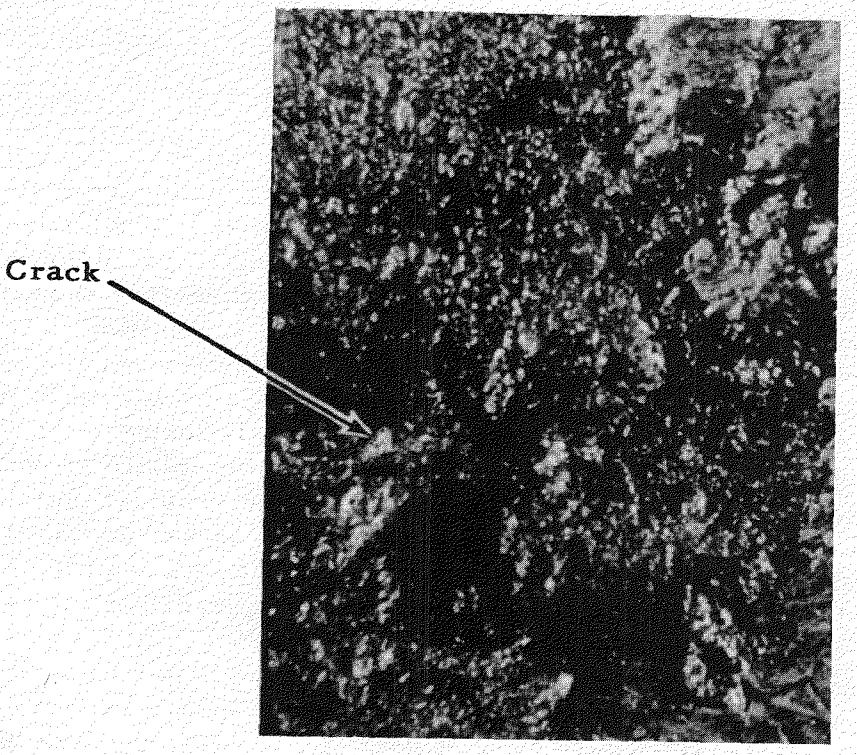

Fig. 3-3. External view (34x) of crack in Si-SiC coating of specimen FA-8 (E6) after irradiation in Capsule SP-4.

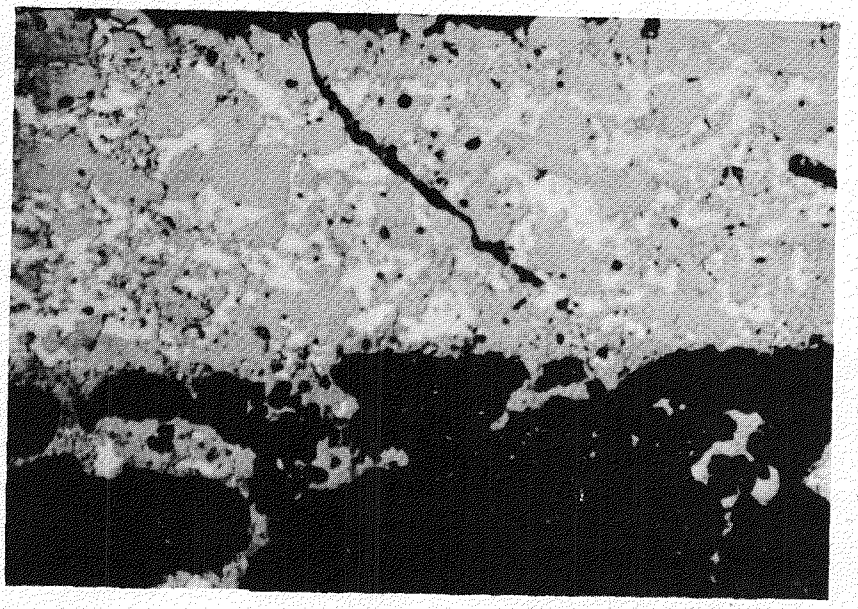

Fig. 3-4. Crack in Si-SiC coating of specimen FA-8 (E6) after irradiation in Capsule SP-4. View at 100x.

3.1.2 Fission Product Retention

Coated specimens of the FA-16 and the FA-23 types were tested for fission product retention during Phase II by three different tests - neutron activation, furnace capsule, and sweep capsule.

Furnace capsule SPF-2 contained specimen FA-16(S15), fueled with normal enrichment uranium. A total of 13 off-gas samples from this experiment were analyzed for long-lived noble fission product gases covering an operating temperature range of 200°F to 1900°F. Initial operation of this capsule was in a thermal flux of 1.7×10^{10}. The fission product retention was so good for this specimen that the capsule was ultimately moved into a flux of 3×10^{12} to achieve maximum sensitivity. A summary of the data obtained is given in Table 3-4.

TABLE 3-4

Summary of Fission Product Release Data
For Si-SiC Coated FA-16 Specimen in Furnace Capsule SPF-2

Sample No.	Temp, °F	Flux n/cm^2-sec	R/B, (Rate of Release/Rate of Production) Xe 133	Xe 135	Kr 85m	Kr 87	Kr 88
1	200	1.7×10^{10}	(No detectable release)				
2	1000	"			"		
3	1000	3×10^{11}			"		
4	1000	"			"		
5	1000	"			"		
6	1500	3×10^{12}	6.1×10^{-6}	6.1×10^{-7}	5.1×10^{-7}	$< 1.3 \times 10^{-7}$	3.0×10^{-7}
7	1500	"	2.8×10^{-6}	2.0×10^{-7}	8.1×10^{-7}	"	2.7×10^{-7}
8	1500	"	2.1×10^{-6}	1.6×10^{-7}	3.1×10^{-7}	"	1.7×10^{-7}
9	1500	"	1.7×10^{-6}	1.1×10^{-7}	3.1×10^{-7}	"	1.7×10^{-7}
10	1900	"	2.6×10^{-6}	3.8×10^{-7}	6.7×10^{-7}	"	1.5×10^{-7}
11	1900	"	4.5×10^{-6}	4.2×10^{-7}	4.1×10^{-7}	"	1.2×10^{-7}
12	1900	"	8.2×10^{-6}	2.0×10^{-7}	7.0×10^{-7}	"	3.0×10^{-7}
13	1900	"	4.3×10^{-6}	2.5×10^{-7}	4.7×10^{-7}	"	1.0×10^{-7}

As can be noted in Table 3-4, the release rates for these long-lived fission gases are extremely low. No significant effect of temperature on leakage rate can be noted. An alpha assay of FA-16(S15) indicated a surface uranium contamination of about 5×10^{-7} of the total uranium in the sphere. A neutron activation test of FA-16(S15) at 1650°F showed that

less than 5×10^{-5} (limit of sensitivity) of the Xe133 in the specimen was released in a 3 hr. period. These factors together with the lack of temperature dependence indicates that the observed "leakage" rates are most probably due to fissioning of the slight uranium contamination on the surface of the specimen.

In preparation for irradiation in Sweep Capsule SP-5, specimen FA-23(E8-7) was subjected to a neutron activation test. This specimen was activated in an integrated thermal neutron flux of 3.6×10^{13} nvt at ambient temperature and then heated at 2000°F for 4 hours. During this heating period, the Xe 133 release was below the detection limit of 2.2×10^{-7} of the Xe133 present inside the specimen. Consequently, this specimen was selected for one of the two sweep compartments in Capsule SP-5. An additional specimen, FA-23(E8-12), was placed in the static compartment.

The design and operating conditions for Capsule SP-5 are described in Section 8.2. Briefly, the FA-23(E8-7) specimen operated at 1.6 KW heat generation and 1300°F surface temperature. The leakage data for long lived xenon and krypton isotopes from this specimen are given in Table 3-5.

TABLE 3-5

Long-Lived Xe and Kr Release From Si-SiC Coated Specimen FA-23(E8-7) in Capsule SP-5

Sample No.	Days of Irradiation	R/B, (Rate of Release/Rate of Production)				
		Kr 85m	Kr 87	Kr 88	Xe 133	Xe 135
1	11	Nil	Nil	Nil	Nil	Nil
2	12	Nil	Nil	Nil	Nil	Nil
3	16-17(a)	1.9×10^{-9}	Nil	1.5×10^{-9}	5.7×10^{-9}	1.5×10^{-9}
4	21	(b)	(b)	(b)	7.9×10^{-3}	(b)
5	21	4.9×10^{-4}	2.0×10^{-4}	1.7×10^{-4}	3.0×10^{-3}	1.1×10^{-4}
6	21	2.8×10^{-3}	1.2×10^{-3}	6.6×10^{-4}	6.3×10^{-3}	9.3×10^{-4}
7	32	2.8×10^{-4}	1.3×10^{-4}	2.0×10^{-4}	5.2×10^{-4}	1.0×10^{-4}

(a) Sample collected over 22 hr period (rather than 2 hr period) because of low release rate.

(b) These species decayed out during long cooling period necessitated by high activity in this sample.

Extremely low fission product release was noted during the first 17 days of irradiation. Sample No. 4 was taken just after Capsule SP-5 was brought up to power for the third cycle. Just prior to startup, gas flow through the compartment containing the FA-23(E8-7) specimen showed no evidence of high fission product leakage. It is therefore assumed that whatever the type of coating failure which caused the large increase in leakage factors for Sample No. 4, it was associated with the increase in internal temperature gradient as the specimen came up to power. The exact nature of the coating failure will not be known until Capsule SP-5 is opened in the Hot Cell for examination.

No further gas samples were taken for the purpose of measuring long lived fission product release. The helium inlet and outlet valves for the FA-23(E8-7) specimen were shut off. During the day of irradiation when the large increase in fission activity was first noticed, a non-volatile fission product trap was put on-stream for a 2 hr period. The procedures used were similar to those used for the non-volatiles trap experiment with the FA-22 specimen described in Section 4.4.3 except that the helium transit time through the trap was 125 sec.

Due to the long delay time between sampling and the radiochemical analysis, no iodine activity was found. Isotopes which were detected include Sr 89, Ba 140, Ce 141, and Cs 137. Plots of isotope concentration as a function of travel time through the trap again showed excellent agreement with the theoretical prediction based on half-lives of the volatile precursors. The leakage factors shown in Table 3-6 were calculated from these data.

TABLE 3-6

Summary of Short-Lived Volatile Fission Product Release Data From Specimen FA-23(E8-7)in Capsule SP-5.

NOTE: Sample Taken During 21st. Day Of Irradiation

Trap	Precursor		
Species	Species	Half Live	R/B
Cs 137	Xe 137	3.9 min	4.0×10^{-4}
Sr 89	Kr 89	3.2 min	7.2×10^{-4}
Ba 140	Xe 140	16 sec.	3.4×10^{-5}
Ce 141	Xe 141	1.7 sec.	4.6×10^{-6}

The leakage factors in Table 3-6 are in rather good agreement with the long-lived fission product leakage factors on the 21st day shown in Table 3-5. A trend to smaller leakage factors with shorter half life can be noted in Table 3-6. This indicates some delay in the escape of these fission products which causes a greater fraction of the short lived fission products to decay within the sphere thus preventing further escape of their non-volatile daughters. If it is assumed that there is a fault in only the Si-SiC coating in this specimen, then the 1/8" unfueled graphite shell on this specimen could be the primary diffusion barrier which is retarding the escape of the shorter lived volatile fission products.

3.2 Pyrolytic Carbon Surface Coatings

This type of coating contains no metal or metal carbide phase and consists solely of carbon deposited on the fuel element surface by the pyrolysis of a hydrocarbon gas. The type of carbon structure which is formed has an extremely low permeability. The bulk density of the coating can be made to closely approach theoretical carbon density, depending upon the temperature of deposition. The main advantage of this type of coating is that the coating itself will not dictate the temperature limit of the whole fuel element but instead the limit will be set by the properties of the fissile material and the graphite matrix.

Three types of pyrolytic carbon coatings were evaluated during Phase II. These types varied primarily in thickness and, to some extent, in deposition temperature. The thickest coating was on the FA-21 (fueled) and FX-3 (unfueled) types which had similar coatings deposited in the range of 3300 to 3400°F. The FA-21 specimens were made by depositing the coating on FA-19 specimens. Specimens of the second type (FA-20) included some having 2 to 5 mil thick coatings deposited at 3000°F and others with thicker coatings, ranging up to 12 mils, deposited at 3200°F. The FA-20 specimens were made by coating FA-19 specimens. Specimens of the third type are represented by the designation FX-5. This type has a thin 0.5 mil coating deposited at about 3000°F. Test results obtained on these three types of coatings are described below.

3.2.1 Physical Evaluation

Photomicrographs of the three types of pyrolytic carbon surface coatings are shown in Figs. 3-5, 3-6, and 3-7. The FA-20 coating shown in Fig. 3-5 is 5 mils thick. The typical conical growth patterns of pyrolytically deposited carbon can be clearly seen in this picture which was taken under polarized light. Good bonding of the coating to the graphite body was achieved. However, a crack running parallel to the graphite surface can be noted. This type of cracking has been noted in a number of other samples of pyrolytic carbon coating and is due to stresses during fabrication arising from a difference in thermal expansion coefficient of the pyrolytic carbon coating and the graphite sphere. The FA-21 coating shown in Fig. 3-6 is 50 mils thick and has purposely been prepared to be somewhat thicker than the FA-20 coating. Again, the conical growth patterns and the presence of cracks parallel to the base plane can be noted. The FX-5 coating shown in Fig. 3-7 averages only 1/2 mil thick. As noted below, this coating was quite porous but more resistant to impact loads than the FA-20 and FA-21 types.

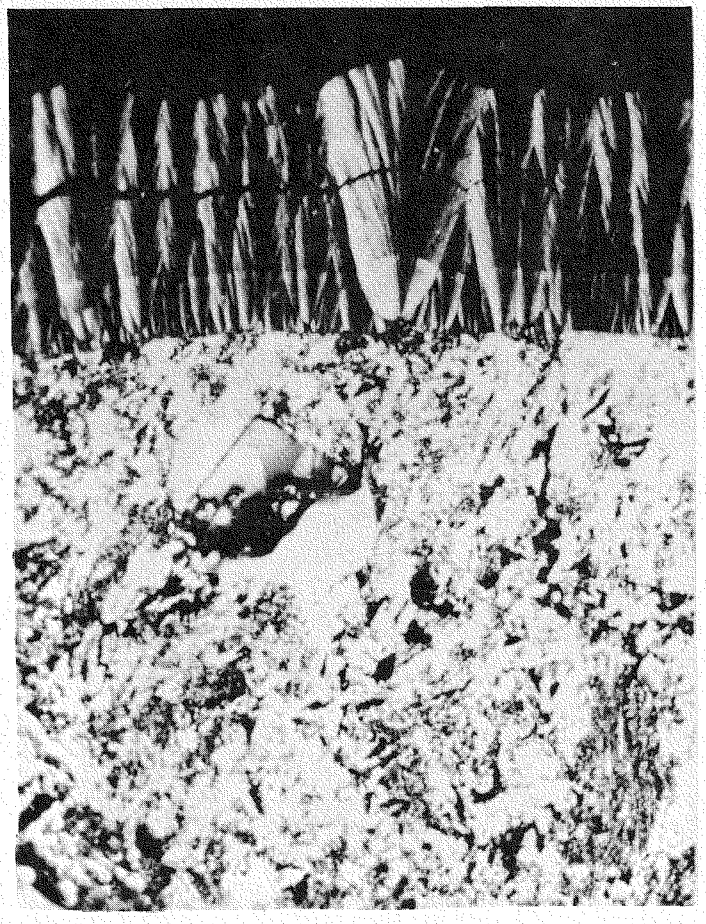

Fig. 3-5. Pyrolytic carbon coating on specimen type FA-20. View at 250x.

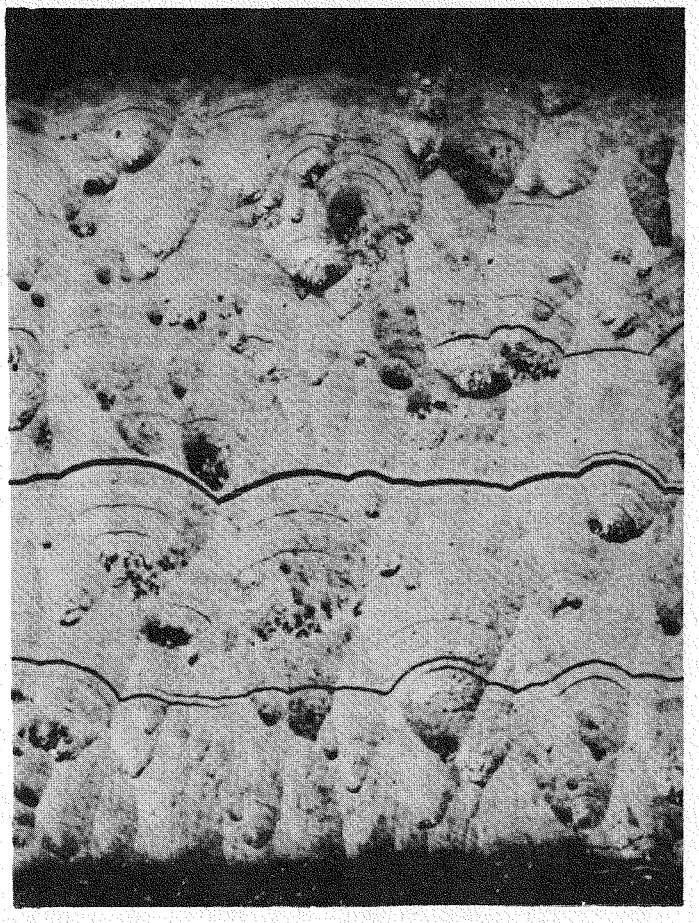

Fig. 3-6. Pyrolytic carbon coating on specimen type FA-21. View at 100x.

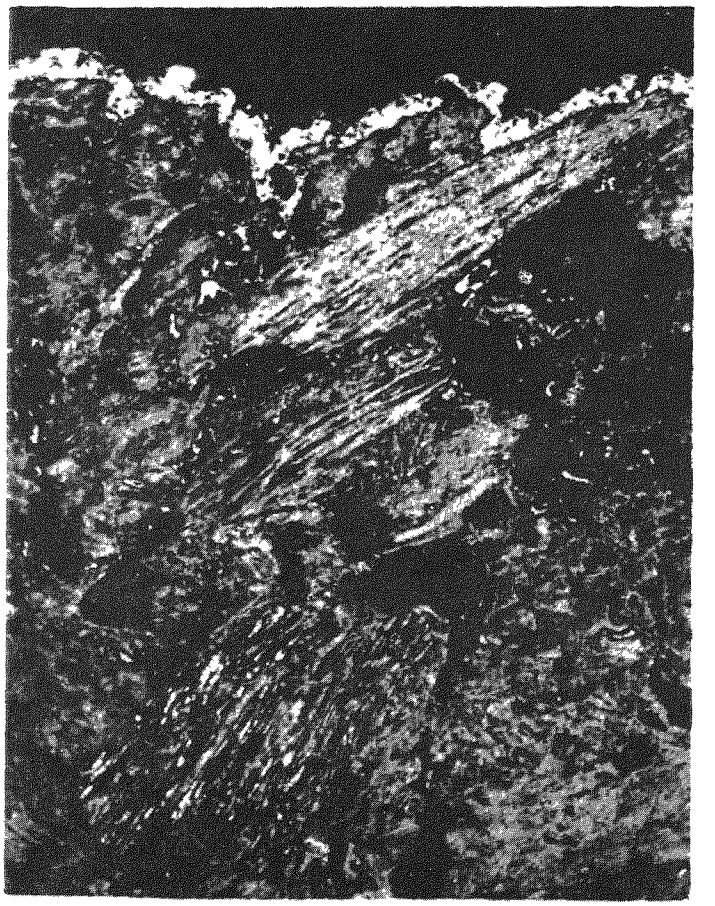

Fig. 3-7. Pyrolytic carbon coating on specimen type FX-5. View at 250x.

Abrasion Tests. Abrasion tests were run on 4 FA-20 specimens and 2 FX-5 specimens. The spheres were tumbled for 60 minutes inside a rotating drum which also contained some dummy graphite spheres. The abrasion test results are summarized in Table 3-7. As can be noted, there was more tendency for coatings to flake off the spheres with the thicker coatings. Even though parts of the coating flaked off specimen 342E, which had the thickest coating, it still did not leak. Some leaks appeared in the thinner coatings. These observations imply that the method of failure in these types of coatings is by chipping off of successive layers and that the innermost layer is most securely bonded to the graphite matrix.

TABLE 3-7

Abrasion Tests On Pyrolytic Carbon Coated Spheres

Specimen No.	Coating Thickness, mils	Time in Hot Oil, Min	Hot Oil Test	Visual Inspection
FA-20(342E)	8.5	8	No leaks	Coating flaked and cracked.
FA-20(427N)	2.7	10	Profuse leaks	Coating flaked
FA-20(431N)	2.3	10	Profuse leaks	Coating flaked
FA-20(435N)	4.1	10	Several small leaks.	No damage
FX-5(X3)	0.5	5	Several leaks(a)	No damage
FX-5(U1)	0.5	5	Several leaks(a)	No damage

(a) These specimens showed general porosity prior to the abrasion tests.

Impact Tests. A summary of impact tests on pyrolytic carbon coated spheres is given in Table 3-8. With the FA-20 specimens, visual damage to the coating (i.e. chipping) and the appearance of a leak usually occurred at the same impact load. In one case (399N), the leak appeared at a higher impact load than required to flake off a portion of the coating. The point of impact failure on FA-21(N1) was "spongy" after the test which indicated that this coating consisted of numerous poorly bonded layers. The thin coatings on the FX-5 type specimens did not break away from the graphite matrix up to point where the sphere broke. In most cases it was not possible to detect whether pinholes developed before the sphere broke due to the porous nature of this coating. All of these results generally confirm the observations noted in the abrasion tests.

TABLE 3-8

Impact Tests on Pyrolytic Carbon Coated Spheres

Specimen No.	Thickness, mils	Impact Load, Ft-Lbs: Coating Failure, Hot Oil Test	Impact Load, Ft-Lbs: Coating Failure, Visual	Impact Load, Ft-Lbs: Graphite Failure
FA-20(433N)	3.4	1.7	1.7	—
FA-20(399N)	4.2	2.2	2.0	—
FA-20(326E)	9.3	1.1	1.1	—
FX-3(44)	50	2.5	2.5	—
FA-21(N1)	50	1.0	1.0	—
FX-5(U1)	0.5	0.4	none	8.0
FX-5(U2)	0.5	(a)	none	7.0
FX-5(X3)	0.5	(a)	8.5	—
FX-5(S)	0.5	(a)	7.5	—

(a) Leakage was too great to define coating failure.

Compression Tests. Compression tests were run on two pyrolytic carbon coated spheres. Specimen FA-20(435N) broke at a load of 2830 lbs. and a deflection of 0.182 in. Specimen FA-20(342E) broke at 3275 lbs and a deflection of 0.200 in. It was not possible to determine whether the coating failed prior to the load at which the sphere failed.

Coating Permeability. All specimens of the FA-20 type were found to pass the hot oil leakage test in the as-received condition. In general, most of the thicker coated FA-21 specimens successfully passed the hot oil tests, although one specimen was found to have a single pinhole type leak. Another FA-21 specimen which had a number of carbon growths about 1/8 inch long protruding from its surface passed the hot oil test. However, when the carbon growths were removed by polishing, pinhole leaks were observed where most of the growths has been. The thin coatings on the FX-5 specimens were all found to be porous by the hot oil leakage test.

Uranium Contamination. Since the pyrolytic carbon is deposited directly on the fueled graphite surface, it was of interest to know whether uranium would migrate through the coating or otherwise contaminate the

coating surface. A number of FA-20 and FA-21 specimens were assayed for surface uranium contamination by alpha counting. The results are tabulated in Table 3-9. Occasionally, several spots on the sphere have been found to have a somewhat higher uranium contamination but on the whole, it can be seen that there is no serious uranium contamination of this type of coating.

TABLE 3-9

Surface Uranium Contamination Of PyC Coated Specimens

	Equivalent Fraction of Total U in Sphere		
Sphere No.	Position 1	Position 2	Position 3
FA-20(399N)	2.1×10^{-6}	—	—
FA-20(427N)	1.7×10^{-6}	—	—
FA-20(431N)	5.9×10^{-7}	—	—
FA-20(433N)	7.8×10^{-7}	—	—
FA-20(435N)	1.4×10^{-6}	—	—
FA-20(429N)	5.9×10^{-7}	7.8×10^{-7}	1.7×10^{-6}
FA-20(338E)	7.1×10^{-7}	5.7×10^{-7}	7.1×10^{-7}
FA-20(345E)	5.7×10^{-7}	6.3×10^{-7}	2.3×10^{-6}
FA-20(325E)	4.8×10^{-7}	2.1×10^{-6}	3.2×10^{-7}
FA-20(329E)	1.6×10^{-7}	8.8×10^{-6}	3.2×10^{-6}
FA-20(344E)	1.6×10^{-7}	4.4×10^{-7}	nil
FA-21(N1)	5.9×10^{-7}	7.8×10^{-7}	1.9×10^{-7}
FA-21(N2)	1.9×10^{-7}	5.9×10^{-7}	nil

Radiation Effects. An FA-20 specimen had been subjected to high burnup in Static Capsule SP-4 with the primary objective of determining the effect of irradiation on the pyrolytic carbon material and also to see whether radiation induced changes to the fueled graphite sphere would weaken the coating in any way. This irradiation started in August, 1959 and was completed during Phase II. The design and operating conditions for Capsule SP-4 are described in Section 8.1. The Hot Cell examination of the irradiated specimen was also completed in Phase II. A summary of the irradiation conditions, weight changes, and dimensional changes are given in Table 3-10.

TABLE 3-10

Summary Of Irradiation Results For Pyrolytic Carbon Coated Specimen FA-20(336E) In Capsule SP-4.

Heat Generation Rate	2.0 KW
Measured Graphite Block Temp.	1250°F
Calculated Surface Temp.	1550°F
Calculated Center Temp.	1750°F
Burnup	6700 KWH
Weight, pre-irradiation and change during irradiation	52.2367 gms, + 0.19%
Diameter, pre-irradiation and change during irradiation:	
Position 1	1.4904", -0.17%
Position 2	1.4948", -0.42%
Position 3	1.4976", -0.31%
Position 4	1.4978", -0.28%
Position 5	1.5028", -0.93%

Visual examination of the specimen upon its removal from the capsule revealed a band of 5 parallel hairline cracks all spaced within a 1/4 inch wide band running completely around the sphere. These cracks can be seen in Fig. 3-8. As expected, there was profuse leakage from the cracks when the specimen was subjected to the hot oil test. There appeared to be some slight leakage in areas removed from the crack region. However, due to the profuse bubbling from the crack region, the presence of other pinholes could not be definitely confirmed. The weight gain listed in Table 3-10 was similar to that observed for the Si-SiC coated specimen also in Capsule SP-4 and it probably associated with the readmission of atmospheric air through the cracks which developed in the coating. In view of the importance of trying to determine the cause of the cracks in the coating, the scheduled impact test on this specimen was omitted. The specimen was mounted in plastic so that it could be sectioned and polished to further study these cracks. Figure 3-9 is section through the coating of the irradiation specimen FA-20(336E). One of the five cracks in the coating can be seen in this view. The coating appears to have been pulled apart. A surface crack in the graphite beneath the coating can also be seen. Cracks of this type have not previously been noted in the surface of uncoated graphite and it is possible that strains in the coating actually caused this crack in the graphite. Due to the orderly nature of the coating

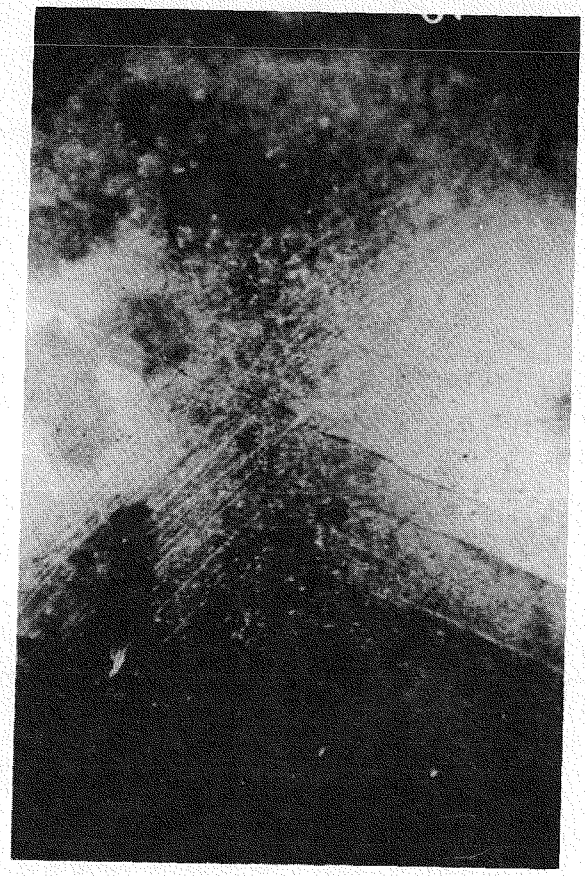

Fig. 3-8. Cracks in surface of pyrolytic carbon coated specimen FA-20 (336E) after irradiation in Capsule SP-4. View at 4x.

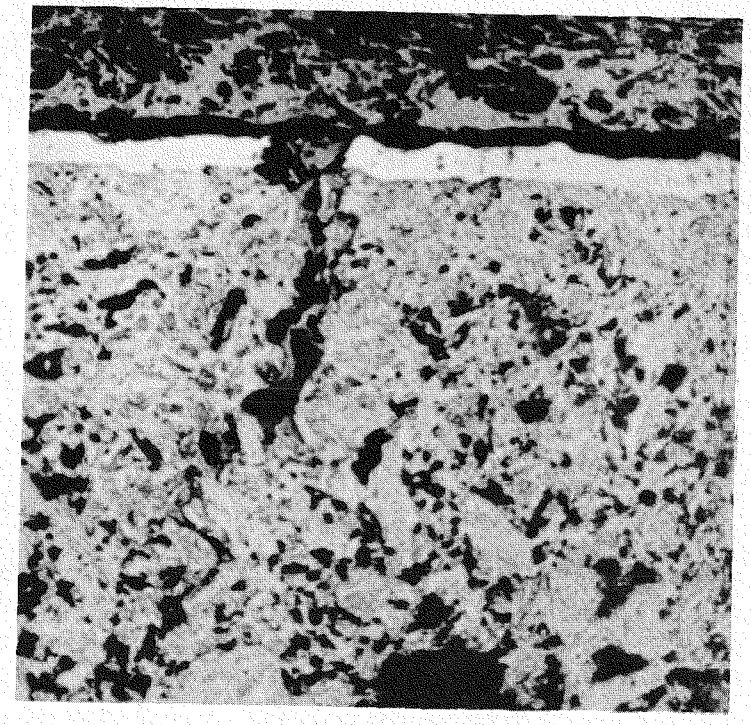

Fig. 3-9. One of the cracks in the surface of pyrolytic carbon coated specimen FA-20 (336E) after irradiation in Capsule SP-4. View at 100x.

cracks, the most likely cause is a radiation induced differential dimensional change in the graphite which caused a tensile stress in the coating in the region of the cracks. Although there may have been some radiation damage to the coating itself, it is believed that if this were the dominant factor, the crack pattern in the coating would have been more random than the orderly cracks actually observed.

Another FA-20 specimen had been under low level irradiation in Furnace Capsule SPF-1. Leakage factors (rate of release/rate of production) for the long lived noble fission product gases (Kr 85m, Kr 87, Kr 88, Xe 133 and Xe 135) at temperatures of 150°F to 1900°F were found to range from about 10^{-4} to 5×10^{-2} (4). Experiments at four temperatures were conducted in the following order: 1500°F, 1000°F, 1900°F, and 150°F. The release rate was somewhat higher than anticipated, particularly during the final run at 150°F. Consequently, it was decided to open Capsule SPF-1 in order to examine the specimen. The post-irradiation of FA-20(310N) was conducted during Phase II. Upon removal of the specimen from the capsule, a large number of pits were readily visible in the surface of the specimen as shown in Fig. 3-10. The pits are seen to be largely concentrated in one region of the specimen. They had the appearance of corrosion pits in metal. Many of the pits appeared to be undercut, that is, the underlying graphite had been removed to a greater extent than the pyrolytic carbon surface coating. From these observations, it was concluded that the sweep helium stream for transporting fission products from the specimen to the trapping system must have become contaminated with oxygen or moisture. Although the gas stream was not analyzed for contaminants, some difficulty had been experienced during the shakedown runs on Capsule SPF-1 with cold trap plugging due to excessive moisture believed to come from the particular helium tank in use at the time. It is probable that the rate of attack did not become excessive until the 1900°F run, causing the significant release rates during the subsequent 150°F run.

3.2.2 Fission Product Retention

A summary of the neutron activation tests on pyrolytic carbon coated specimens is given in Table 3-11. All of these specimens showed good fission product retention since most of the Xe 133 release was below the limit of sensitivity of the test apparatus. Only at 2300°F on one of the specimens was there a detectable amount of Xe 133 release. These results indicate the pyrolytically deposited carbon has an extremely low permeability to fission product gases, many orders of magnitude below normal graphite.

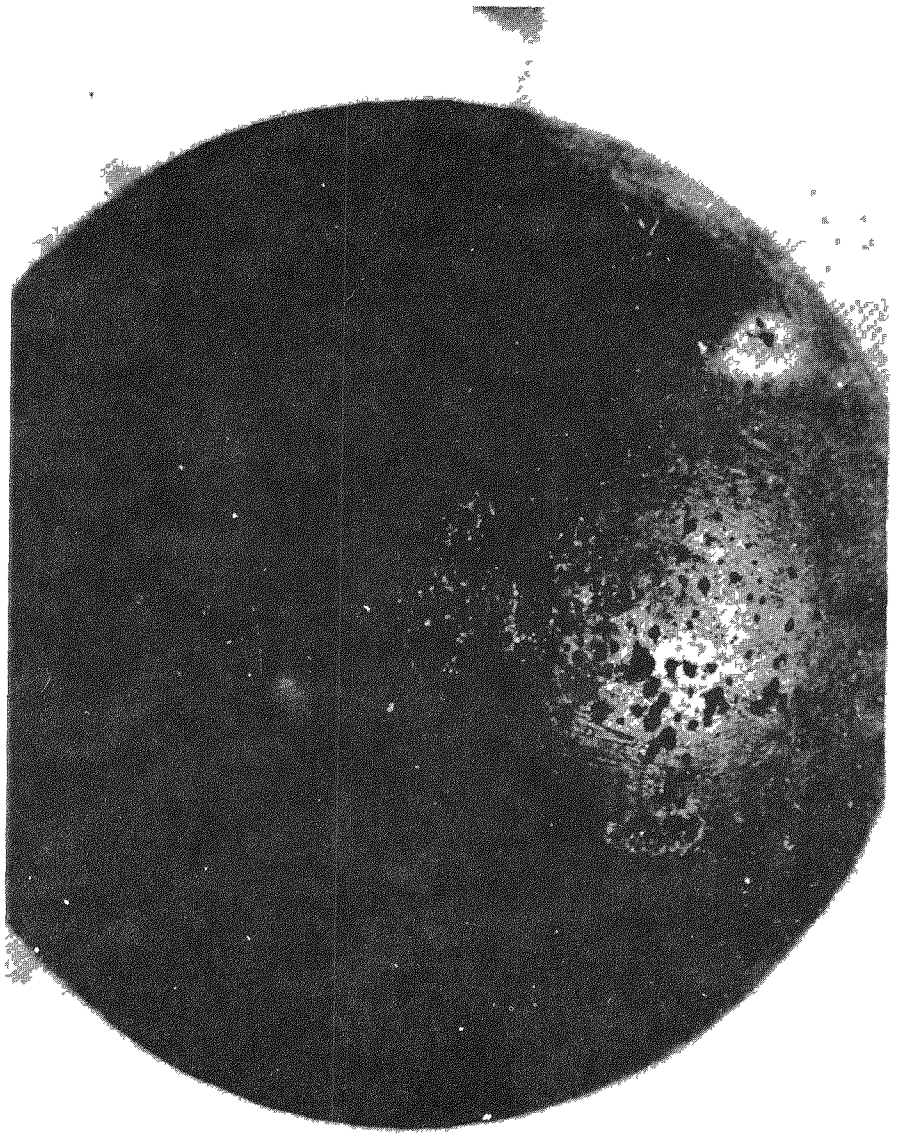

Fig. 3-10. Corrosion pits in surface of pyrolytic carbon coated specimen FA-20 (310N) after exposure in Furnace Capsule SPF-1.

TABLE 3-11

Neutron Activation Tests on Pyrolytic Carbon Coated Specimens

Specimen No.	Coating Thickness, mils	Test Temp °F	Time Min.	Fractional Release of Xe 133
FA-20(429N)	4.9	1700	70	$<4 \times 10^{-5}$
		2200	100	$<4 \times 10^{-5}$
FA-20(338E)	9.5	1900	180	$<9.3 \times 10^{-7}$
FA-21(N2)	50	1650	75	$<4 \times 10^{-5}$
		2300	80	4×10^{-5}

Fission product retention experiments on specimen FA-20(310N) in Furnace Capsule SPF-1 were completed in Phase I and correlated with neutron activation data on this same specimen (4). During Phase II, data at 1000°F, 1900°F and 150°F were obtained. All data is summarized in Table 3-12.

TABLE 3-12

Summary of Fission Product Release From Specimen FA-20(310N) in Furnace Capsule SPF-1

Specimen Temp.	R/B, (Release Rate/Production Rate)				
	Kr 85m	Kr 87	Kr 88	Xe 133	Xe 135
150°F	.00038	.00016	(a)	.0046	.0015
1000°F	.0043	.0023	.0038	.0057	.0039
1500°F	.016	.013	.016	.041	.009
1900°F	.026	.0107	.0224	.067	.019

(a) Not detectable.

During the final run at 150°F, the release rates were higher than anticipated. Consequently, Capsule SPF-1 was opened in the Hot Cell in order to examine the specimen. As described in Section 3.2.1, a number of pits were found in the coating which were responsible for the high release at 150°F.

4.0 Alumina Coated Fuel Particles

Another method of retaining fission products in a uranium-graphite fuel element is to place a coating on each individual fuel particle of an admixture type element. There are several advantages of coatings on fuel particles. Fission products are retained at their source. The coating material is not subjected to such external loads as impact, compression, or abrasion, nor such internal loads as thermal stress which are normally applied to a PBR fuel element. The fracture of a PBR fuel element will not expose uncoated fuel particles, thus fission product retention will be maintained. There should be a minor beneficial effect on manufacturing costs since the graphite fabricator will not have to handle exposed fuel. There may well be an advantage in reprocessing in that the graphite matrix can be removed and disposed of with little regard for the contained uranium and fission products inside the particle coatings.

Development work on a sintered alumina coating for UO_2 particles began during Phase I at the Battelle Memorial Institute. This process consisted of preparing fuel particles from a sintered grade urania powder, dusting the fuel particles with a sinterable grade alumina powder while in a pelletizing drum, isostatically pressing the coated particles and then sintering them. A typical coated particle produced by this process can be seen in Fig. 4-12. The main problems with this type of coated particle were the lower sintering shrinkage of UO_2 compared with the alumina coating, and reproducibility, particularly when thinner coatings (i.e. in the range of coating thickness equal to the fuel particle radius) are employed. A number of variations in the fuel particle were tried. These included the use of UO_3, mixtures of UO_3 and UO_2, and the addition of alumina monohydrate to the starting UO_2 powder. The best solution to the differential shrinkage problem was found to be the addition of 65 w/o UO_3 to the UO_2. However, it was found that reproducibly good coatings could only be made with excessive coating thicknesses (i.e. coating thickness equal to the fuel particle diameter). Consequently, this work on sintered alumina was abandoned during Phase II in favor of another process proposed by Battelle.

This new process, known as vapor deposited alumina, was first attractive because extremely thin coatings (i.e. 10 microns and less) could be produced and the material appeared dense and impermeable. Subsequent development work and irradiation test results obtained during Phase II showed that this was indeed a most promising type of coating. The work on alumina coated UO_2 described in the following sections all relates to vapor deposited alumina.

4.1 Coated Particle Fabrication

The process for applying vapor deposited alumina coatings on UO_2 particles was performed at Battelle in a fluidized bed. The apparatus used for all work reported herein was a 1" diameter externally heated quartz tube having a conical bottom to support the bed of UO_2 particles. The particles were fluidized by a hydrogen stream containing aluminum chloride vapor. An additional stream of hydrogen is introduced into the lower part of the bed through a water vaporizer. About 50% of the alumina formed by hydrolysis at approximately 1800°F is deposited on the surfaces of the UO_2 particles. The remainder of the alumina passes out of the reaction vessel as fines along with the by-product HCl. Measurement of HCl production is used to follow the alumina production rate. The convenient batch size for the experimental apparatus is 100 gms of UO_2. High-fired UO_2 spherical shot was used for practically all of the runs.

Uranium contamination of the coating by UO_2 dusting during the initial stages of fabrication is minimized by stopping the process after several microns of alumina have been deposited, rinsing both the particles and the reaction vessel, and restarting the process. When large coating thicknesses are desired, volumetric expansion of the coated particle bed limits the run, making it necessary to split the batch in half and continue coating each half in separate runs.

The large number of particle collisions during the fluidized coating process, each tending to form a new growth site, is believed to be a major factor in forming the dense coating. No sintering step is required after the fluidization process. The deposition temperature is perhaps the most important process variable. In the 1800°F to 2000°F range, a dense impermeable alpha-phase alumina is formed while at a lower temperatures a porous coating is formed. A further description of the manufacturing process is given in reference (10).

A summary of all alumina coated UO_2 particles made to date is given in Table 4-1. Batches which have been used to fuel graphite spheres are also indicated.

TABLE 4-1

Alumina Coated Particles and Fueled Graphite Spheres Made During Phase II

Batch No.	UO_2 Size, μ	Uranium Enrich.	Coating Thick, μ	Deposit. Temp., °F	No. of Spheres
1B	105/149	Nat.	20	1830	3
2A	105/149	Nat.	38	1830	2
3C	105/149	Nat.	50	2010	0
4E	105/149	Enr.	55	1830	3
5D	250/420	Dep.	40	2010	0
6F	105/149	Enr.	42	1830	0
6H	105/149	Enr.	48	1830	5
6J	105/149	Enr.	66	1830	0
7H	105/149	(a)	40	1830	0
7J	105/149	(a)	44	1830	0
8G	297/350	Nat.	150	1380(b), 1830	0
9	105/149	Nat.	14	1830	0
9A	105/149	Nat.	26	1830	0
11C	105/149	Enr.	59	1380(b), 1830	0

(a) Particle composition was ThO_2 and UO_2 in 11:1 ratio.
(b) 20 microns of porous Al_2O_3 was deposited at this temperature.

Batches 1B and 2A. These were the first batches of alumina coated UO_2 made for the PBR Fuel Element Development Program. Batch 1B was prepared in 3 stages and was subjected to a nitric acid leach after the first stage (9 microns) to remove uranium contamination. Batch 2A was prepared by making two additional runs on batch 1B. Particles from Batch 1B are seen in Fig. 4-1 and particles from batch 2A are seen in Fig. 4-2 All runs were done at 1830°F. No evidence of laminations between the successive runs can be noted. The dense continuous appearance of the particles on all coatings was most encouraging.

Batches 3C and 5D. Two variables were studied in these batches. A higher deposition temperature (2010°F) was used for batch 3C and both the 2010°F deposition temperature and larger particles were used in batch 5D. A greater amount of included porosity was noted in batch 3C as seen in Fig. 4-3. The porosity does not appear to be interconnected in the radial direction but does appear to be oriented parallel to the coating surfaces. The UO_2 used in batch 5 D was somewhat irregular in shape as seen in Fig. 4-4. More evidence of included porosity can be noted. In spite of the angular nature of the UO_2, all surfaces are uniformly coated.

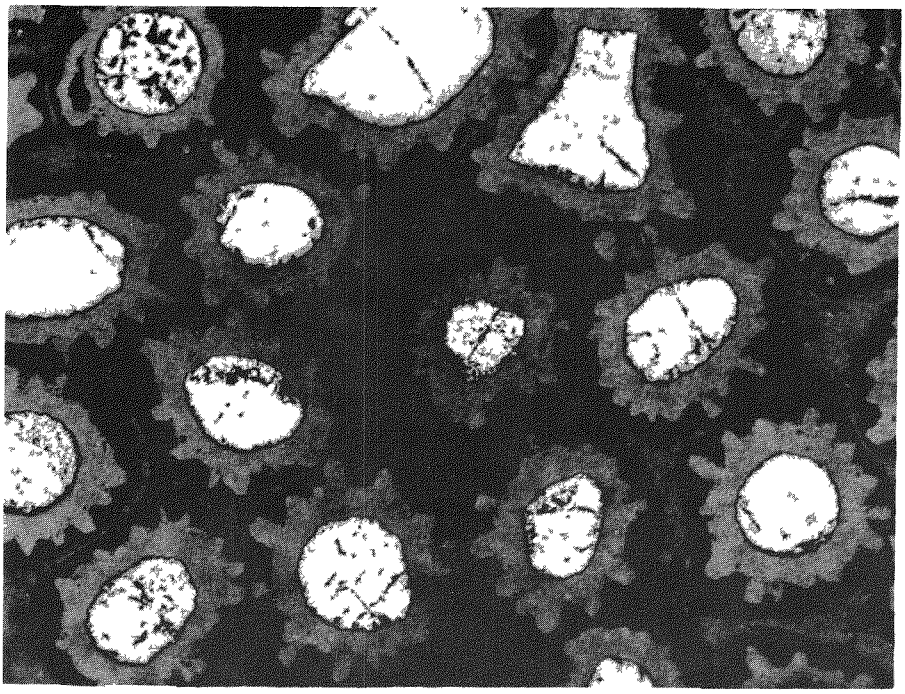

Fig. 4-1. Al_2O_3 coating on UO_2, from batch No. 1B 100x

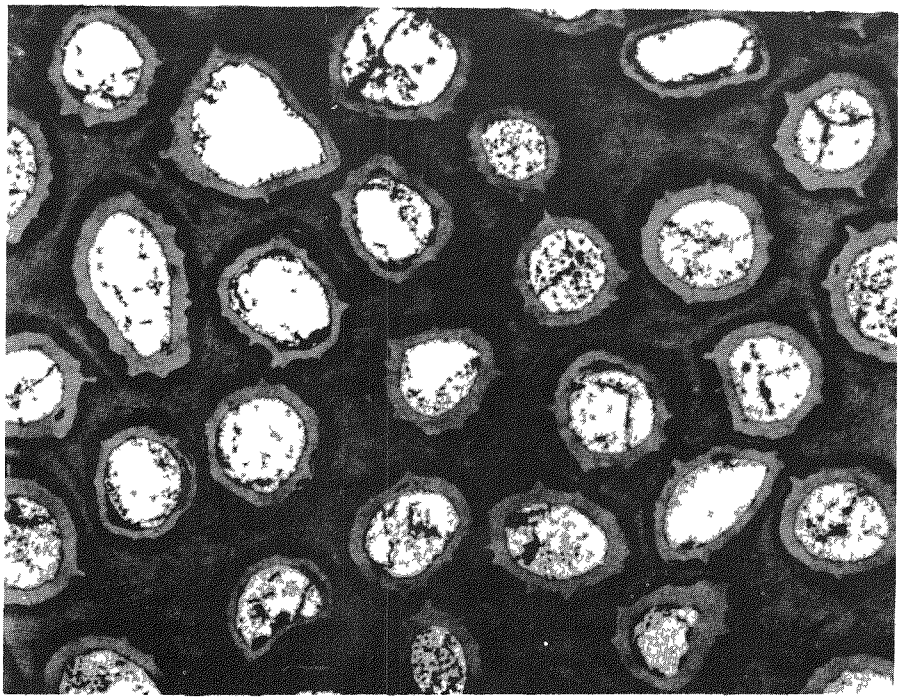

Fig. 4-2. Al_2O_3 coating on UO_2, from batch No. 2A 100x

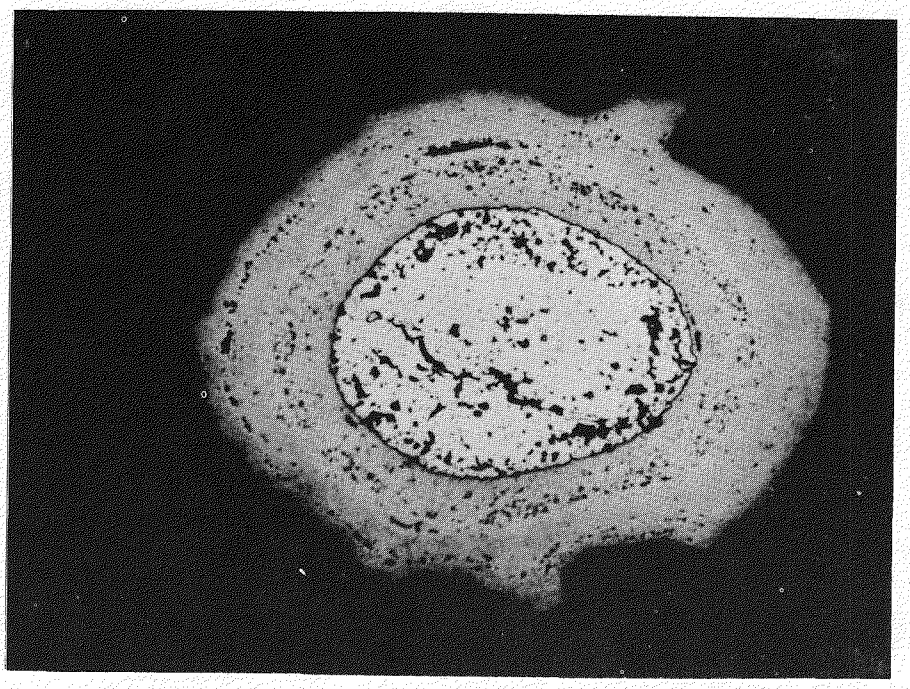

250x

Fig. 4-3. Al_2O_3 Coating on UO_2 from batch No. 3C

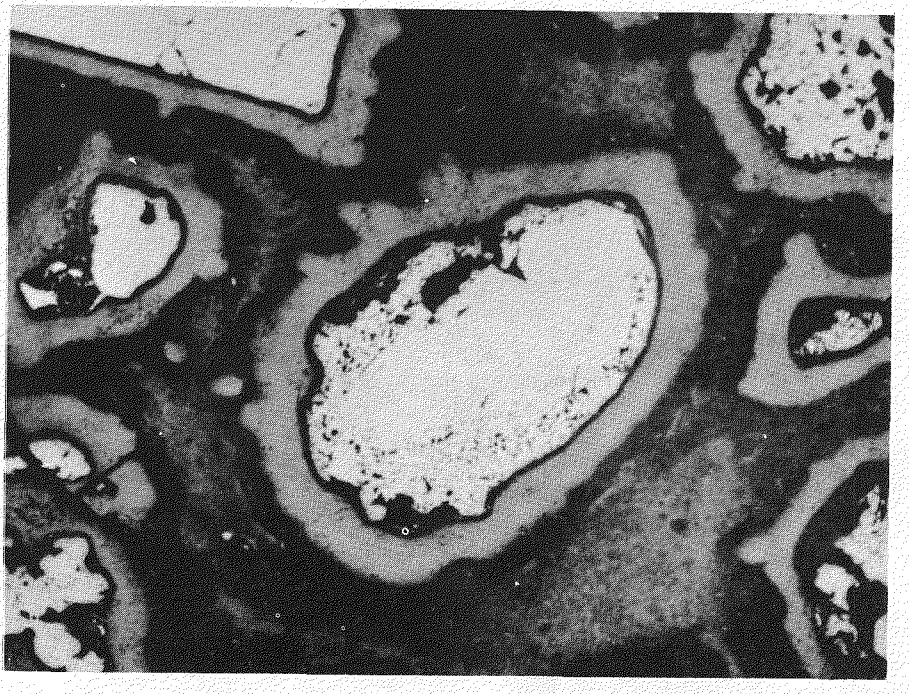

Fig. 4-4. Al_2O_3 Coating on UO_2 from batch No. 5D

Batch 4E. The batch of enriched UO_2 shot was coated for high level irradiation testing. Particles from this batch were eventually incorporated into the FA-22 specimens which were irradiated in Capsule SP-5. Figure 4-5 shows a 500X view of a particle from this batch together with a 5000X picture which was taken in order to study the structure of the coating in more detail. The dark band in the coating is now believed to be a porous alumina region which was inadvertently deposited during the fabrication of this batch. In the 5000X view, the dense and continuous band of impermeable alumina can be noted between the UO_2 and the porous alumina. Grain boundaries can be clearly noted in the UO_2. The absence of such boundaries in the alumina phase is the major reason why this type of coating has shown such good fission product retention.

Batches 6F, 6H, and 6J. These batches containing enriched uranium were made in order that additional fueled graphite spheres could be prepared for irradiation in the in-pile loop (see Section 9.0). A single batch of enriched UO_2 particles was first coated with 23 microns of alumina in 3 steps. The batch was then split with batch 6F being produced in 3 more runs on one half and batch 6H being produced in 2 more runs on the other half. Batch 6J, which approaches the maximum thickness to diameter ratio considered for use in the PBR, was prepared by making two additional runs on a portion of batch 6F. Fig. 4-6 is a photomicrograph of particles from batch 6F where the good bonding between successive coating runs is apparent by the lack of any visible interfaces within the coating.

Batches 7H and 7J. Thoria-urania particles were used in batches 7H and 7J to determine whether there would be any unanticipated effects due to the presence of thoria. The nominal 11:1 Th/U atom ratio used in these particles resulted from a design study of a 125 eMW Pebble Bed Reactor Steam Power Plant (1). A single batch of ThO_2/UO_2 particles was first coated with 24 microns of alumina in 5 steps. After splitting this batch, 3 more runs were made on each half to produce batches 7H and 7J. A photomicrograph of a typical batch of coated particles from batch 7H is seen in Fig. 4-7. Although the ThO_2/UO_2 particles are somewhat irregular, all particles are seen to be adequately coated with no evidence of gaps between successive coating layers.

Batch 8G. This batch was prepared with two special features in mind: (1) a large UO_2 particle was used (297/350 micron) so that a thick coating could be applied and not exceed limitations on carbon moderator displacement when dispersed in a graphite sphere, and (2) a porous inner layer of alumina

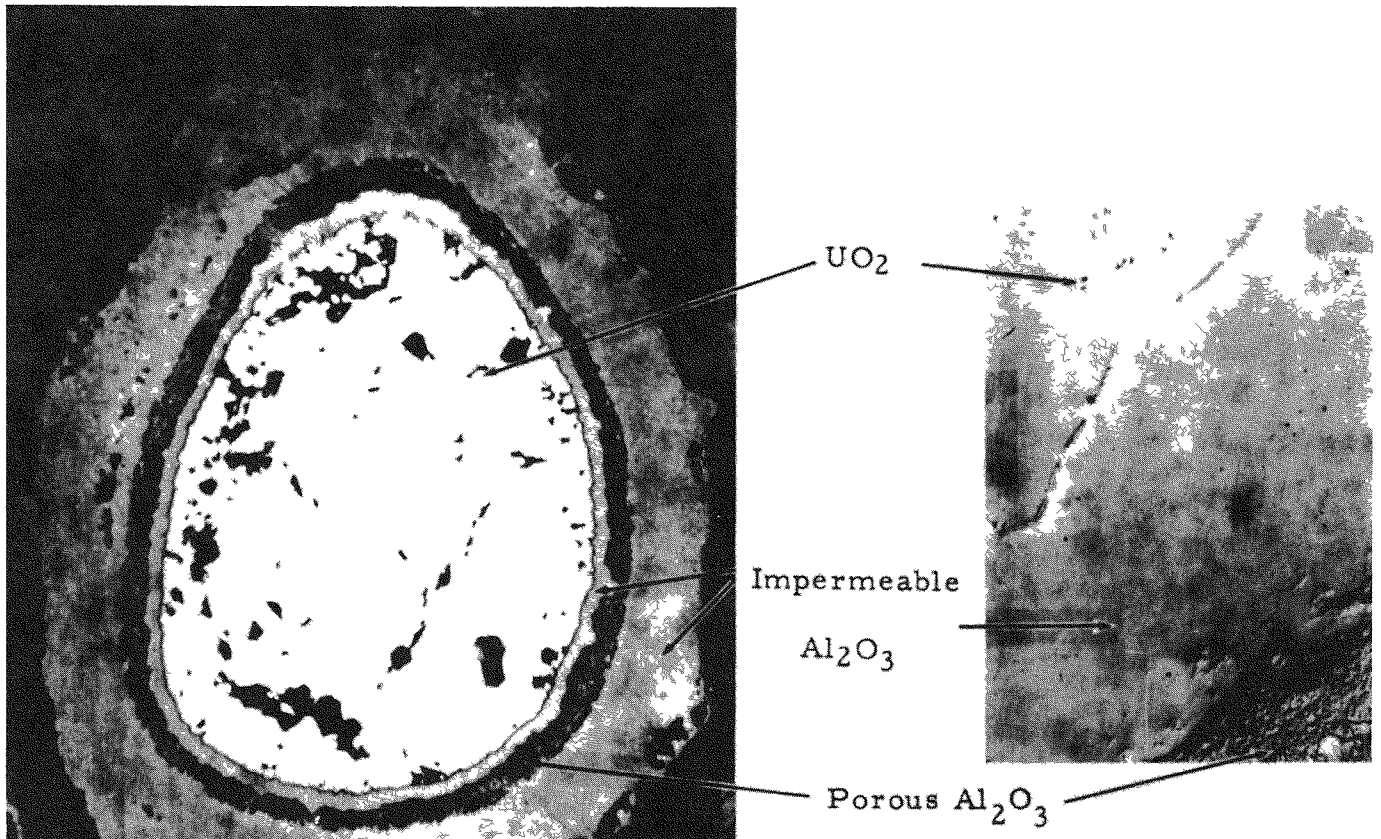

Al_2O_3 coated UO_2 particle from Batch 4E (500X).

5000X magnification at Al_2O_3-UO_2 interface. Unetched.

Fig. 4-5

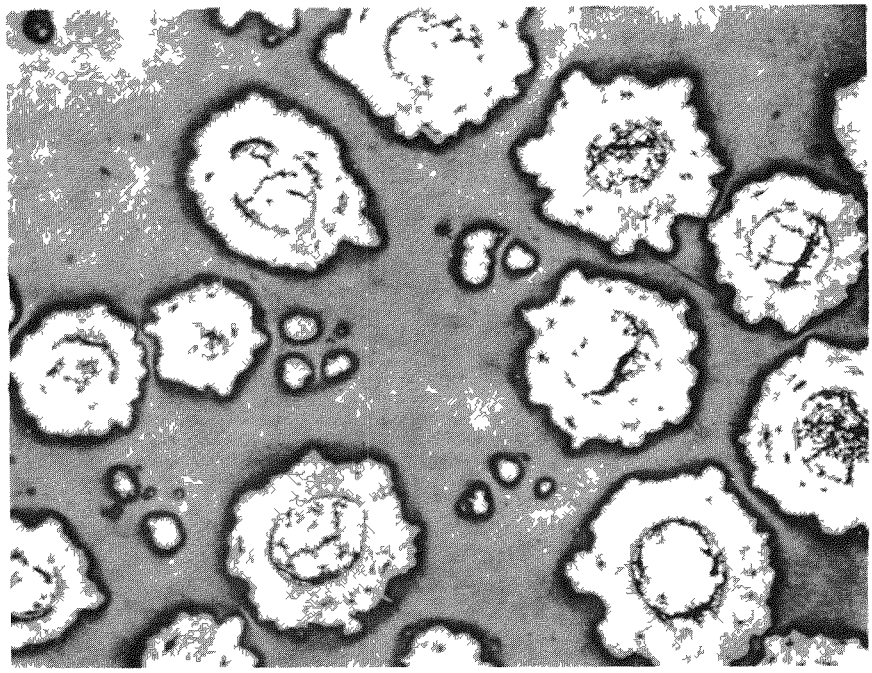

Fig. 4-6. Al_2O_3 Coating on UO_2, from batch 6F. 100x

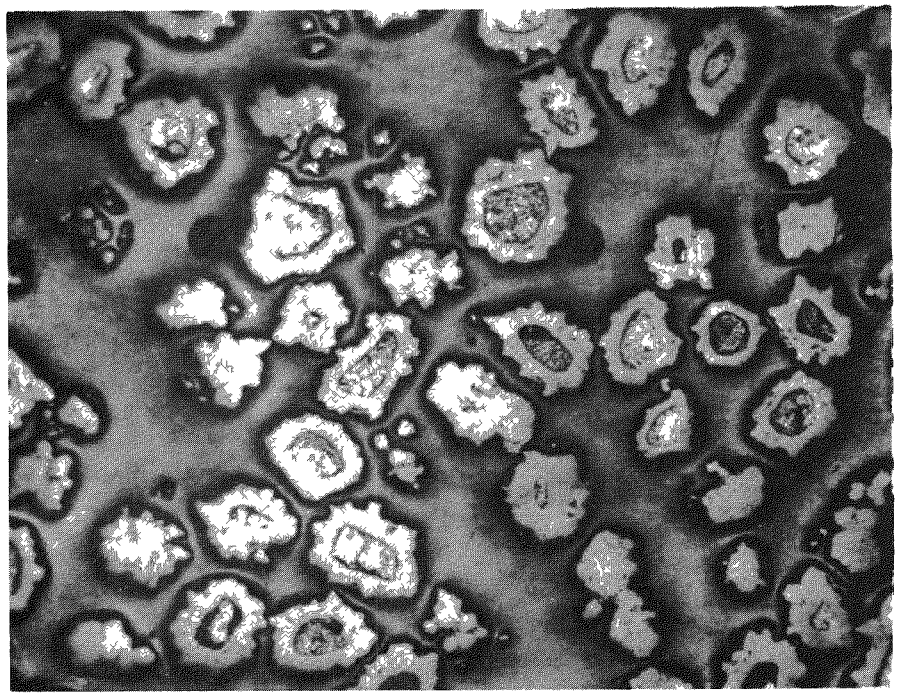

Fig. 4-7. Al_2O_3 Coating on ThO_2/UO_2 from batch 7H 50x

was used which would have the advantage of providing a reservoir for fission gases and a cushion to prevent thermal cycle fracture of the outermost impermeable alumina coating. A thin 2 micron coating was first deposited at 1830°F so that any uranium contamination arising from dusting of the bare UO_2 particles during the early stages of fluidization could be leached away. Next, a 20 micron layer of porous Al_2O_3 was deposited at 1380°F. Additional impermeable alumina was deposited at 1830°F until a total alumina thickness of 150 microns was reached. 5 gm. samples were removed from the batch at coating thickness of 30, 50, 77, 106, 122 and 150 microns in order to evaluate the effect of coating thickness of thermal cycle rupture. Fig. 4-8 shows a particle from batch 8A which has been coated with only the thin impermeable layer and the porous layer of alumina. Fig. 4-9 shows several particles from the final batch, 8G. The dark band near the UO_2 particle is the porous alumina. Some evidence of annular porosity in the UO_2 particles can be noted. Occasional growths of alumina can be seen to protrude from the outer surface of the coating. In several instances, a dust particle inclusion can be noted at the base of alumina growths. Similar growths have been noted in pyrolytically deposited carbon coatings which were also believed to arise from soot particles.

Batches 9 and 9A. These batches were prepared in order to explore the effect of faster deposition rate on coating integrity. All previous batches were prepared at a deposition rate of about 6 gms/hr which would not cause excessive plugging of the exhaust system by Al_2O_3 fines. This rate was increased to 12, 24, and 48 gms/hr as a result of improvements in operating procedure and equipment design. No difficulties were experienced at 12 gms/hr (Batch 9). At 24 gms/hr (Batch 9A), a plug formed at the top of the reaction vessel after several hours of operation. Further plugging was observed at 48 gms/hr.

Batch 11C. This batch was prepared with fully enriched UO_2 and was intended to be a duplicate of batch 8G, containing a porous inner layer of Al_2O_3. A supply of irregularly shaped enriched UO_2 was used because of the extended delivery time for large spherical shot. After 59 microns had been deposited, it was noted that portions of the coatings on many of the particles had chipped off. Efforts were made to weed out the faulty particles by leaching and thermal cycling but this did not help. This type of difficulty is believed due to the combination of the porous inner layer on irregularly shaped particles. Further coating of this batch was abandoned.

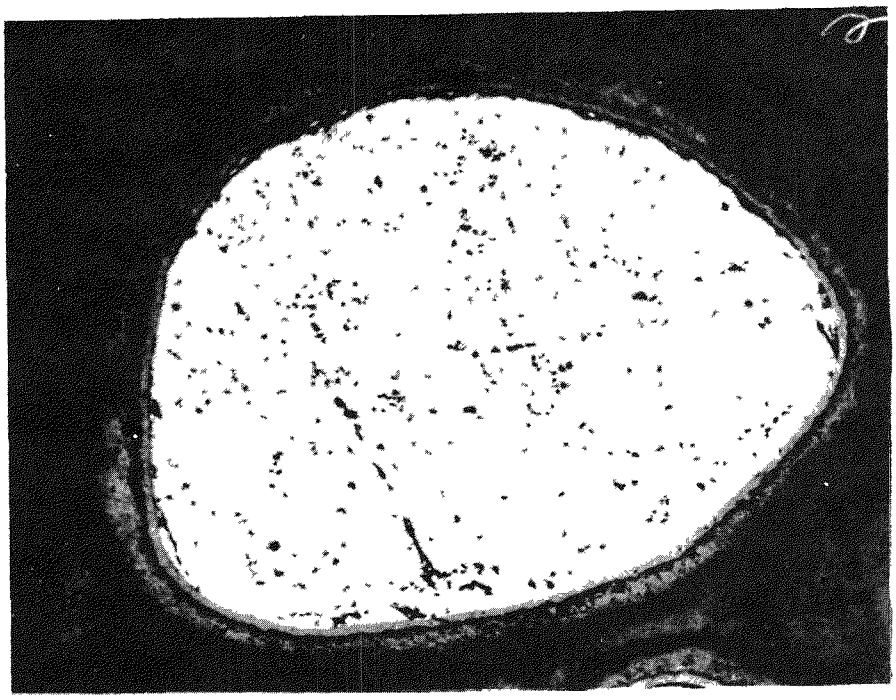

Fig. 4-8. Batch 8A showing thin impermeable layer of Al_2O_3 and porous layer of Al_2O_3 on UO_2 particle (500X).

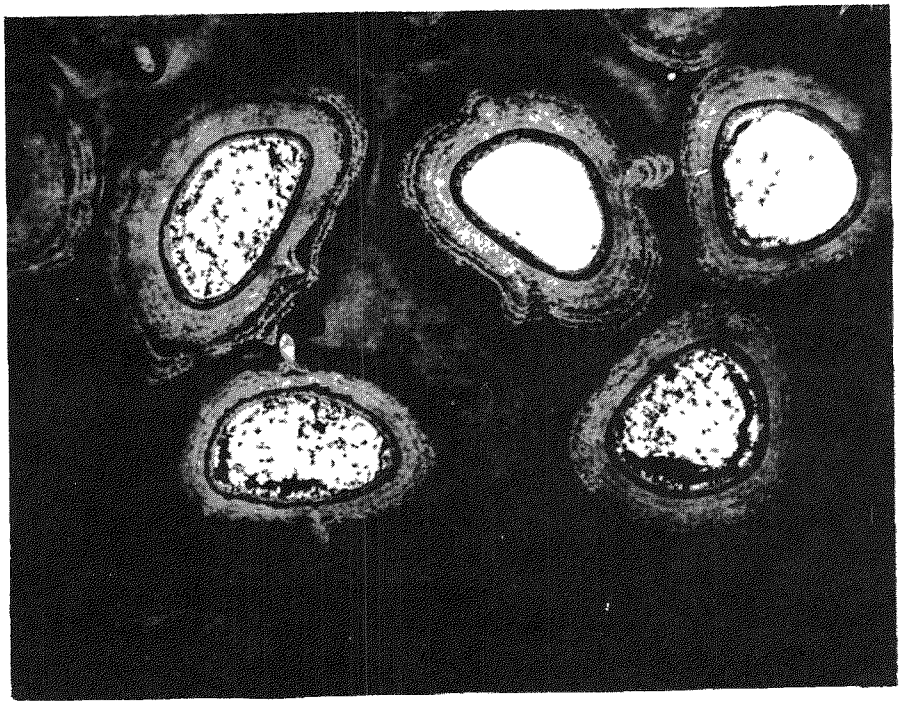

Fig. 4-9. Batch 8G showing Al_2O_3 coating with porous inner layer on UO_2 (50X).

4.2 Pre-Irradiation Testing of Coated Particles

A number of standard screening tests are used for alumina coated fuel particles. In general, each batch of particles which has been fabricated is subjected to the following tests:

1. Alpha Assay: Uranium contamination on the surface of the particles is detected by placing a thin layer of the coated particles in a 2π proportional gas flow counter and measuring the alpha emission rate.

2. Coating Integrity: Coated particles are exposed to air at 1200°F. Any faults in the coating cause the underlying UO_2 to be oxidized to U_3O_8 which further ruptures the coating due to expansion of the fuel particle. Thus, weight gain after this test is a measure of lack of coating integrity. An entire batch of particles can be subjected to this test so that exposed uranium can be subsequently removed from faulty particles by leaching.

3. Thermal Cycling: Particles are thermal cycled between room temperature and 2500°F in an inert atmosphere to determine whether the slightly higher expansion coefficient of UO_2 as compared with the alumina coating will cause the coating to fail when the particle is heated above its fabrication temperature.

4. Metallographic Examination: Routine metallography is done up to 500X. On occasion, electron microscopy is used for more detailed study.

Table 4-2 is a summary of pre-irradiation test results on Al_2O_3 coated particles. The most striking results are from the coating integrity tests where uniformly good coatings were found for every batch. Even in the later batches where the entire batch was subjected to the hot air oxidation test, extremely small weight changes were found. In earlier work with other types of particle coatings, weight gains as high as 10% to 50% were often found in similar tests. The weight loss reported for some batches is due to further devolatilization of adsorbed air and moisture.

Since the thermal expansion coefficient of UO_2 (10×10^{-6}/°C) is slightly higher than for Al_2O_3 (8.5×10^{-6}/°C), it was of interest to learn whether heating the coated particles above their fabrication temperature would rupture the Al_2O_3 coatings. A top temperature of 2500°F was selected for the thermal cycle tests because this appeared to be the upper limit due to reaction between Al_2O_3 and graphite. The first thermal cycle test was run on batch 2A and was done in air. The alpha count was found to increase

TABLE 4-2

Pre-Irradiation Tests on Alumina Coated Fuel Particles

1.	Batch No.	1B	2A	3C	4E	5D	6F	6H	7H	7J	8G	9	9A
2.	UO_2 Size, μ	105/149	105/149	105/149	105/149	250/420	105/149	105/149	105/149	105/149	297/350	105/149	105/149
3.	Coating Thickness, μ	20	38	50	55	40	42	48	40	44	150[f]	14	26
4.	UO_2 Constant, w/o	71.0	48.9	32.6	36.0	66.1	27.3	26.6	35.4[e]	34.5[e]	42.8	-	-
5.	As Fabricated												
	(a) Alpha assay [a]	7.3 ± 1.3	1.4 ± 1.0	0.8 ± 0.8	20.7 ± 2.5	0.2 ± 0.8	0.4 ± 1.2	0.4 ± 1.2	2.0 ± 0.4	0.5 ± 1.0	1.0 ± 0.6	-	-
	(b) Exposed U[b]	1.5×10^{-5}	4.5×10^{-6}	4.0×10^{-6}	3.0×10^{-5}	4.5×10^{-7}	4.5×10^{-7}	4.5×10^{-7}	9.0×10^{-6}	2×10^{-7}	3.5×10^{-6}	-	-
6.	Coating Integrity [c]												
	(a) Sample Wt, gms	19.66	5.0	28.1	61.6122	2.81	109	125	89	132	162	-	-
	(b) Weight Change, gms	-.0027	nil	+.10	-0.0343	-.001	+.0004	-.0410	-.0005	nil	+.0005	-	-
	(c) Alpha Assay [a]	-	76.1 ± 5.2	0.8 ± 0.8	-	-	-	-	-	-	0.6 ± 0.7	46.0 ± 3.1	1.8 ± 0.8
7.	Thermal Cycle[d]												
	(a) Weight Change, %	-	-0.25	-0.02	-	10.0	-	-	-	-	-	-	-
	(b) Alpha Assay[a]	-	-	2.0 ± 1.0	-		-	-	5.9 ± 2.0	0.4 ± 0.8	3.4 ± 1.2	193 ± 6.0	32.6 ± 2.6

(a) Reported as cpm/gm of sample
(b) Reported as fraction of total uranium in sample
(c) Sample heated in 1200°F air for 5 hours
(d) Sample heated 3 times to 2500°F in inert atmosphere
(e) $ThO_2 + UO_2$ content
(f) Consists of 20 microns of porous Al_2O_3 and 130 microns of impermeable Al_2O_3

to 44.2 ± 2.0 cpm from the as-fabricated value of 1.4 ± 1.0 cpm. Metallographic examination revealed that some of the coatings were cracked. In order to determine whether oxygen diffusion into the particles at 2500°F might have been the cause, the thermal cycle test was repeated in a reducing atmosphere of N_2 + 10 v/o H_2 using material from both batches 2A and 3C. Metallographic examination of both batches revealed no cracks in the coatings of either batch. An alpha assay of the batch 3C material showed an increase in exposed uranium of only a factor of 2. Alpha assays of batches 7H, 7J, and 8G after thermal cycling also showed no significant change. Thus, when the Al_2O_3 coating thickness is at least 30% of the UO_2 diameter, no damage occurs to the coating when the particles are heated up to 500°F above their fabrication temperature. However, significant coating failure was found when a thickness-to-diameter ratio of 10% was used (batch 5D) in a similar thermal cycle test as evidenced by weight gain in a subsequent hot air test.

ThO_2/UO_2 particles were used to prepare batches 7H and 7J and, as expected, no differences were found compared with an all-UO_2 fuel particle.

In the preparation of batch 8G, a number of smaller batches having intermediate coating thicknesses were withdrawn for examination. The results of tests on these intermediate batches are shown in Table 4-3.

TABLE 4-3

Evaluation of Batches 8A through 8G which Incorporate a Porous Inner Layer of Alumina

Batch No.	Coating Thick, μ	Weight Gain, %[b]	Alpha Count Rate, cpm/gm sample		
			As-Fab.	Hot Air[b]	Thermal Cycle[c]
8A	22[a]	2.8	53.0 ± 3.3	—	—
8B	30	0.5	1.4 ± 0.7	—	—
8C	50	0.03	0.4 ± 0.5	106 ± 5	90.6 ± 4.3
8D	77	0.003	0.2 ± 0.4	51.8 ± 3.3	—
8E	106	0.04	0.8 ± 0.6	10.8 ± 1.6	6.4 ± 1.4
8F	122	0.04	0.4 ± 0.5	5.0 ± 1.2	—
8G	150	0.0003	1.0 ± 0.6	0.6 ± 0.7	3.4 ± 1.2

(a) Includes 2 micron flash coat (impermeable Al_2O_3) and 20 micron coat of porous Al_2O_3.
(b) After exposure to 1200°F air for 5 hrs.
(c) After nine cycles between 550°F and 2500°F in a reducing atmosphere.

A relatively high weight gain can be noted in batch 8A which contains a 2 micron impermeable alumina layer which probably was cracked, and a 20 micron porous layer. However, improvement can be seen in subsequent coating thicknesses. The alpha assay of the as-fabricated batches showed uniformly good quality once the first impermeable layer had been placed over the porous material (batches 8B through 8G). The hot air test showed uniformly good quality from batches 8C through 8G by the weight gain method. However, the somewhat more sensitive alpha assay technique showed a decreasing contamination with increasing coating thickness indicating that some surface uranium was covered by successive coating layers. In the thermal cycle test, there was some evidence of failure in batch 8C, but batches 8E and 8G showed no significant effect. In general, the batches with the thickest coatings passed all tests well.

Batches 9 and 9A were prepared in the course of studies to increase the Al_2O_3 deposition rate. The thicker coating on batch 9A resulted in lower uranium contamination after the coating integrity test. It is believed that the damage in thermal cycle testing was due to the lower coating thickness-to-UO_2 diameter ratio rather than effects of the increased Al_2O_3 deposition rate used in making these batches.

4.3 Graphite Matrix Fueled With Alumina Coated Particles

There are a number of conditions imposed upon alumina coated particles when they are considered for use in a graphite matrix. The volume occupied by the coated particles should be low enough so that the strength of the graphite matrix is not impaired. The size of the coated fuel particle should be small enough so that uniform mixtures of coated particles in graphite can be achieved. The coatings should be strong enough to prevent their damage during the mixing and molding steps. The temperature to which the fueled body is subjected during manufacture and operation should be low enough to prevent reaction between the Al_2O_3 and the graphite. The coated particles should be securely attached to or buried within the graphite matrix to prevent their loss during use.

As noted in Table 4-1, 13 graphite spheres fueled with Al_2O_3 coated UO_2 have been made to date. The primary function of these spheres was to provide specimens for irradiation testing, however some information relating to the conditions cited above was obtained.

4.3.1 Sphere Manufacture

Most of the spherical fuel element specimens made to date have been molded in dies which leave a rather prominent molding flash around the equator of the sphere. Since close tolerances were required for specimens used in high flux capsule irradiations, the standard practice for specimens fueled with uncoated fuel particles was to grind off the molding flash. In view of the potential damage to Al_2O_3 particle coatings, special alpha assays were made on three FA-22 specimens where the molding flash was removed by grinding. The results of this test are shown in Table 4-4 were positions E are on the equatorial molding flash and positions N and S are at opposite ends of the diameter perpendicular to the plane of the molding flash. The molding flash was removed by hand filing. As can be noted, a large increase in uranium contamination was found for specimens 436N (fueled with batch 1B material) and 448N (fueled with batch 2A material) indicating significant damage to the Al_2O_3 coatings. No significant damage to the particles in specimen 39-9N (fueled with batch 1B material) was noted. However, a subsequent radiograph of an equatorial slice from these specimens (see Fig. 4-10) showed an unexplained deficiency of fuel particles at the surface of specimen 39-9N. It was concluded that since the molding flash could not be safely removed, an allowance would be made in the design of the graphite blocks which hold the FA-22 specimen in place during capsule irradiation and no surface machining would be done on FA-22 specimens. Future designs of molds for PBR will minimize or eliminate the molding flash so that loss of fuel material by abrasion or impact will be avoided.

TABLE 4-4

Alpha Assays of FA-22 Specimens Where Molding Flash Has Been Removed

Specimen No.	Molding Flash Removal	Position	Net Alpha Count Rate, cpm(a)
FA-22(436N)	Before	N	12.6 ± 7.0
	"	S	2.8 ± 5.6
	"	E	1.4 ± 5.6
	After	E	636 ± 31
	"	E	318 ± 22
	"	N	22.4 ± 8.4
FA-22(448N)	Before	N	8.4 ± 6.3
	"	S	nil
	"	E	16.8 ± 6.3
	After	E	224 ± 19
	"	E	274 ± 21
	"	N	5.6 ± 6.3
FA-22(39-9N)	Before	N	16.8 ± 6.3
	"	S	4.2 ± 5.6
	"	E	7.0 ± 6.3
	After	E	2.8 ± 6.3
	"	E	2.8 ± 6.3
	"	E	14.0 ± 7.7

(a) Normalized to Whole Sphere Surface.

Uniform dispersions of Al_2O_3 coated UO_2 particles in graphite have been obtained, as seen in radiographs of slices from specimens FA-22(436N) and FA-22(448N) shown in Fig. 4-10. The apparent high particle density in 448N is due to the thicker Al_2O_3 coatings on these particles. It is concluded that there is no problem with achieving uniform particle dispersions up to the 250 micron size.

Several tests have been made to determine the extent of particle coating damage during the mixing and molding steps of sphere fabrication. Tests used to date have included alpha assays of the graphite mix, of the surface of the completed sphere, and of an unfueled graphite sphere. This last step was to determine whether equipment contamination was a possible source of uranium contamination. Since it is not possible to measure uranium

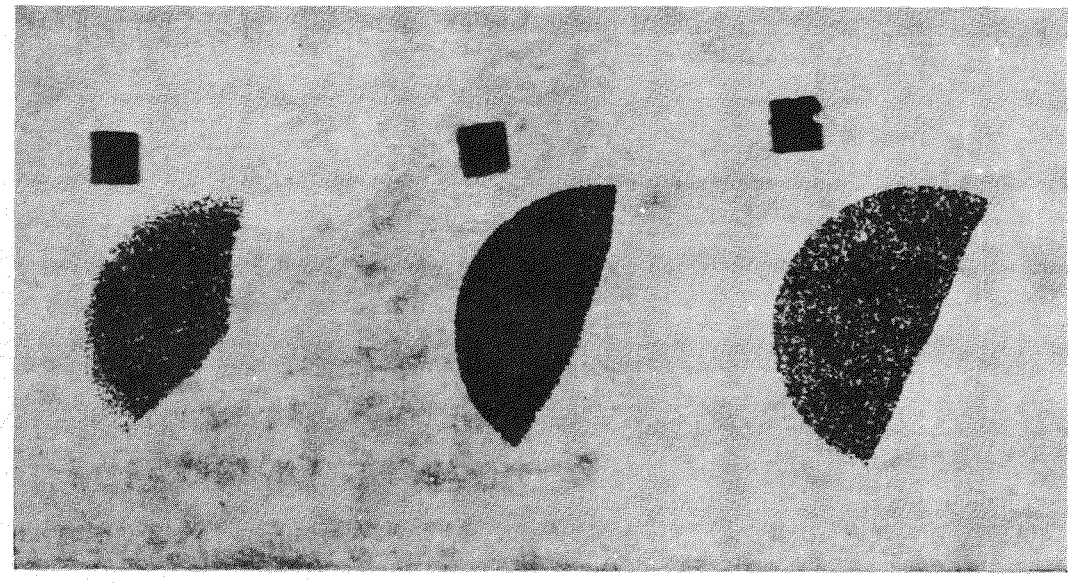

Fig. 4-10. Radiographs of slices cut from graphite spheres fueled with Al_2O_3 coated UO_2. #1 is from FA-22(39-9N), #2 is from FA-22(448N), #3 is from FA-22(436N).

contamination throughout the entire graphite matrix without destroying the finished sphere, a neutron activation test is considered the final test in determining whether coating fracture during manufacturing has been significant. A summary of alpha assays relating to particle damage are given in Table 4-5.

TABLE 4-5

Effect of Manufacturing Processes on Damage To Fuel Particle Coatings

	Net Alpha Count Rate, cpm[a]	Uranium Contamination[b]	Fraction of Xe 133 Released [c]
A. Particles Only			
1. Batch 1B	7.3 ± 1.3	1.5×10^{-5}	3.3×10^{-4} (2400°F, 210 min)
2. Batch 2A	1.4 ± 1.0	4.5×10^{-6}	1.3×10^{-6} (1500°F, 144 min)
3. Batch 4E	20.7 ± 2.5	3.0×10^{-5}	—
4. Batch 6H	0.4 ± 1.2	4.5×10^{-7}	—
B. Sphere Surface			
1. FA-22(437N)-(1B)	1.4 ± 5.6	4.0×10^{-7}	1.0×10^{-4} (2300°F, 140 min)
2. FA-22(449N)-(2A)	4.7 ± 5.8	1.3×10^{-6}	7.5×10^{-6} (1500°F, 270 min)
3. FA-22(471E)-(4E)	16.3 ± 6.1	9.2×10^{-7}	7.7×10^{-6} (1950°F, 240 min)
4. FA-22(548E)-(6H)	14.7 ± 5.9	8.4×10^{-7}	6.3×10^{-7} (2000°F, 240 min)
C. Graphite-Particle Mix (Using batch 6H)	114 ± 20	—	—
D. Unfueled Sphere (Made after Sphere 548E)	7.7 ± 2.1	—	—

(a) All values normalized to equivalent surface of 1 1/2" sphere except for particles which are reported as cpm/gm sample.
(b) Reported as ratio of uranium on surface to contained uranium in sample.
(c) See Neutron Activation Test results in Section 4.3.4.

Uranium contamination on the surfaces of the spheres is seen to be about equal to or less than the contamination on the particles. This implies that there was no major damage to the particles even though the sphere assay only relates to the sphere surface and not to the contamination of the interior portions of the graphite matrix. Comparison of the neutron activation data for batch 2A particles before and after incorporation into a sphere showed only a slight increase in Xe 133 release. The assay of the graphite-coated particle mixture did indicate that some slight damage occurred

during the mixing process. The alpha assay of the unfueled sphere showed that contamination from equipment can be an additional source of uranium contamination. Thus, it can be concluded that there is no gross damage to Al_2O_3 coated UO_2 when incorporated into graphite spheres but that slight contamination can come from three sources: the coated particles as made, coated particle damage during ball fabrication, and from process equipment.

Figure 4-11 shows the surface of an FA-22 specimen which was made for capsule irradiation. The appearance of many fuel particles right at the surface can be noted. Future fuel element designs will incorporate features to prevent loss of these particles from the surface. These features will include surface coatings of either pyrolytic carbon or silicon carbide, carbonaceous layers added to the particles before mixing to permit better bonding to the graphite matrix, or an unfueled shell of graphite on the fueled sphere.

The presence of alumina in a graphite matrix imposes a temperature limitation in order to avoid reaction between the alumina and the graphite. There are indications in the literature (11) that this temperature may be as high as 3600°F. However, to avoid any possibility of damage to the particles during the manufacturing process, the short time graphite bake cycle was limited to a maximum temperature of 2500°F. A series of long time carburization tests was performed using several types of alumina and graphite. These results are reported in the following section 4.3.2.

4.3.2 Carburization Studies

Two series of tests have been run to study the reaction between Al_2O_3 and graphite. The first series involved sintered Al_2O_3 coated UO_2 in graphite samples prepared by Battelle. Three types of graphite were used: (1) AGOT graphite flour with Barrett pitch binder, (2) AGOT graphite flour with BV1600 resin binder, and (3) Texas 55 coke flour with Barrett pitch binder. Samples with resin binder and with coke flour showed severe reaction between the Al_2O_3 and the graphite at 2500°F. The sample with graphite flour and pitch binder showed no reaction after 168 hrs at 2500°F as seen in Fig. 4-12. However, when this latter material was held at 3000°F for only a 6 hr. period, a severe reaction was noted, as seen in Fig. 4-13.

The second series of tests involved vapor deposited alumina. Specimens were heated for periods of 168, 500 and 1000 hrs. at 2500°F based on results from the sintered alumina carburization test. The samples used in the second series are described in Table 4-6.

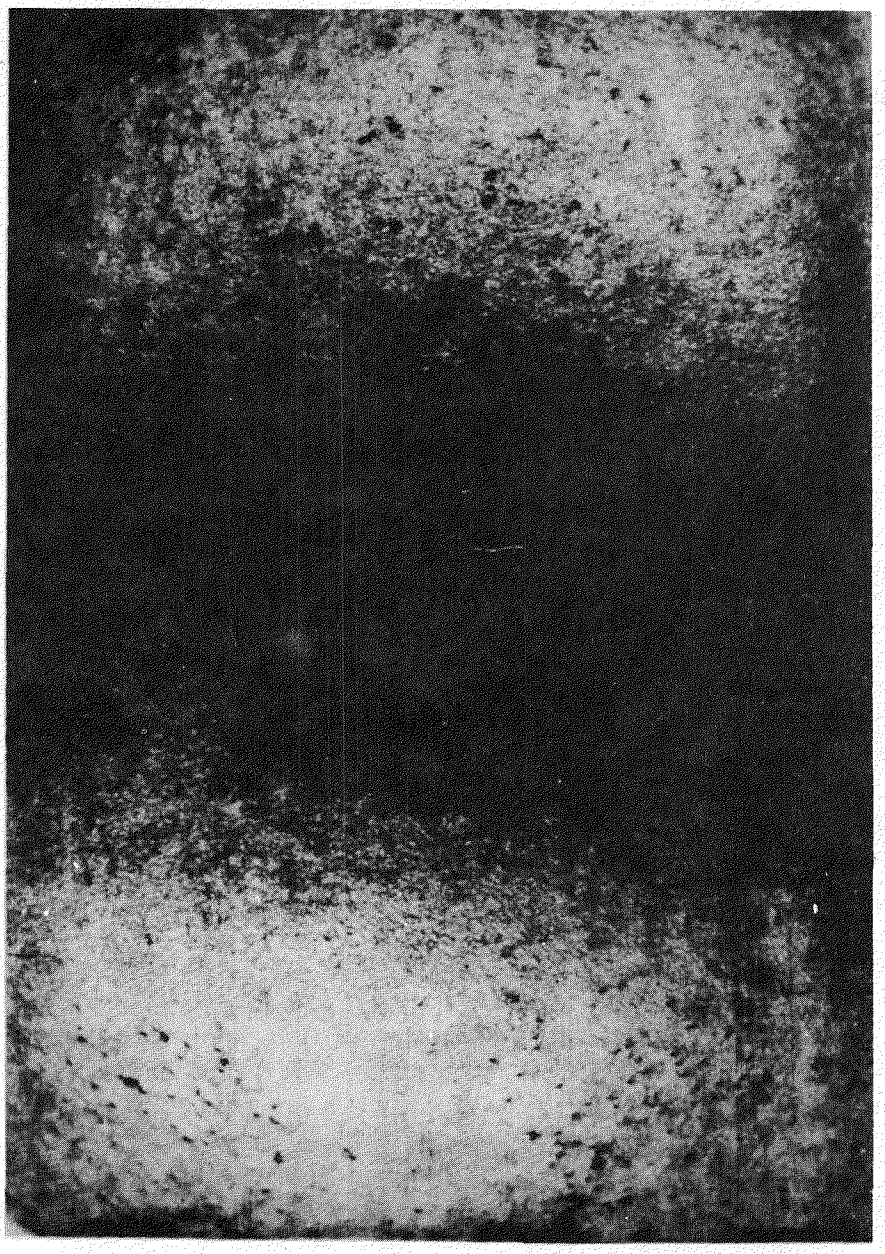

Fig. 4-11 External view of an FA-22 specimen showing Al_2O_3 coated UO_2 particles at the surface.

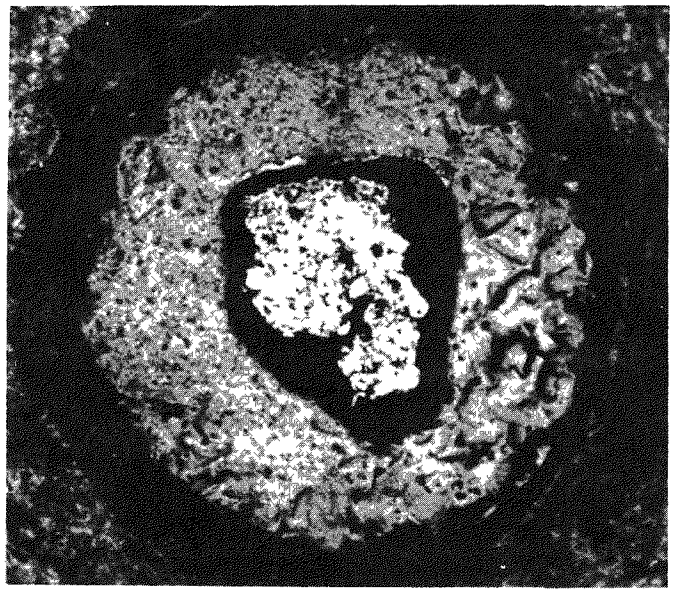

Fig. 4-12 Sintered Al_2O_3 on UO_2 heated in graphite at 2500°F for 168 hrs. (50x)

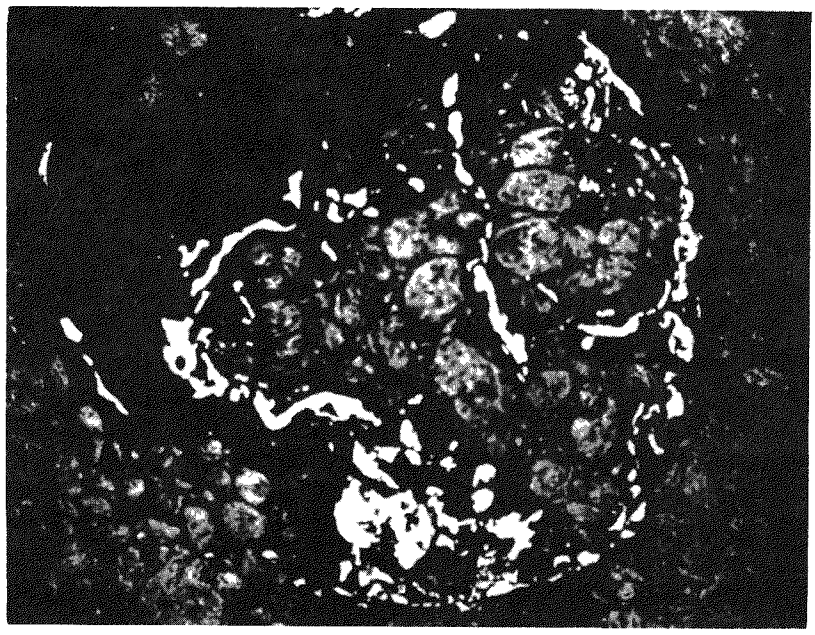

Fig. 4-13 Sintered Al_2O_3 coated UO_2 particle after reaction with graphite at 3000°F for 6 hrs. (50x)

TABLE 4-6

Samples Used in Second Carburization Test

Sample Type No.	Particle Batch No.	Graphite Filler	Pitch Binder	Max. Bake Temp., °F
1	1B	AGOT		1700
2(a)	1B	2301	Coal Tar	2300
3(a)	2A	2301	Coal Tar	2300

(a) Pieces from an FA-22 fuel element.

In all three heating runs, a deposit formed on the inside walls of the furnace tube. The deposits consisted of alumina, silicon carbide, aluminum nitride, and/or iron silicide in addition to an unidentified phase. It is believed that the silicon and the alumina came from the Mullite insulation tube, the iron from the graphite, and nitrogen from the furnace atmosphere. The unidentified phase was found on both the furnace walls and the specimen surfaces.

Typical results of this test are shown in Figures 4-14 through 4-23. Table 4-7 lists the sample number and heating time for each of these figures.

TABLE 4-7

List Of Figures Showing Results Of Graphite-Alumina Reaction Test

Figure No.	Sample Type No.	Heating Time at 2500°F	Location of Particle in the Sample
4-14	Type 1	none	——
4-15	"	168 hrs.	surface
4-16	Type 2	none	——
4-17	"	168 hrs.	center
4-18	"	500 hrs.	center
4-19	"	500 hrs.	surface
4-20	Type 3	none	——
4-21	"	500 hrs.	center
4-22	"	1000 hrs.	center
4-23	"	1000 hrs.	surface

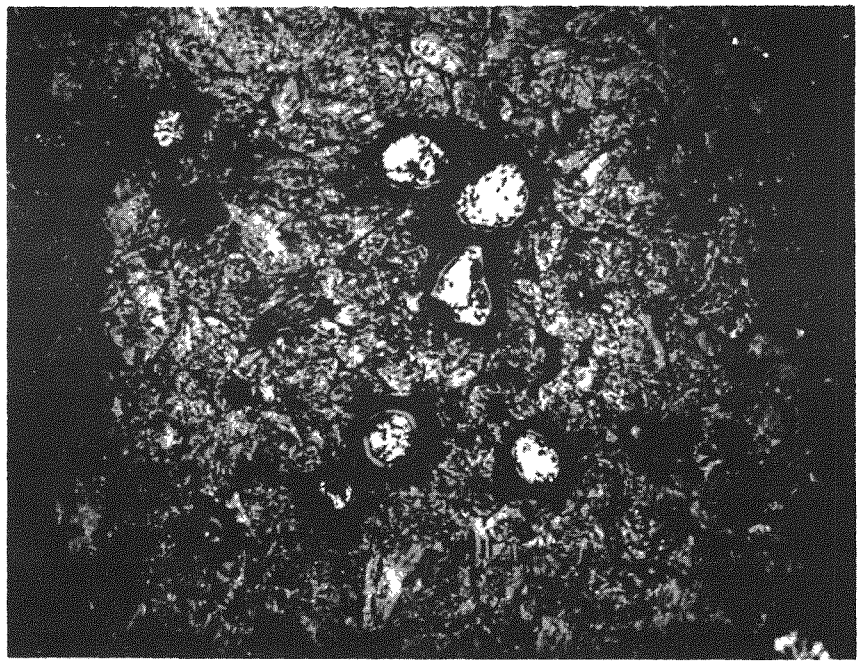

Fig. 4-14. Graphite-Al_2O_3 Specimen Type 1, as fabricated (50X).

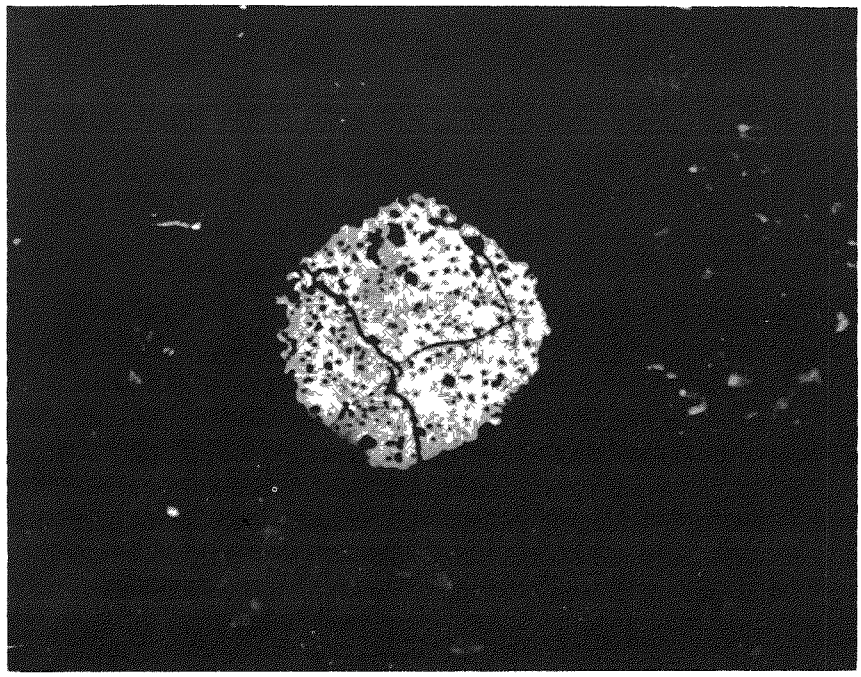

Fig. 4-15. Graphite-Al_2O_3 Specimen Type 1, after 168 hrs at 2500°F (250X).

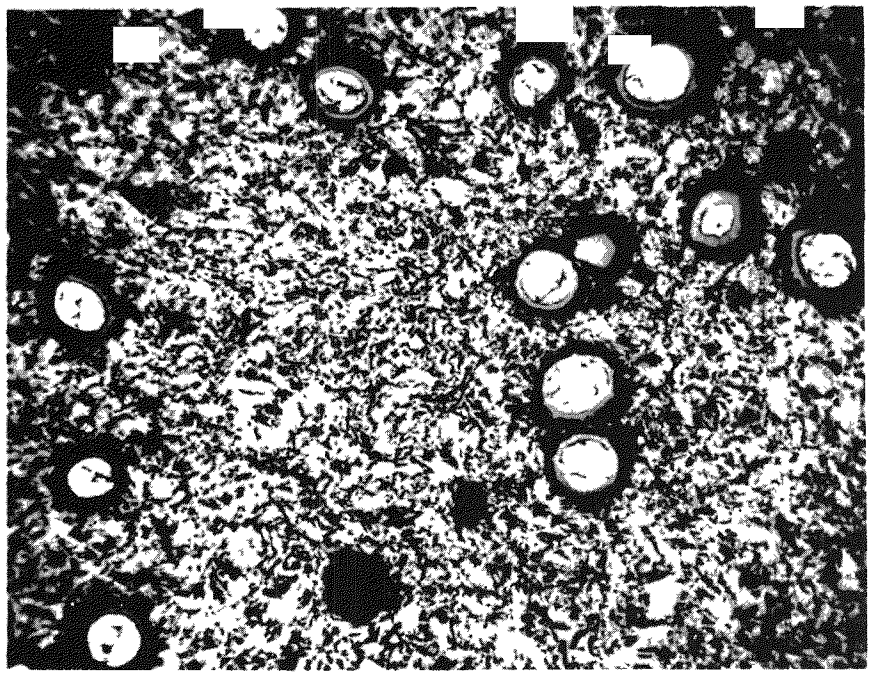

Fig. 4-16 Graphite-Al_2O_3 Specimen Type 2, as fabricated (50X).

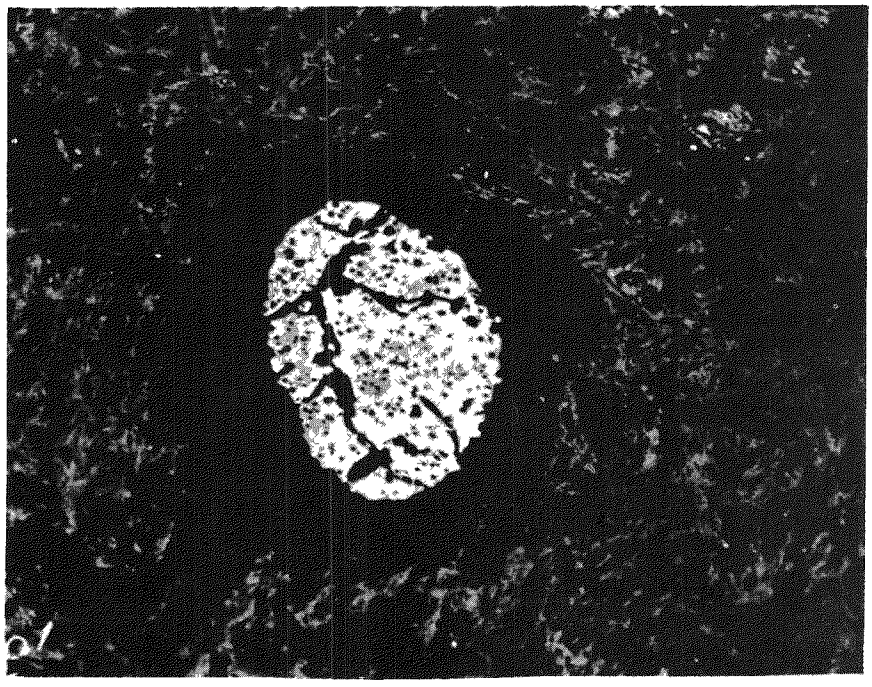

Fig. 4-17. Graphite-Al_2O_3 Specimen Type 2, after 168 hrs at 2500°F. View at center of specimen (250X).

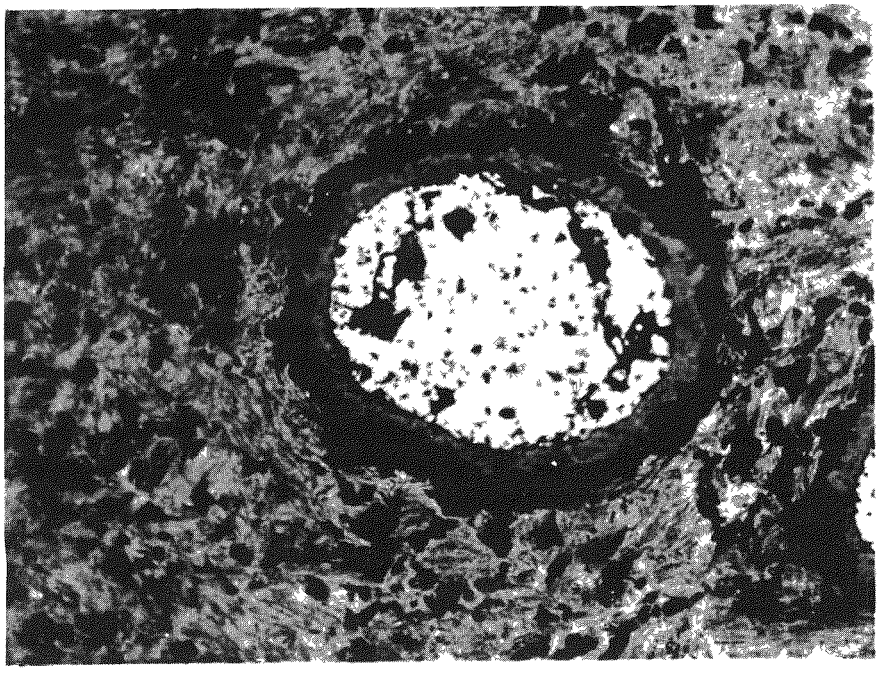

Fig. 4-18 Graphite-Al_2O_3 Specimen Type 2, after 500 hrs at 2500°F. View at center of specimen (250X).

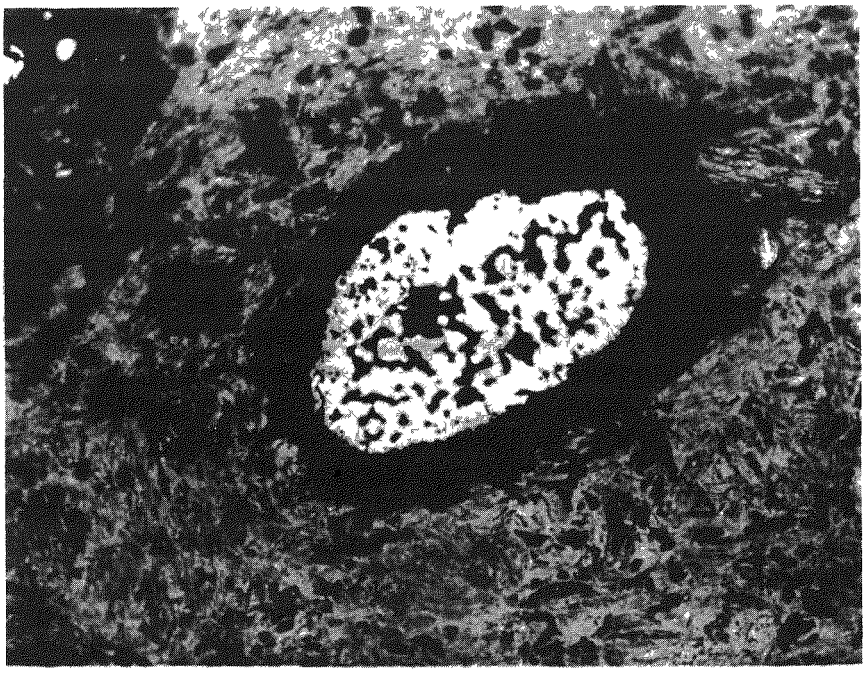

Fig. 4-19. Graphite-Al_2O_3 Specimen Type 2, after 500 hrs at 2500°F. View near surface of specimen (250X).

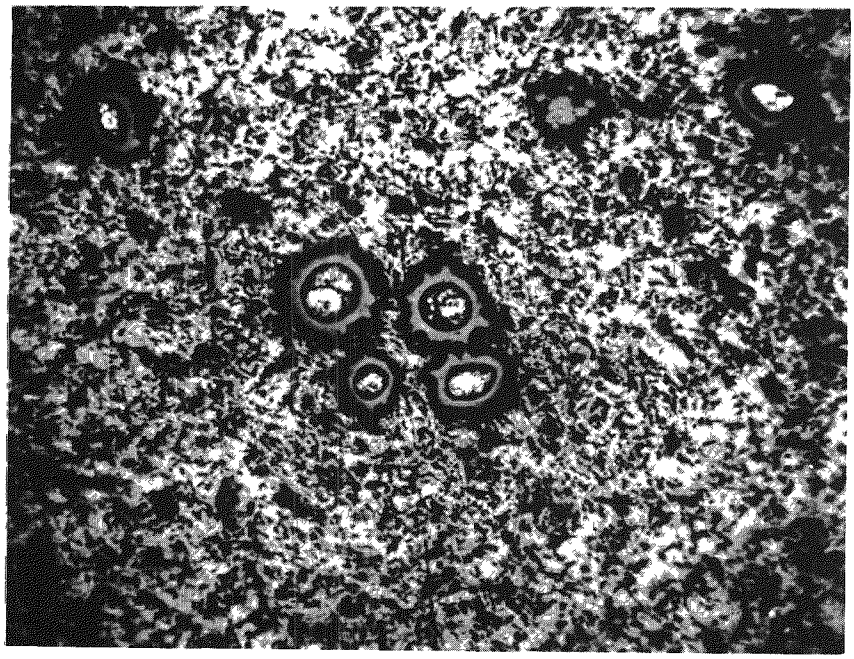

Fig. 4-20 Graphite-Al_2O_3 Specimen Type 3, as fabricated (50X).

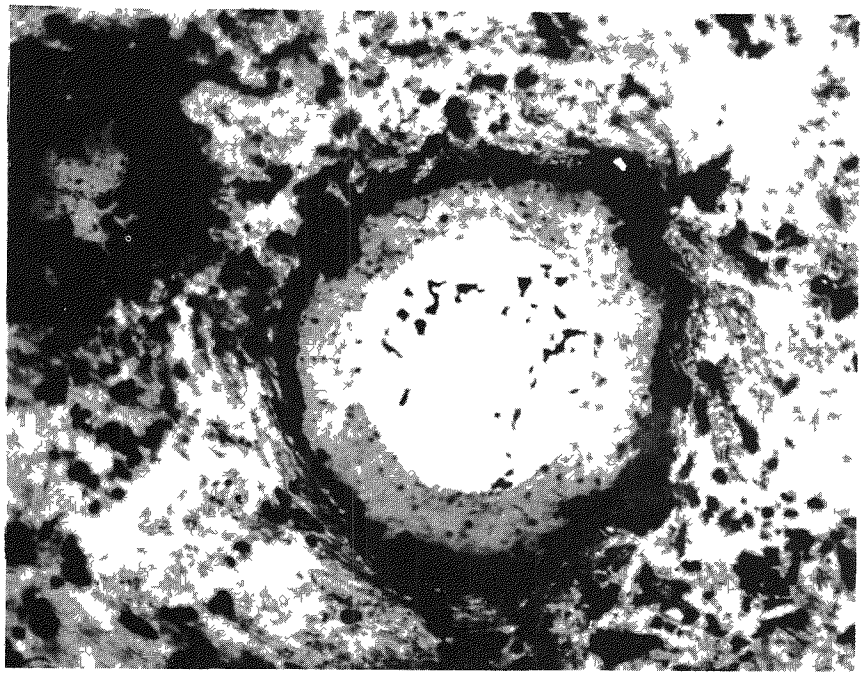

Fig. 4-21 Graphite-Al_2O_3 Specimen Type 3, after 500 hrs at 2500°F. View at center of specimen (250X).

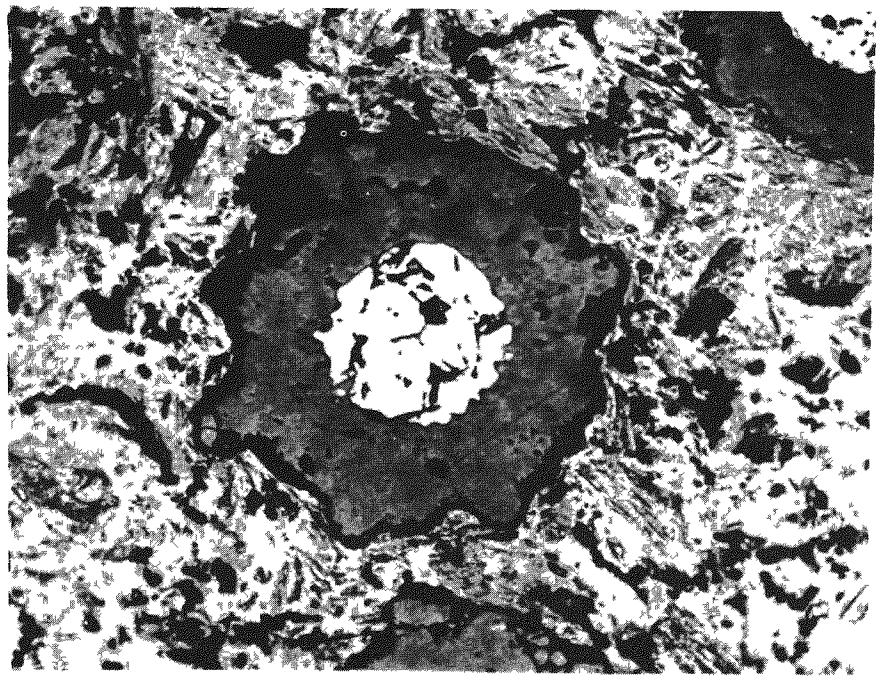

Fig. 4-22 Graphite-Al_2O_3 Specimen Type 3, after 1000 hrs at 2500°F. View at center of specimen (250X).

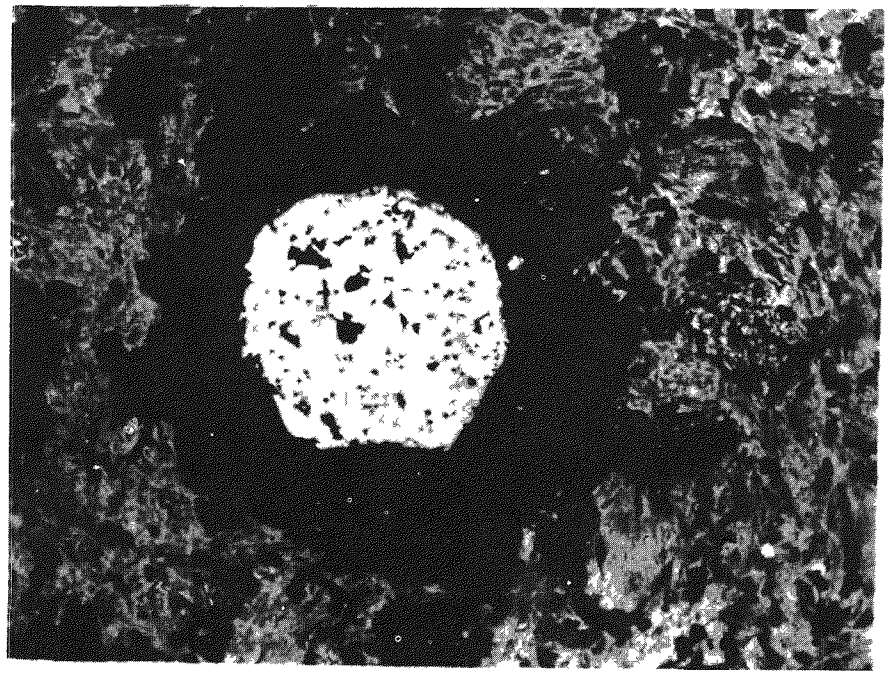

Fig. 4-23 Graphite-Al_2O_3 Specimen Type 3, after 1000 hrs at 2500°F. View near surface of specimen (250X).

No effect can be noted on the particle coatings in the as-fabricated condition except that some of the coatings in the Type 1 sample are cracked which undoubtedly influenced some of the results obtained for this type. After 168 hrs, several particles in Type 1 were attacked (see Figure 4-15); and there was essentially no attack to Type 2 (see Figure 4-17) and Type 3. After 500 hrs the coatings in Type 1 were completely destroyed; some thinning of the coatings in Type 2 was noted (see Figure 4-18); and some attack was beginning to occur to the Type 3 coatings (see Figure 4-21). Figure 4-19 is a view of the 500 hr. test on Type 2 except the particle shown was near the edge of the sample rather than at the center of the sample as in Figure 4-18. The coating is completely gone in Figure 4-19 which indicates a much greater reaction on particle coatings near the sample surface. The bright regions in the remaining fuel particle in Figure 4-19 are unidentified metallic appearing phases, possibly containing aluminum, which were also noted in the Type 1 fuel particle. After 1000 hrs, the particles in Type 1 were almost completely converted to a metallic phase; and the coatings in Type 2 were almost entirely destroyed, with greater attack being noted at the edge of the sample. Coatings near the center of Type 3 samples were generally intact although there was some deterioration of the alumina (see Figure 4-22). Near the surface of the sample, complete coating attack was again noted (see Figure 4-23). It is possible that the spurious deposits noted in the furnace tube were responsible for accelerating the attack on particle coatings near the surfaces of the graphite samples.

In these tests with vapor deposited Al_2O_3 the resin binder material (Type 1) again showed the greatest degree of attack. However, the initial crackings in the coatings of Type 1 and the thin coatings of both types 1 and 2 could have been factors in the more rapid deterioration of these coatings by early exposure of the UO_2 particles. Since there was some evidence of attack even in the thickest alumina coating in graphite having a coal tar pitch binder, the maximum safe temperature must be below 2500°F.

4.3.3 Evaluation of Fueled Spheres

Due to the small number of graphite spheres fueled with Al_2O_3 coated UO_2 (Type FA-22) which were procured primarily for irradiation testing, there has only been a limited amount of test data on these spheres, exclusive of the data on fission product retention which is described in Section 4.4.

A complete summary of all alpha assays performed on the surfaces of FA-22 specimens is given in Table 4-8. Each data point represents

TABLE 4-8

Surface Uranium Contamination of Graphite Spheres Fueled with Al_2O_3 Coated UO_2.

Specimen No.	Coated Particle Batch No.	Net α Count Rate, cpm	Equivalent Surface Uranium, mg.
FA-22(436N)	1B	12.6 ± 7.0	0.017
		2.8 ± 5.6	0.0037
		1.4 ± 5.6	0.0019
FA-22(437N)	1B	2.8 ± 5.6	0.0037
		nil	nil
		1.4 ± 5.6	0.0019
FA-22(448N)	2A	8.4 ± 6.3	0.011
		nil	nil
		16.8 ± 6.3	0.022
FA-22(449N)	2A	2.8 ± 5.6	0.0037
		7.0 ± 6.3	0.0092
		4.2 ± 5.6	0.0055
FA-22(39-9N)	1B	16.8 ± 6.3	0.022
		4.2 ± 5.6	0.0055
		7.0 ± 6.3	0.0092
FA-22(470E)	4E	16.8 ± 6.3	0.0046
		28.0 ± 7.7	0.0076
		221 ± 18.2	0.060
FA-22(471E)	4E	23.8 ± 7.0	0.0065
		12.6 ± 5.6	0.0034
		12.6 ± 5.6	0.0034
FA-22(472E)	4E	44.8 ± 9.8	0.012
		18.2 ± 7.0	0.0050
		16.8 ± 7.0	0.0046
FA-22(546E)	6H	49.0 ± 9.1	0.013
		11.2 ± 5.6	0.0030
		39.2 ± 7.0	0.011
		70.0 ± 10.5	0.019
FA-22(547E)	6H		0.0115
		1.12 ± 13	0.030
		64.4 ± 9.8	0.017
		70.0 ± 10.5	0.019
		30.8 ± 17.7	0.0084
FA-22(548E)	6H		0.0186
		22.4 ± 7.0	0.0061
		7.0 ± 4.9	0.0019
		5.6 ± 4.9	0.0015
		23.8 ± 7.0	0.0065
FA-22(549E)	6H	14.7 ± 5.9	0.0040
		33.6 ± 8.4	0.0091
		25.2 ± 7.0	0.0068
		75.6 ± 10.5	0.021
		199 ± 17	0.054
FA-22(550E)	6H		0.0227
		12.6 ± 5.6	0.0034
		22.4 ± 7.0	0.0061
		12.6 ± 5.6	0.0034
		14.0 ± 6.3	0.0038

a different portion of the sphere surface and the value shown has been normalized to the whole surface. Since each specimen is fueled with 4.75 gms of uranium, the fraction of exposed uranium on the surface of these specimens ranges from 3×10^{-7} to 1.3×10^{-5} as predicted by these alpha assays. A rather uniform pattern of uranium contamination can be seen over the surfaces of the specimens. The locally high reading obtained in a few cases was probably due to a collection of slightly damaged particles right at the surface.

Several impact and compression tests have been run on FA-22 specimens. The graphite used in the FA-22 specimens is similar to that used in the FA-1 specimens. A fully graphitized filler material is used in both specimens but the pitch binder is not graphitized due to the low bake temperature in order to avoid graphite reactions with the Al_2O_3 or the UO_2. The bake temperatures were 2560°F for the FA-1 type and 2300°F for the FA-22 type. Impact and compression data for these two types are summarized in Table 4-9.

TABLE 4-9

Impact and Compression Tests on FA-22 and FA-1 Specimens

Specimen Type	Compression Failure		Impact Failure
	Load, lbs.	Reflection, in	Load, ft-lbs
FA-22	4465	0.079	7.0
	4435	0.078	
FA-1	2410	0.0433	11.5
	2865	0.0508	11.5
			7.3

Both of these specimen types in Table 4-9 are fueled with same volume fraction of UO_2 but the FA-22 type has the added volume fraction of the Al_2O_3 coatings. From the test data, the presence of the Al_2O_3 is seen to have no deleterious effect on the strength of the graphite sphere. The significantly higher compressive strength of the FA-22 specimens was thought to be associated with its slightly lower bake temperature. However, the rupture modulus (load to deflection ratio) is the same for both types of material.

In order to determine the extent of damage to the Al_2O_3 coatings when the graphite spheres were broken, portions of several of the specimens were alpha assayed on their fractured surfaces. In addition, one specimen was subjected to repeated low level impact loads on one spot. The results are summarized in Table 4-10. The specimen fueled with the massive sintered Al_2O_3 coatings showed no significant increase in uranium contamination while there was evidence of some damage to the thinner vapor-deposited Al_2O_3 coatings.

TABLE 4-10

Alpha Assays of Fractured FA-22 Specimens

Sphere Condition	Al_2O_3 Coating Thickness, μ	Net Alpha Count Rate on Fractured Surface, cpm[a]
1. After Compressive Failure	250	4.2 ± 3.5
		1.4 ± 2.8
		8.4 ± 4.9
2. 100 impacts of 3 in-lbs.	48 [b]	11.2 ± 2.8 (before)
		166 ± 6 (after)
3. After Impact Failure	48 [b]	202 ± 18
		411 ± 25
		488 ± 27

(a) Normalized to surface area of 1 1/2" sphere.
(b) On enriched UO_2 particles.

4.4 Fission Product Retention

Al_2O_3 coated UO_2 particles have been subjected to all three of the standard fission product retention tests, namely neutron activation, furnace capsule irradiation, and sweep capsule irradiation. Test specimens have included both coated particles and 1-1/2" graphite spheres fueled with coated particles.

4.4.1 Neutron Activation Tests

Table 4-11 summarizes the results of neutron activation tests on Al_2O_3 coated UO_2. Although the specimens have some variation in coating, very low amounts of Xe 133 were released during the test periods. A comparison of these release fractions with surface uranium contamination estimated from alpha assays in Table 4-5 indicates the Xe 133 was most likely released from this external contamination and that no conclusion can be drawn about fission product diffusion through the coatings because these amounts are about equal or less than the exposed uranium content.

4.4.2 Furnace Capsule Tests

Furnace Capsule SPF-3 contained specimen FA-22(449N) fueled with Al_2O_3 coated UO_2 from batch 2A. One of the objectives of this experiment was to determine whether there was any significant increase in fission product leakage through the Al_2O_3 coatings as the specimen temperature was raised to 1900°F, the maximum capability of this type of capsule.

The leakage factors obtained from this specimen during the course of the experiment are listed in Table 4-12. The capsule was operated during March 1960 at 1000°F and 1500°F using the gas train which is normally used for Sweep Capsule experiments. However, with the startup of Sweep Capsule SP-5, operation of Furnace Capsule SPF-3 was suspended until August while a separate gas train was constructed. Data was taken over the range of 280°F to 1900°F, with repeat samples being taken at several temperatures. These repeat samples, taken within a 2-week period, showed excellent reproducibility. However, it is not known why the earliest samples taken at 1000°F and 1500°F (Samples 1 and 2) are approximately one order of magnitude lower than the later samples. Shortly after the 1900°F sample (No. 13), a failure in the inner container caused a loss of vaccum in the outer jacket. This caused a drop in specimen temperature to about 1000°F at the same heat input. With maximum heat input, a specimen temperature of 1800°F was achieved for the last two samples.

TABLE 4-11

Neutron Activation Tests on Al_2O_3 Coated UO_2

Specimen	Test Temp, °F	Time, Min.	Fractional Release of Xe 133
1. Batch 1B	1850	100	$<1.7 \times 10^{-4}$
	2250	75	1.7×10^{-4}
	2400	135	1.6×10^{-4}
2. FA-22(437N) fueled with Batch 1B	1650	80	$<8.1 \times 10^{-6}$
	1800	50	1.6×10^{-5}
	2200	60	4.9×10^{-5}
	2350	30	2.6×10^{-4}
3. Batch 2A	1500	144	1.3×10^{-6}
	1500	60	$<3.7 \times 10^{-5}$
	2000	50	$<3.7 \times 10^{-5}$
4. FA-22(449N) fueled with Batch 2A	1500	270	7.5×10^{-6}
	1900	60	$<9.4 \times 10^{-6}$
	1900[a]	60	$<9.4 \times 10^{-6}$
	1900[a]	135	$<9.4 \times 10^{-6}$
5. FA-22(471E) fueled with Batch 4E	1950	240	7.7×10^{-6}
6. FA-22(548E) fueled with Batch 6H	2000	240	6.3×10^{-7}

TABLE 4-12

Summary of Fission Product Release Data from Specimen FA-22 (449N)

In Furnace Capsule SPF-3

Sample No.	Date	Temp. °F	R/B (Release Rate/Production Rate) Kr 85	Kr 87	Kr 88	Xe 133	Xe 135
1	3/17	1000	5.6(-7)[a]	4.2(-7)	2.6(-7)	1.2(-6)	1.7(-7)
2	3/18	1500	2.0(-6)	1.0(-6)	3.2(-7)	5.8(-6)	1.7(-6)
3	8/3	290	1.1(-6)	<2.0(-7)	2.0(-7)	7.8(-6)	3.8(-7)
4	8/8	280	<8.0(-7)	<2.0(-7)	<2.0(-7)	<4.8(-6)	1.9(-7)
5	8/12	460	3.6(-6)	8.2(-7)	1.8(-6)	2.0(-5)	1.5(-6)
6	8/18	560	1.9(-6)	1.3(-6)	6.8(-7)	6.4(-6)	1.9(-6)
7	8/26	1020	6.2(-6)	1.7(-6)	2.1(-6)	1.8(-5)	4.5(-6)
8	8/31	1120	5.2(-6)	1.7(-6)	2.2(-6)	1.4(-5)	3.6(-6)
9	9/14	1100	2.3(-6)	4.7(-7)	9.2(-7)	4.2(-6)	1.1(-6)
10	9/23	1480	1.6(-5)	3.5(-6)	6.8(-6)	3.7(-5)	6.2(-6)
11	9/27	1510	1.4(-5)	3.4(-6)	5.3(-6)	3.8(-5)	9.5(-6)
12	9/30	1500	1.4(-5)	2.9(-6)	6.2(-6)	3.7(-5)	1.0(-5)
13	10/6	1895	4.6(-6)	9.2(-7)	1.7(-6)	9.0(-6)	2.7(-6)
14	10/12	1035	1.7(-7)	<2.0(-7)	<2.0(-7)	1.4(-6)	2.6(-7)
15	10/27	1800	5.2(-5)	1.6(-5)	2.2(-5)	2.8(-4)	5.6(-5)
16	10/28	1790	1.8(-5)	3.6(-6)	1.1(-5)	9.5(-5)	1.1(-5)

(a) Numbers in parentheses denote power of 10.

The leakage factors for 2 of the 5 fission products measured in this experiment (Kr 87, Xe 133) are plotted in Figure 4-24 as a function of specimen temperature. The leakage factors for the other three fission products (Kr 85m, Kr 88, Xe 135) follow the same trend with temperature and have been omitted from Figure 4-24 for clarity. Also, data from samples 1, 2, 13, and 14 have been omitted. As can be noted, increasing the specimen temperature from about 300°F up to about 1100°F causes essentially no increase in fission product leakage. An increase in specimen temperature from 1100°F to about 1800°F then causes about a 1 order of magnitude increase in leakage. It is most probable that the greatest contribution to the fission product release from this specimen is due to exposed uranium contamination and that increasing the specimen temperature has merely affected the fission products escaping from this exposed uranium through the graphite matrix. Although the total irradiation time for this specimen was of the order of 100 days, radiation damage effects are believed to be insignificant due to the use of normal enrichment uranium and a thermal flux of only 3×10^{11} nv.

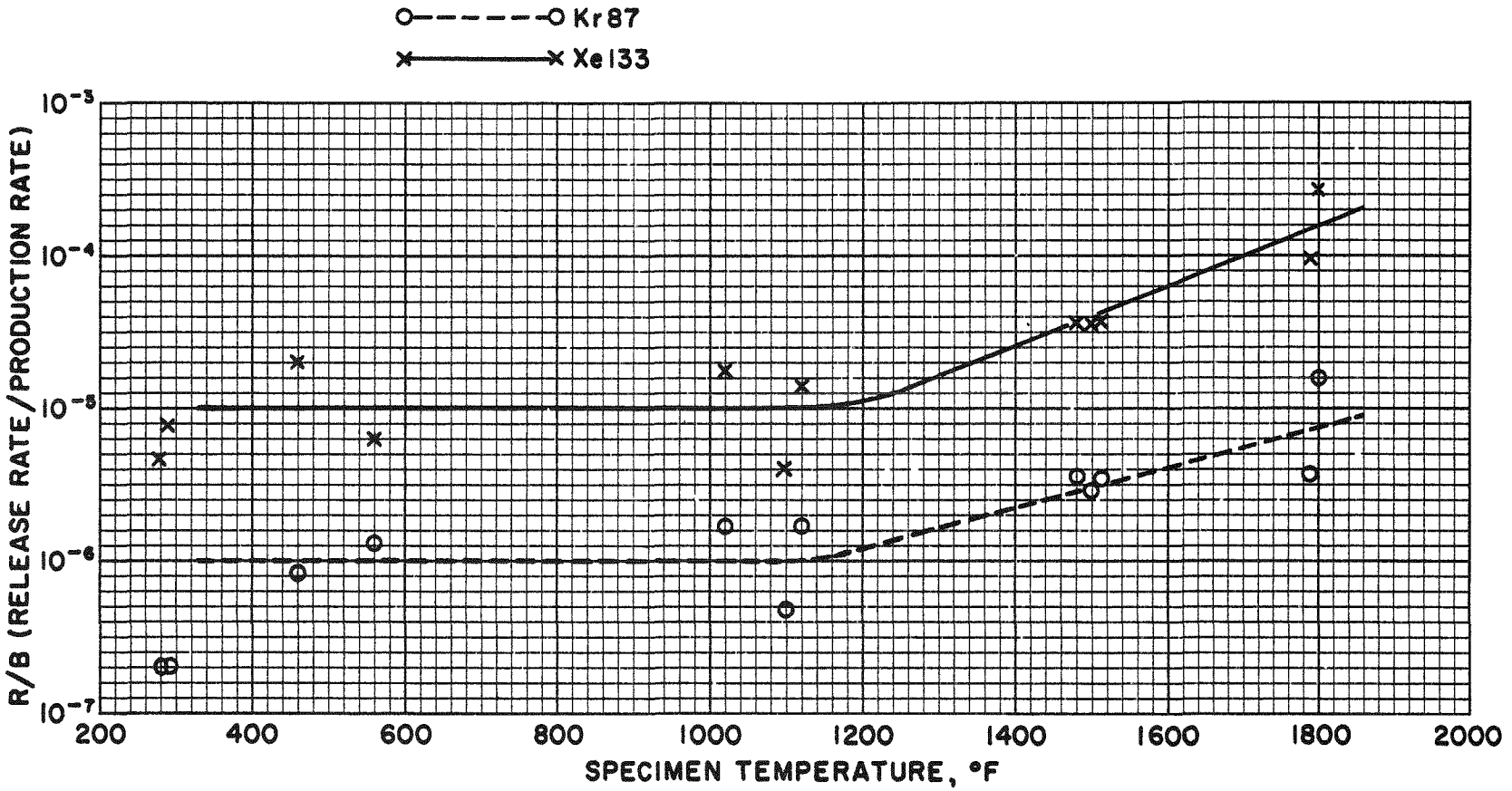

TYPICAL FISSION PRODUCT RELEASE DATA
FOR SPECIMEN FA-22(449N)
IN FURNACE CAPSULE SPF-3

FIG. 4-24

4.4.3 Sweep Capsule Tests

Specimen FA-22(471E) fueled with Al_2O_3 coated UO_2 from batch 4E was encapsulated in the sweep compartment of Sweep Capsule SP-5 in order to determine the effect of irradiation on fission product retention by the Al_2O_3 coatings. An additional FA-22 specimen was included in the static compartment of Capsule SP-5. The design and operating conditions of Capsule SP-5 are described in Section 8.2. Briefly, specimen FA-22(471E) operated at nominal conditions of 1.5 KW, a surface temperature of 1350°F and a central temperature of 1550°F. Capsule SP-5 was under irradiation from April to October, 1960, the end of Phase II. The estimated burnup in specimen FA-22(471E) based on the thermal data is 6 a/o U235.

During the course of the irradiation, 22 samples of the off-gas stream were analyzed for long-lived gaseous fission products and 2 samples were taken using a special non-volatiles trap to measure the leakage factors for short-lived gaseous fission products and other isotopes such as iodine and cesium.

The leakage factors for the long-lived fission product gases are listed in Table 4-13. This data is plotted in Fig. 4-25 which also includes a plot of the temperature history for this specimen. No data was taken during the period between samples 9 and 10 while certain revisions were made to the gas train. Although there was no helium flow over the specimen during this period, it remained under full power irradiation. Samples 11 and 12 were taken on the same day to check reproducibility of the sampling and analysis procedure. Good agreement was found between these two samples. Although there were several perturbations in the trends of the leakage factors, some of which appear to be associated with specimen temperature variations, some special tests were made to determine whether the 2 order of magnitude dip in sample 15 (i.e. at 111 days) was in any way attributable to the sampling procedure. The sample trap used for #15 was used again for sample #16 but with the addition of a backup trap. For sample #16, less than 1% of the total activity was found in the backup trap indicating that the first sampling trap was in good condition. Thus, it was concluded that the charcoal may have been contaminated with air or moisture when sample 15 was taken resulting in little or no fission product adsorption. It was estimated that if the activity present in sample 15 was present only in the gas spaces in the charcoal bed, the calculated leakage factors would have been of the same order as those reported for sample 16.

TABLE 4-13

Summary of Long-Lived Gaseous Fission Product Release from Specimen FA-22(471E) in Capsule SP-5

Sample No.	Days of Irradiation	R/B (Rate of Release/Rate of Production)				
		Kr 85m	Kr 87	Kr 88	Xe 133	Xe 135
1	5	1.6(-8)(c)	(a)	2.2(-9)	1.8(-7)	1.9(-8)
2	9	5.9(-8)	1.8(-8)	2.7(-8)	1.0(-7)	4.0(-8)
3	19	4.7(-7)	1.8(-7)	2.9(-7)	1.9(-6)	4.9(-7)
4	23	7.3(-6)	(b)	(b)	5.8(-6)	2.1(-6)
5	24	2.6(-8)	(a)	1.6(-8)	1.3(-7)	8.2(-9)
6	27	7.0(-9)	(a)	7.1(-9)	4.8(-8)	4.2(-9)
7	28	3.1(-9)	(a)	4.7(-9)	4.0(-8)	1.6(-9)
8	32	1.8(-8)	(a)	7.7(-9)	9.1(-7)	1.2(-8)
9	38	7.6(-9)	(a)	1.9(-9)	5.0(-8)	4.0(-9)
10	72	4.0(-6)	1.6(-7)	(a)	2.8(-4)	7.8(-7)
11	83	5.9(-6)	1.3(-7)	(a)	8.0(-4)	7.9(-7)
12	83	2.1(-6)	2.0(-7)	6.2(-7)	2.1(-4)	5.3(-7)
13	91	6.1(-6)	2.9(-7)	1.0(-6)	1.2(-3)	1.5(-6)
14	102	1.2(-5)	1.1(-6)	3.2(-6)	1.1(-3)	4.2(-6)
15	111	1.2(-7)	3.7(-8)	(a)	2.6(-5)	2.0(-7)
16	122	4.7(-4)	(a)	(a)	4.1(-3)	1.4(-4)
17	132	2.5(-4)	7.6(-6)	4.8(-5)	4.7(-3)	1.4(-4)
18	134	4.8(-4)	3.3(-5)	1.4(-4)	8.1(-3)	2.4(-4)
19	137	2.5(-4)	1.9(-5)	7.4(-5)	1.7(-2)	1.9(-4)
20	143	4.6(-4)	2.7(-5)	1.1(-4)	9.7(-3)	2.3(-4)
21	148	3.0(-5)	5.9(-6)	1.2(-5)	6.9(-4)	2.2(-5)
22	149	3.7(-5)	6.3(-6)	1.6(-5)	1.5(-4)	1.8(-5)

(a) Below sensitivity
(b) Decayed out prior to analysis
(c) Numbers in parentheses denote power of 10

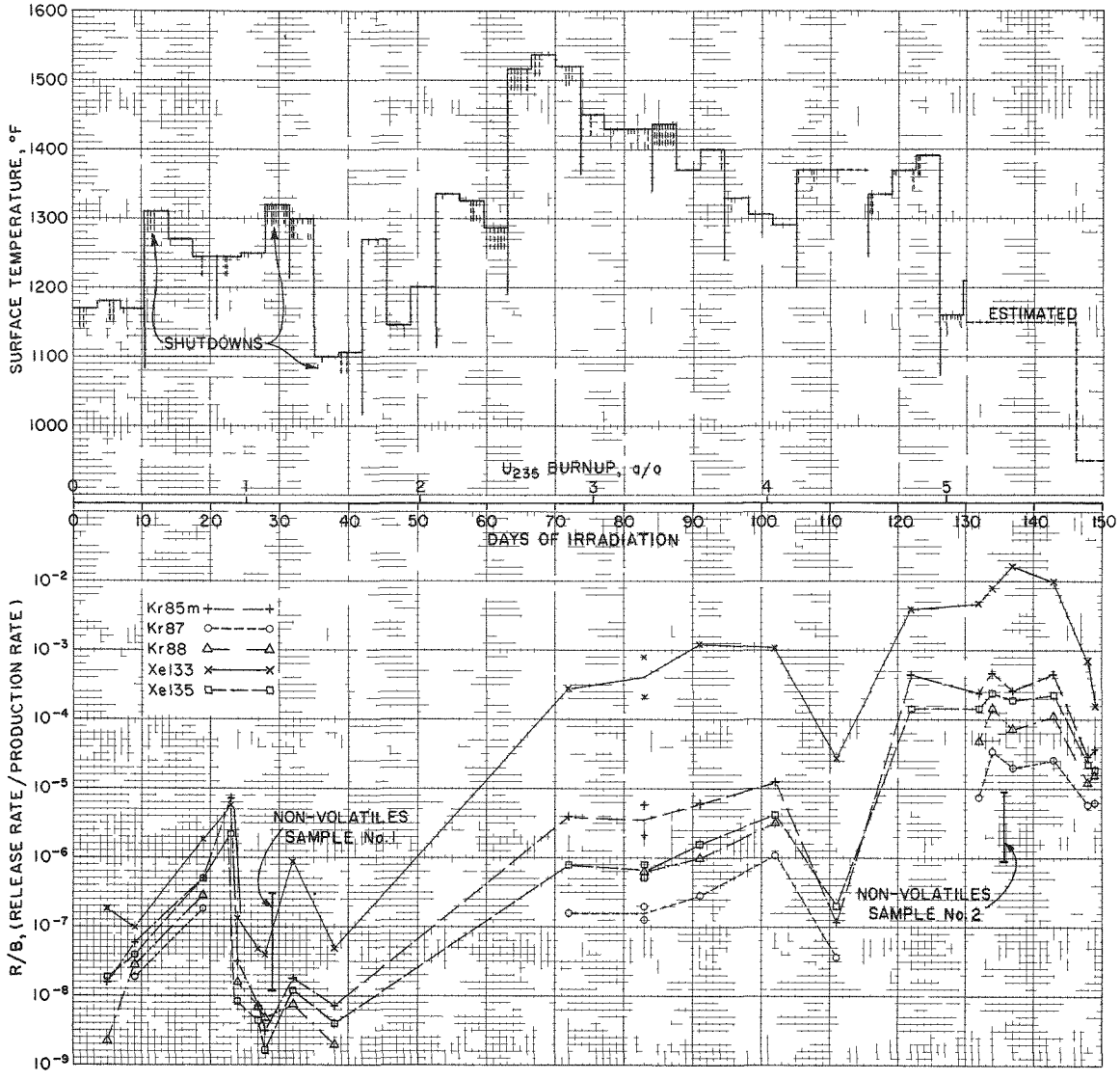

PERFORMANCE OF SPECIMEN FA-22(471E) IN SWEEP CAPSULE SP-5

FIG 4-25

The two non-volatile trap samples were taken at approximately 1 a/o and 5 a/o burnup. These traps are located in the BRR pool near Capsule SP-5 so that the transit time from the capsule to the trap is only 2 sec. A description of the non-volatiles trap is given in Section 8.2. In normal capsule operation, the helium stream bypasses the non-volatiles trap. When a sample is taken, the helium stream is diverted through the trap for a 48 hr period with a residence time of 90 sec. During this time isotopes which are non-volatile at the pool water temperature are deposited in the trap. Species of interest include strontium, barium, and cerium which are daughter products of certain short lived gaseous products, and iodine, tellurium, and cesium which could themselves diffuse out of the fuel element.

Since the trap consists of a number of stainless steel mesh pads in series, the pattern of fission product deposition as a function of residence time (i.e. trap length) can be measured. Conventional radiochemical techniques are used to separate, identify, and assay the individual isotopes. A check of the trap walls showed that more than 98% of the Sr 89, Ba 140 and Ce 141 activity was in the stainless steel mesh pads so that wall effects were neglected in reporting the data.

Typical results obtained from this type of experiment are shown in Fig. 4-26 (Sr 89, Ba 140, Ce 141) and Fig. 4-27 (I 131, I 133) which are the data from non-volatiles trap sample #1. If it is assumed that non-volatile daughter products deposit on the stainless steel mesh immediately upon the decay of its volatile parent isotope, then the concentration of the non-volatile daughter product through the trap should be a function of the half-life of the gaseous precursor. These predicted deposition curves are also shown in Figure 4-26. As can be noted, there is excellent agreement between the theoretical curves and the actual data points. Essentially all of the Ba 140 and Ce 141 was deposited in the trap. Only about 30% of the Sr 89 was deposited in the trap with the remainder passing out of the trap as undecayed Kr 89. There is practically no decay of the I 131 and I 133 during their passage through the trap. The assumption of a constant removal efficiency per inch of trap would explain the exponential nature of the iodine curves seen in Figure 4-27. Essentially all of the iodines are removed by the trap.

Somewhat similar results were obtained for non-volatiles trap sample #2. During a portion of the sampling period for Trap #2, the flow rate was inadvertently lowered (i.e. gas transit time increased) so that the data for Sr 89, Ba 140, and Ce 141 would consequently be expected to fall on curved lines rather than straight lines as in Fig. 4-26. This was

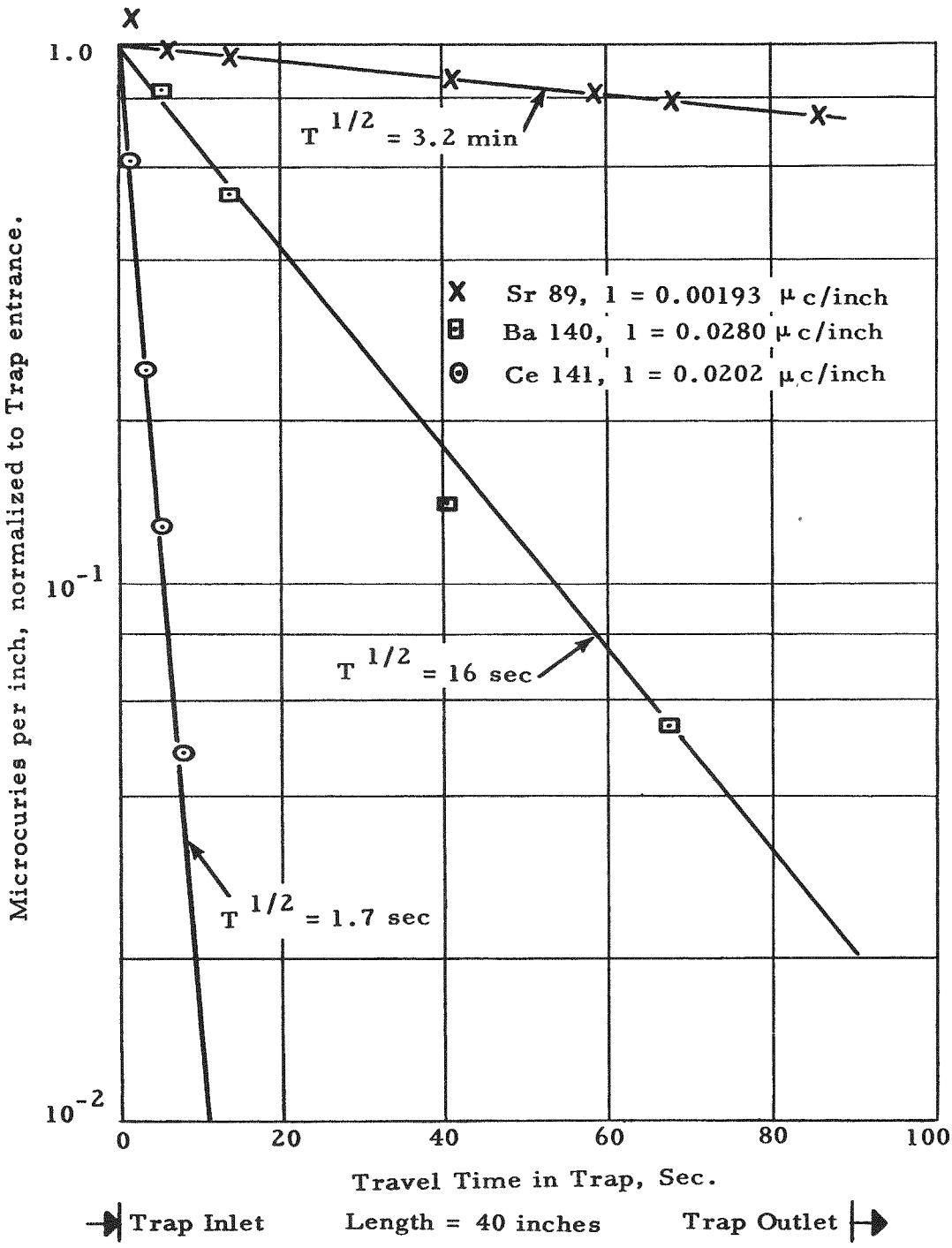

Fig. 4-26 Distribution of Sr 89, Ba 140, and Ce 141 in Non-Volatiles Trap for Specimen FA-22(471E).

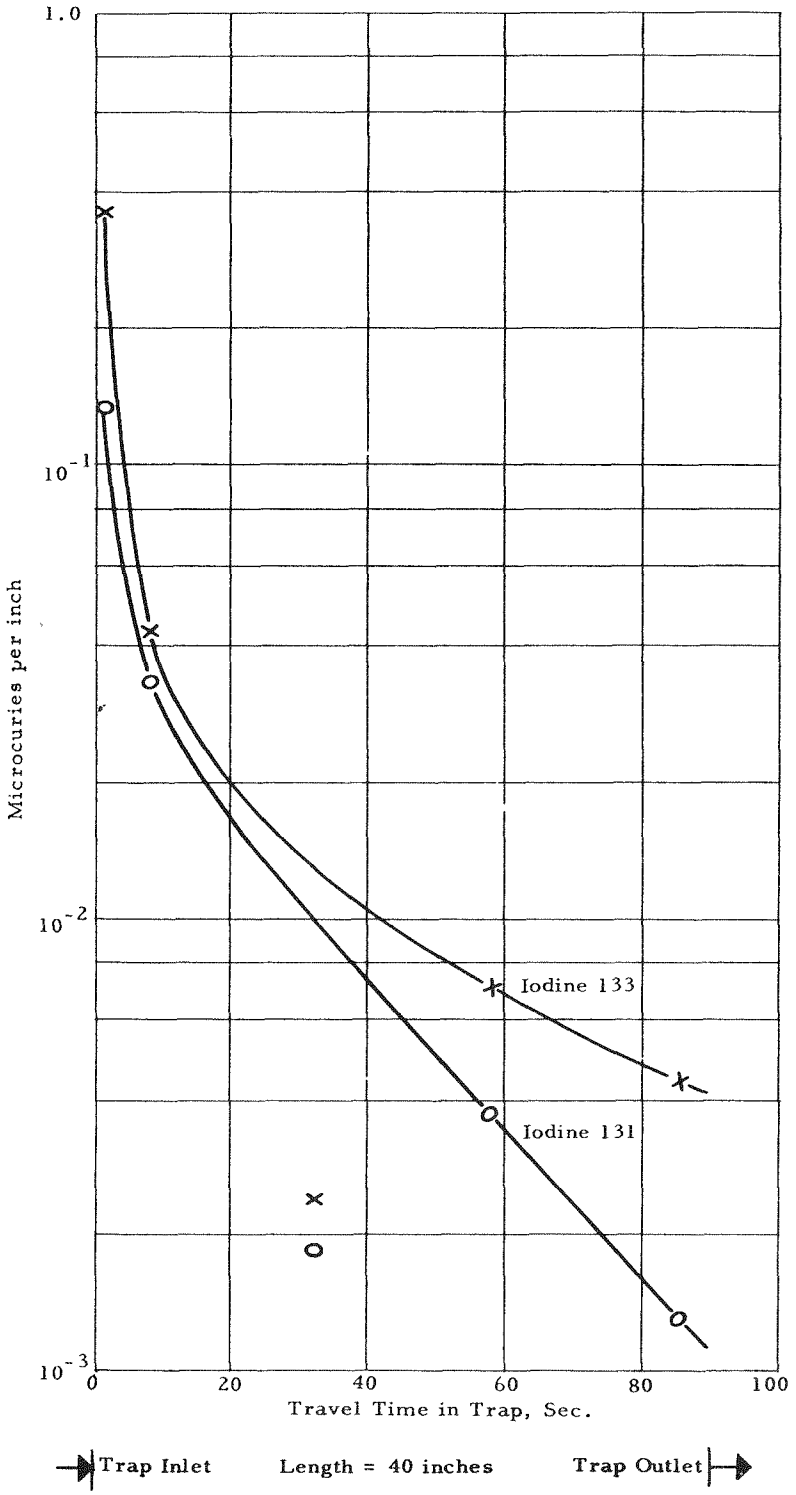

Fig. 4-27. Distribution of I 131 and I 133 in Non-Volatiles Trap for Specimen FA-22(471E)

found to be the case. However, the activity distributions for I 131 and I 133 were both found to be maximum at the trap inlet and outlet and minimum in the center of the trap. The cause for this type of distribution is not known.

The leakage factors for these various isotopes are based on the non-volatiles trap data and are summarized in Table 4-14 and also superimposed on Fig. 4-25. In addition to the isotopes plotted in Figs. 4-26 and 4-27, Cs 137, Te 132, and Y 91 were also found. The Cs 137 was detected in Trap #1 in such a small amount that leakage factors could not be calculated. However, the Cs 137 activity was sufficiently high in Trap #2 that its distribution plot was found to coincide with the predicted distribution based on Xe 137 diffusion from the specimen. This implies that cesium isotopes which have a boiling point of 1240°F probably did not diffuse from the fuel element and that the Cs 137 found in the trap came from Xe 137 which diffused from the fuel element and decayed in the trap. The slight traces of Te 132 found in each trap indicate that there may have been some diffusion of tellurium which is molten at the specimen operating temperature.

TABLE 4 -14

Summary of Non-Volatile Trap Data for Specimen FA-22(471E) in Capsule SP-5

Trapped Species		Principal Gaseous Precursor			
				Leakage Factors (a)	
Isotope	Half-Life	Isotope	Half-Life	Trap #1	Trap #2
Sr 89	54d	Kr 89	3.2m	3.0×10^{-7}	8.9×10^{-6}
Y 91	64.4h	Kr 91	9.8s	(e)	4.0×10^{-6}
Ba 140	12.8d	Xe 140	16s	1.0×10^{-7}	9.2×10^{-7}
Ce 141	32d	Xe 141	1.7s	1.3×10^{-7}	1.4×10^{-6}
Cs 137	25.6y	Xe 137	3.9m	(b)	7.1×10^{-6}
I 131	8.05d			1.2×10^{-8}(c)	(d)
I 133	20.8d			1.4×10^{-8}(c)	(d)
Te 132	77h			(b)	(b)

(a) Release rate/production rate; Trap #1 at 1 a/o burnup, Trap #2 at 5 a/o burnup.
(b) Activity level only high enough to permit qualitative identification.
(c) Leakage factor for the trapped iodine isotope.
(d) Due to peculiar distribution within the trap, the release rate for this isotope could not be calculated.
(e) Chemical analysis for Y was not performed for Trap #1.

4.4.4 Analysis of the Data

The term R/B (i.e. the ratio of release rate to the production rate) is used because it is a convenient way of expressing the fission product leakage data. The experimentally determined release rates are simply divided by an equilibrium production rate which is based on the estimated flux, uranium loading in the specimen, and the fission yield. Also, the R/B term can be used directly to compute the reduction in equilibrium primary loop activity when comparing coated fuel element performance with that for uncoated fuel. However, if fission products are released by a diffusion mechanism, the actual isotope concentration (rather than production rate) at the time of sampling determines the release rate. Fortunately, most of the isotopes of interest reach an equilibrium concentration level within 24 hours after startup which is the minimum time period before samples are taken. The one exception is Xe 133 which requires nearly 30 days to reach equilibrium concentration.

A mathematical model has been devised by S.D. Beck of BMI to approximate fission product diffusion from a coated fuel particle. This model is based on the assumption that equilibrium conditions have been achieved, that fission products are generated uniformly in fuel particles only, and that the diffusion coefficients are equal for both the fuel particle material and the coating material. The relationship is:

$$\frac{R}{B} = \frac{3(a/b)^3}{a\sqrt{\lambda/D}\,\sinh a\sqrt{\lambda/D}}\left[b\sqrt{\lambda/D}\,\cosh b\sqrt{\lambda/D} - \sinh b\sqrt{\lambda/D}\right]$$

where:

- R = rate of release, atoms/sec
- B = rate of production, atoms/sec
- a = outer radius of coating, cm
- b = inner radius of coating, cm
- λ = decay constant, sec^{-1}
- D = diffusion coefficient, cm^2/sec

This relationship has been used to construct a graph of R/B as a function of half life with D as a parameter for use in analyzing the data

from the FA-22(471E) in Capsule SP-5 as shown in Figure 4-28. Although the assumptions used to derive this relationship are over simplified, the diffusion model does show the very strong effect of isotope decay constant on fission product leakage. When a volatile isotope is diffusing through the coating and it decays into a non-volatile isotope, it is assumed that no further diffusion occurs. Thus, very low leakage rates would be expected for short-lived isotopes.

The leakage data at 1 a/o and 5 a/o burnup are plotted on Figure 4-28. At 1 a/o burnup, the leakage factors for all isotopes are approximately equal in the range of 10^{-6} to 10^{-8} and there is no tendency for the data to fall along lines of constant diffusion coefficients. This indicates that the "leakage" from the specimen most probably arises from uranium contamination external to the fuel particle coatings. There was no significant leakage through the coatings. The leakage factors are of the same order as found in the low level irradiation test of another FA-22 specimen in Capsule SPF-3 (see Figure 4-24). However, at 5 a/o, the leakage factors for the longer-lived isotopes do tend to approximate the lines of constant diffusion coefficient implying a measurable diffusion through the coatings. The leakage factors for the short-lived isotopes at 5 a/o burnup show only a slight half-life dependency and are about an order of magnitude higher than the corresponding 1 a/o data. This could mean that a portion of the coatings have cracked, exposing bare fuel.

As can be noted in Figure 4-25, certain of the perturbations in the R/B curve can be associated with temperature variations in the specimen, most noticeably the 1 to 2 order of magnitude decrease of leakage factor for the last two samples corresponding to a temperature drop of about 1150°F to 950°F. This indicates a strong temperature dependency for the highly irradiated coatings in distinction to the small temperature dependency at low burnups noted in Capsule SPF-3. The perturbations during the early part of the irradiation do not entirely correspond to temperature changes and it is not clear whether other factors in the test procedure were responsible for these variations.

Based on this data, it is deduced that up to about 1.5 a/o the leakage was due to uranium contamination, that somewhere between 1.5 a/o and 3 a/o radiation damage to the coated particles began to be significant, and that at the end of the irradiation the permeability of a majority of the particle coatings had increased and, in addition some of the coatings had cracked. It is expected that hot cell examination of this specimen will further clarify this point.

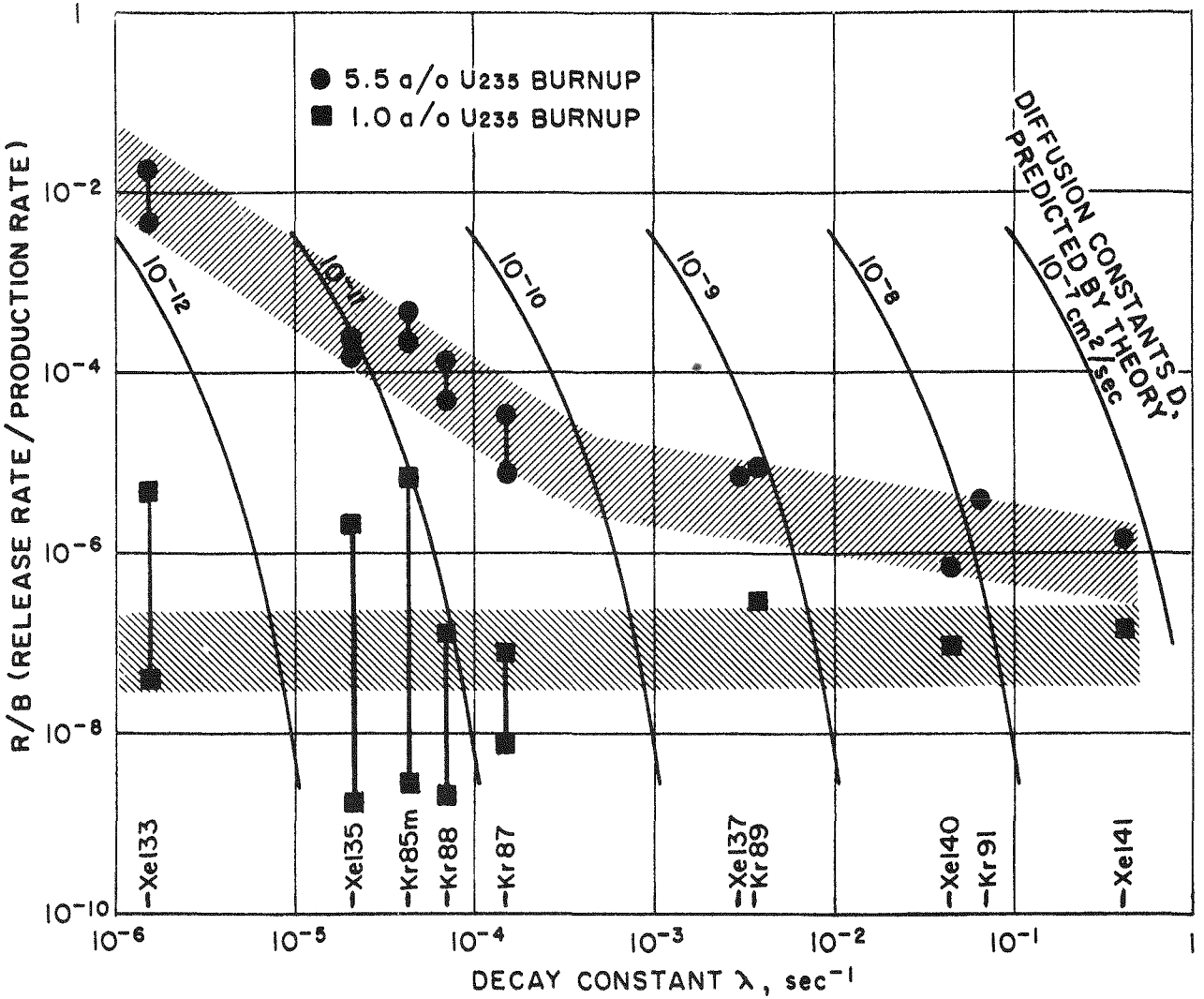

COMPARISON OF DATA FOR SPECIMEN FA-22(471E)
IN SWEEP CAPSULE SP-5
WITH THEORETICAL PREDICTIONS

FIG. 4-28

It will be desirable to extend the useful life of Al_2O_3 coated UO_2 particles as a "clean" fuel element system beyond the 1.5 a/o burnup level found in the capsule SP-5 irradiation. There are several possibilities which warrant further investigation. These include the use of a porous inner layer (such as the batch 8G material) to minimize fission gas pressure buildup and a fundamental study of neutron damage to the molecularly deposited Al_2O_3 material to determine whether other process conditions or the use of coating additives will minimize radiation induced porosity.

5.0 Pyrolytic Carbon Coated Fuel Particles

Interest in pyrolytic carbon coated fuel particles stems from previous experience with pyrolytic carbon coatings on the surface of fuel elements. Advantages of pyrolytic carbon as a particle coating material are that it removes the temperature limitation imposed by the chemical reaction between metal oxide particles coatings and the graphite matrix and that the pyrolytic carbon coating material does not effectively displace moderating material when dispersed in graphite.

During Phase II, an exploratory program on pyrolytic carbon coated UC_2 particles was conducted at the Battelle Memorial Institute. Also, several types of these particles were procured from commercial sources for evaluation.

5.1 Fabrication

Pyrolytic carbon is formed by the pyrolysis of a hydrocarbon gas which causes a layer of carbon to build up on the surface to be coated. A fluid bed process was used at Battelle to coat UC_2 particles. The basic apparatus consisted of a 1" diameter by 24" long reaction tube, located inside an electrical resistance furnace. A helium stream containing either acetylene or methane was used to fluidize the bed. An enlarged disentrainment section was located above the reaction tube. For the 1800°F runs, a quartz reaction tube was used and a thermocouple well was located inside the reaction tube. For the 2400°F runs, a Mullite reaction tube was used with an external thermocouple.

A summary of the process conditions for the particles fabricated at Battelle is given in Table 5-1. UC_2 particles for batches PyC-1 and PyC-2 were obtained from the Carborundum Co. and were crushed and sieved from UC_2 pellets. The spherical UC_2 shot used in batches PyC-5 and PyC-6 was obtained from the Minnesota Mining & Mfg. Co.

TABLE 5-1

Pyrolytic Carbon Coated Fuel Particles Prepared At Battelle

Batch No.	UC_2 Shape	UC_2 Size, μ	Gas	Temp, °F	Coating Thickness, μ	w/o U
PyC-1	Irreg.	177/250	CH_4	2060	7	
			C_2H_2	1870	21	
			C_2H_2	1990	12(a)	70.6
PyC-2	Irreg.	177/250	C_2H_2	1860	17	84.4
PyC-5	Spher.	150/250	C_2H_2	2450	160	22.9
PyC-6	Spher.	150/250	C_2H_2	2450	80	53.8

(a) Final coating thickness was 40 μ.

Photomicrographs of particles from batches PyC-1 and PyC-2 are shown in Figs. 5-1 and 5-2. As seen in both figures, all particles have been rather uniformly coated with a continuous carbon phase in spite of the irregular shapes of the UC_2. One particle from batch PyC-1 in Fig. 5-1 has a crack at one end through the inner two coating layers but the outer layer is continuous over the crack. The interface between the second and third coating layers can be readily detected which indicates that successive layers of pyrolytic carbon are not as well bonded as in the case of Al_2O_3.

The thickness of pyrolytic carbon applied in a single run at about 1900°F (Batches PyC-1 and PyC-2) was limited by carbon soot formation which tended to plug the discharge lines from the reaction vessel. Several attempts were made to eliminate this problem by introducing CO_2 to react with the excess carbon but no significant effect was found.

Batch PyC-5 was prepared with the objectives of determining whether the higher deposition temperature would resolve both the soot problem and the thermal cycle fracture problem, and also to utilize spherically-shaped UC_2 particles. The UC_2 shot used in batches PyC-5 and PyC-6 was procured from the Minnesota Mining and Manufacturing Co.

When batch PyC-5 was fabricated, the coating process was found to proceed at a very rapid rate. The entire 160 micron coating was deposited in only two hours. The absence of soot formation at the higher deposition temperature permitted this thick coating to be deposited in one step. A photomicrograph of particles from batch PyC-5 is shown in Figure 5-3.

Fig. 5-1. Batch PyC-1 showing pyrolytically deposited carbon coatings on UC_2 particles (100X)

Fig. 5-2. Batch PyC-2 showing pyrolytically deposited carbon coatings on UC_2 particles (100X)

The spherical UC_2 particles are seen to be uniformly coated. However, an increasing amount of annular porosity can be noted with increasing radius producing an "onion-skin" effect. The individual layers of pyrolytic carbon appear to be continuous. The layer formation is believed to be due to either recycle of particles between hot and cold zones in the reaction vessel or the differences in thermal contraction rates in the normal and tangential directions in the pyrolytic carbon.

The next run was made with the same materials at the same conditions but the run was stopped when only half of the previous coating thickness (i.e. 80 microns) was deposited. A photomicrograph of particles from batch PyC-6 is seen in Figure 5-4. As can be noted there is no gross porosity in the coatings on this batch. The coatings are somewhat similar to the inner half of the coatings on batch PyC-5 in Figure 5-3. The dark band between the coating and UC_2 particles is a void region formed by the greater contraction of the UC_2 particle in cooling down from the deposition temperature. In general, the uniformly dense and impermeable appearance of these coatings was most encouraging.

Two additional types of pyrolytic carbon coated UC_2 were obtained from commercial sources during Phase II. Batch PyC-7 made by Minnesota Mining & Mfg. Co. is shown in Fig. 5-5 and Batch PyC-8 made by High Temperature Materials, Inc. is shown in Fig. 5-6. Both of these batches utilized 177/250 micron spherical UC_2 shot supplied by the Minnesota Mining & Mfg. Co. and were coated with 80 microns of pyrolytic carbon. Batch PyC-7 was treated at a maximum temperature of 3600°F. Some evidence of a layer structure in the coating can be noted. The characteristic conical structure of high temperature pyrolytic graphite can be seen in Fig. 5-6. The coating for this batch was deposited at 3600°F. Evaluation of these two batches will be performed in Phase III.

Several advantages are presently believed to be significant for these higher temperature pyrolytic carbon coatings. First, a higher operating temperature can be used because the higher expansion coefficient of the UC_2 will not rupture the coating when heated up to its deposition temperature. Coating densities closely approaching theoretical carbon density are achieved at deposition temperatures of 3600°F and higher. Also, high temperature pyrolytic graphite is known to have greater strength which could mean less damage during fuel element fabrication.

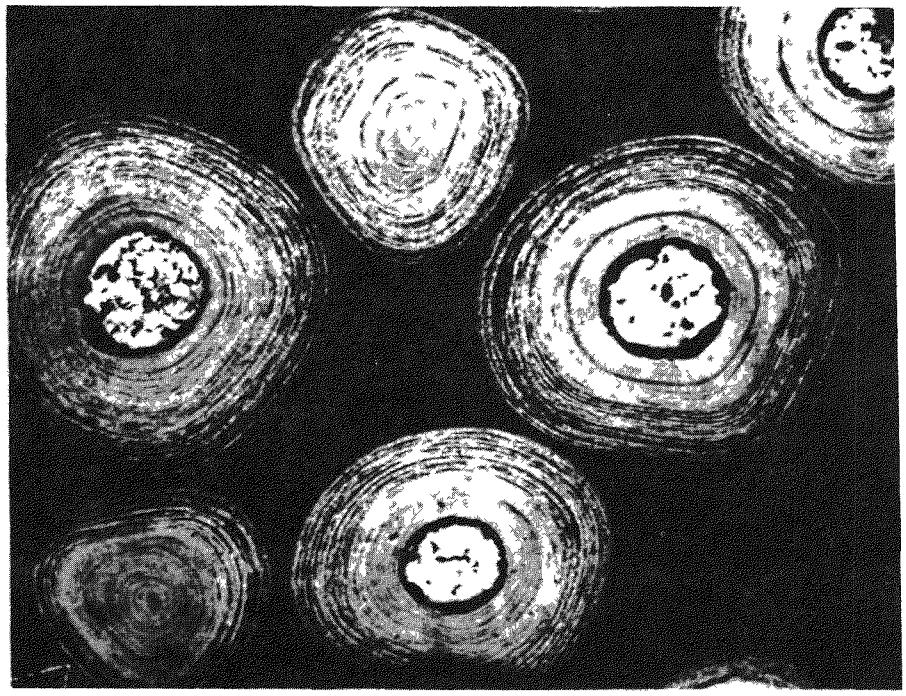

Fig. 5-3. Batch PyC-5 showing pyrolytically deposited carbon coatings on UC_2 (80X)

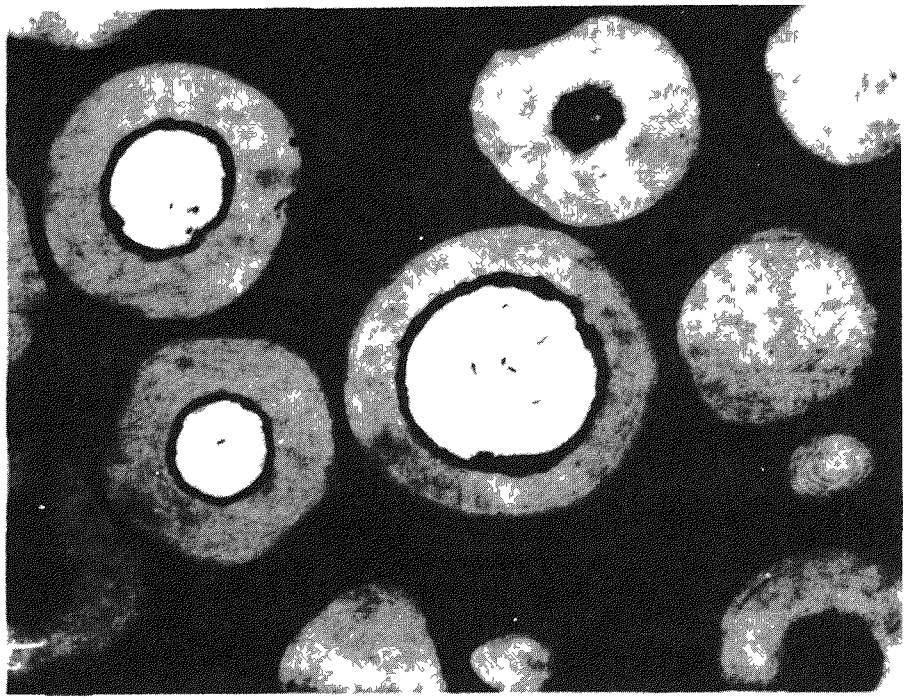

Fig. 5-4. Batch PyC-6 showing pyrolytically deposited carbon coatings on UC_2 (100X)

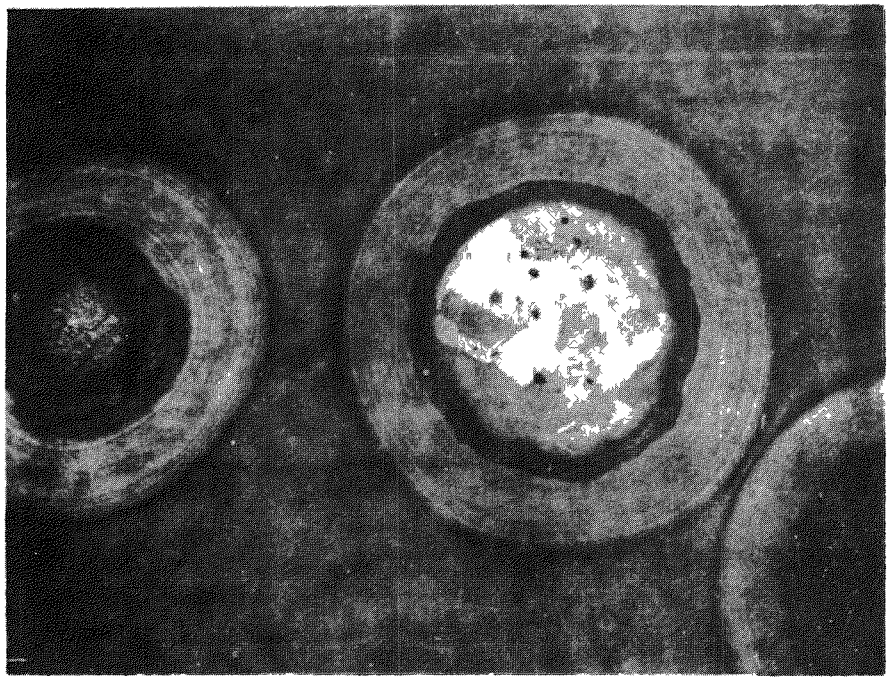

Fig. 5-5. Pyrolytic Graphite coated UC_2 particles by Minnesota Mining & Mfg. Co. (250X).

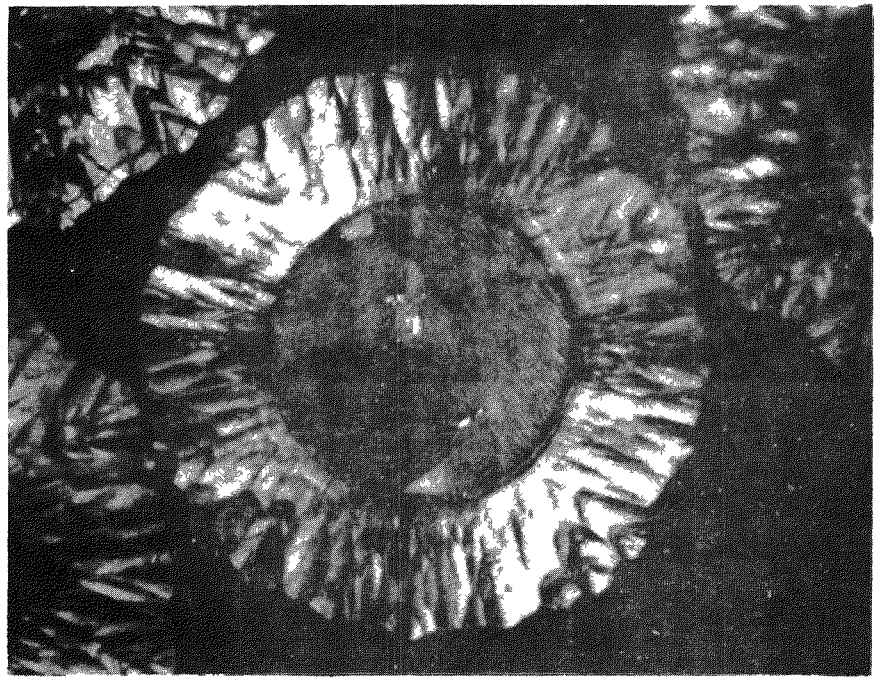

Fig. 5-6. UC_2 particle coated with Pyrographite by High Temperature Materials Inc., after thermal cycling to 3600°F. (250X, polarized light).

5.2 Pre-Irradiation Testing of Pyrolytic Carbon Coated Particles

The standard screening tests performed on pyrolytic carbon coated particles are generally similar to those used on alumina coated particles except that a nitric acid leach is used for the coating integrity test rather than the hot air oxidation test. Test results on pyrolytic carbon coated UC_2 particles are summarized in Table 5-2.

Uniformly good quality was found for the coatings in all batches based on the results of the nitric acid leach test. The uranium contamination was found to be low on all batches except PyC-2. In this case, it is believed that direct alpha recoil from the UC_2 particles through the thin coatings was responsible for the higher alpha count.

The thermal cycle test temperature of 3600°F was selected because of the interest in using the pyrolytic particle coating to prevent chemical reaction between silicon and uranium in an Si-SiC coated specimen. At this temperature, very severe damage to the coatings in batches PyC-1 and PyC-2 was found by the alpha assays after thermal cycling. Fig. 5-7 is a photomicrograph of batch PyC-1 after the thermal cycle test where many of the coating cracks can be seen at the sharper corners of the UC_2 particles. Much less evidence of thermal cycle cracking was noted in the 2450°F coatings on batches PyC-5 and PyC-6. A leach test on batch PyC-5 after thermal cycling indicated that 0.6% of the particles had cracked, on the assumption that all uranium was leached from cracked particles. The best results were obtained on the 3600°F coatings of batches PyC-7 and PyC-8. The photomicrograph of a particle from batch PyC-8 shown in Fig. 5-6 was taken after the thermal cycle test performed by the vendor and no visible evidence of cracking can be noted.

Several 1 1/2" graphite spheres (Type FA-24) were fueled with pyrolytic carbon coated UC_2 from batch PyC-1. An alpha assay of the surfaces of these spheres showed a rather uniform surface contamination of about 2×10^{-3}% of the total uranium in each sphere.

5.3 Fission Product Retention

The only fission product retention test on pyrolytic carbon coated UC_2 particles was the neutron activation test on three batches of particles and a fueled graphite sphere. These results are summarized in Table 5-3.

TABLE 5-2

Pre-Irradiation Tests On Pyrolytic Carbon Coated UC_2 Particles

A. Batch No. [a]	PyC-1	PyC-2	PyC-5	PyC-6
B. As-Fabricated				
1. Uranium Contamination				
a. Alpha Assay [b]	0.7±1.1	244±7	1.9±1.3	1.9±1.3
b. Exposed U [c]	1.3×10^{-6}	4×10^{-4}	9×10^{-6}	5×10^{-6}
2. Coating Integrity [d]				
a. Leach Time, hrs.	8	8	8	8
b. Uranium Removed, %	0.004	0.004	0.001	0.010
C. After Thermal Cycle [e]				
1. Uranium Contamination				
a. Alpha Assay [b]	2610±31	3680±30	21.4±3.7	65.6±5.2
b. Exposed U [c]	5×10^{-3}	6×10^{-3}	1×10^{-4}	1.6×10^{-4}

(a) See Table 5-1 for description of particles
(b) Reported as cpm/gm sample
(c) Reported as fraction of total uranium in sample
(d) Leach in hot nitric acid
(e) Heated to 3600°F in argon atmosphere.

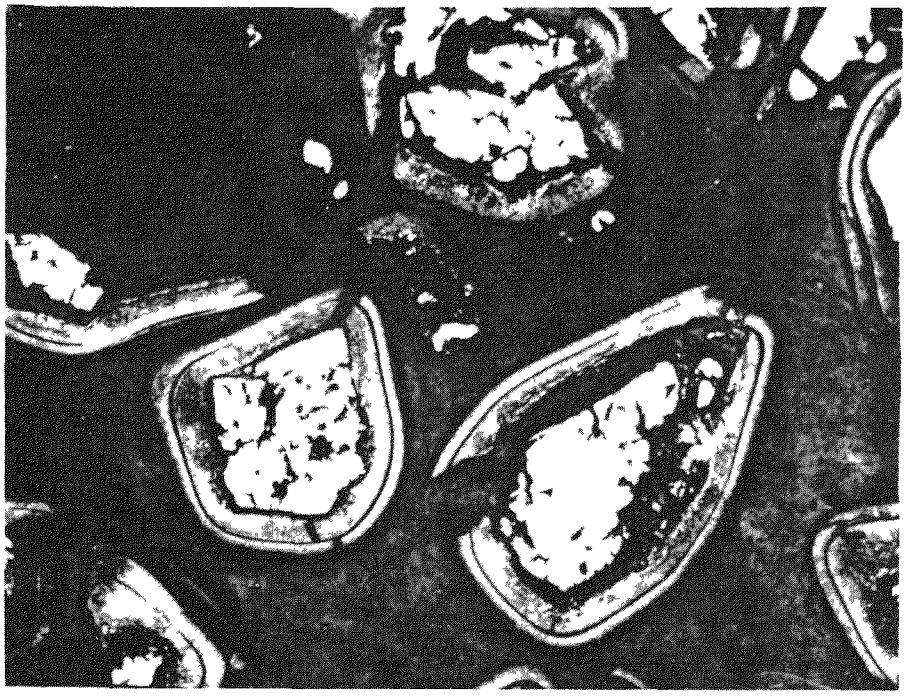

(a) View at 100x.

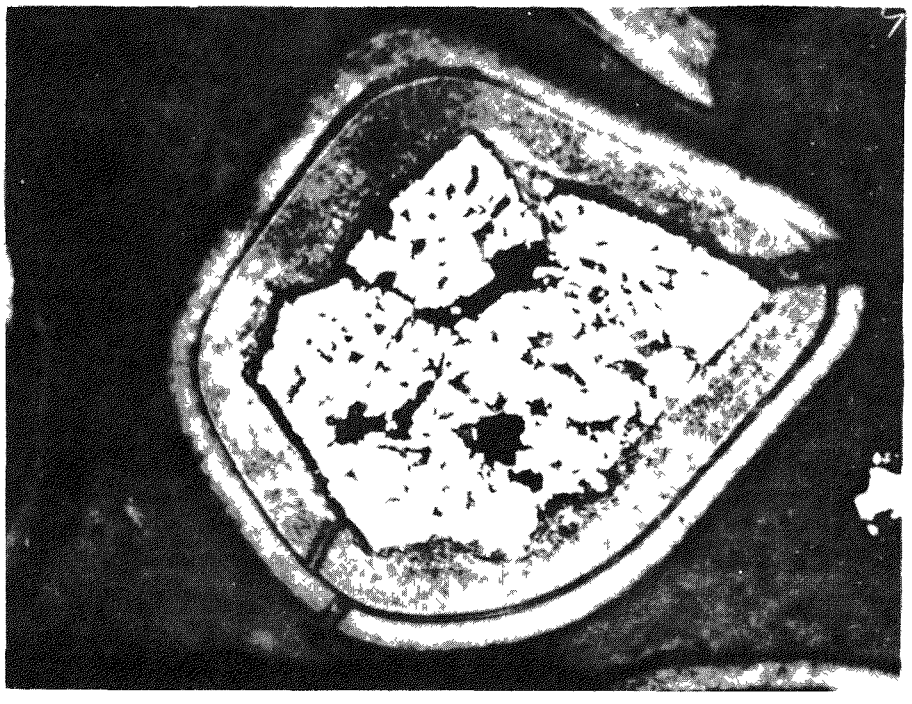

(b) View at 250x.

Fig. 5-7. Particles from batch PyC-1 after thermal cycling to 3600°F

TABLE 5-3

Neutron Activation Tests on Pyrolytic Carbon Coated Particles

Specimen	Test Temp, °F	Time Min.	Fractional Release of Xe133
1. Batch PyC-1	1600	160	$< 4.5 \times 10^{-6}$
	2000	93	$< 4.5 \times 10^{-6}$
	2400	65	4.7×10^{-4}
2. FA-24 Specimen fuel with PyC-1	1000	30	1.7×10^{-3}
	1700	25	3.4×10^{-4}
	2100	60	6.8×10^{-4}
	2500	30	1.5×10^{-3}
	2700	10	4.9×10^{-4}
3. Batch PyC-5	1500	60	(a)
	2000	60	(a)
	2500	65	(a)
	600/2500		$< 6.5 \times 10^{-6}$
	2500	210	2.5×10^{-5}
4. Batch PyC-6	1500	55	(a)
	2000	58	(a)
	2500	55	$< 5.2 \times 10^{-5}$
	600/2500(b)		$< 1.0 \times 10^{-4}$
	2500	240	$> 4.2 \times 10^{-4}$ (c)

(a) Activity level below sensitivity and included in subsequent reading.
(b) Temperature cycled 6 times.
(c) This Xe133 release occured during the last hour of heating.

The results on batch PyC-1 before incorporation in graphite show that up to 2000°F (i.e. the coating deposition temperature), this pyrolytic carbon coating showed good fission product retention. At 2400°F, the increased Xe133 leakage has shown that some of the coatings have cracked which confirms the previous thermal cycle results. Definite evidence of damage to the particles during fabrication of the fueled sphere is also seen. The Xe133 release from the fueled sphere is greater than the 2×10^{-5} surface contamination indicating uranium contamination due to particle damage extended throughout the whole graphite matrix. Many of the coatings

on the irregular fuel particles were evidently cracked during the admixture process.

In spite of the annular porosity in Batch PyC-5, the coatings exhibited good fission product retention. Thermal cycling to 2500°F did not appear to damage the coatings. Batch PyC-6 showed good fission retention up to its coating deposition temperature of 2500°F. After thermal cycling, the release remained low during the first three hours at 2500°F. During the fourth hour, a rise in Xe133 release was noted. A subsequent microscopic examination revealed a crusty, glazed white deposit on some of the particles. Peeling of the coating was noted on some of the particles. It is believed that a reaction between the coating and the Alundum crucible used to hold the particles caused this type of damage to the coatings.

These neutron activation results are comparable to the earlier results obtained on Al_2O_3 coated UO_2 and show that pyrolytic carbon has good possibilities as a fission product barrier. The effects of radiation damage to this material remains to be assessed.

6.0. Other Materials Development

During the course of the PBR Fuel Element Development Program, a number of development programs were sponsored on miscellaneous materials of interest to the Pebble Bed Reactor. These programs included the infiltration of graphite with thorium nitrate, coatings for fission product retention located beneath the surface of a graphite sphere, and the use of natural graphite filler to increase the density of a graphite sphere.

6.1 Thorium Nitrate Infiltration of Graphite

One method of fueling a graphite body is to infiltrate the pores of the graphite body with fuel-bearing solution, dehydrate the body, and bake it to convert the fuel to a stable solid form, deposited in the pores of the graphite. This infiltration procedure has been of interest to the PBR Fuel Element Development Program because of its potential as an economic method of fueling large batches of spheres, particularly when partially decontaminated fuel is used. A number of spheres fueled with approximately 5.4 gms of fully enriched UO_2 (Specimen type FI-1) had previously been prepared for evaluation as core fuel elements, as described in Appendix B of ref. (2).

In order to fully utilize the infiltration process in a Pebble Bed Reactor, the process should also be suitable for preparing blanket elements loaded with ThO_2. However, the available pore volume of a graphite sphere limits the amount of fuel which can be added to the sphere by the infiltration process. Previous studies of a blanketed PBR core (1) showed that 30 to 45 gms. of ThO_2 per 1-1/2 inch diameter graphite sphere would be required in blanket elements. Consequently, the Speer Carbon Co. undertook a study (7) to establish process conditions for graphite spheres loaded with ThO_2 by infiltration with thorium nitrate and also to determine the amount of ThO_2 which can be added to graphite as a function of graphite density.

6.1.1 The Infiltration Process

Six sets of 1-1/2 inch graphite spheres having nominal densities of 1.25, 1.35, 1.45, 1.55, 1.65 and 1.75 g/cc were machined from extruded blocks of Moderator Grade B graphite (Speer Carbon Co.) for use in the program. A summary of the mercury porosimetry data on these spheres is given in Table 6-1.

TABLE 6-1

DENSITIES AND POROSITIES OF GRAPHITE SPHERES

Nominal Density, g/cc	Avg. Apparent Density, g/cc	Avg. Pore Volumes, cc/g			
		Total	D>100μ	100μ<D>.06μ	D<.06μ
1.25	1.240	0.364	0.009	0.305	0.050
1.35	1.339	0.305	0.007	0.250	0.048
1.45	1.421	0.263	0.015	0.200	0.048
1.55	1.579	0.192	0.014	0.118	0.060
1.65	1.666	0.159	0.013	0.110	0.036
1.75	1.732	0.136	0.009	0.074	0.052

After experimenting with several variables, the following standard procedure was adopted for loading the spheres.

1. 3 to 4 spheres of a particular group were outgassed for 15 hrs. to a pressure of 5-15 microns of mercury.
2. A water solution containing 76 w/o $Th(NO_3)_4 . 4 H_2O$ was prepared. This solution was nearly saturated at the infiltration temperature of 25°C.
3. The outgassed spheres were then flooded under vacuum for 30 minutes with the thorium nitrate solution.
4. Atmospheric pressure was applied to flooded spheres for an additional 15 min.
5. The spheres were removed from the solution, wiped clean of solution, and stored at ambient temperature for 16 hours.
6. The spheres were placed in a Vycor tube and heated in a flowing argon stream in accordance with the following schedule:
   a. Temperature raised to 160°C in 30 min. and held for 3 hours to remove water.
   b. Temperature rasied to 700°C in 1 hour and held for 3 hours to decompose thorium nitrate to thorium oxide.
7. Where additional ThO_2 loading was required, the above procedure was repeated.

A number of variations in this process were tried. When a 100°C solution containing 85 w/o $Th(NO_3)_4 . 4H_2O$ was tried, a slight increase in ThO_2 loading per infiltration was found but was not felt sufficient to warrant the complications of providing heated production apparatus. When the vacuum pretreatment was omitted, there was a significant decrease in ThO_2 loading. When longer infiltration times were used, there was no increase in ThO_2 loading. Other variables which were not found to increase the ThO_2 loading were the use of 10 psig pressure during infiltration, a slower heating rate to 700°C, and the use of 12 psig pressure during firing. Shorter heating times at the final temperature and a higher final temperature (950°C) were also investigated. It was found that the standard heating cycle produced complete denitration although some further slight weight losses occurred at the higher temperature due to mechanical losses of ThO_2 and graphite in the further handling.

6.1.2 Results of Infiltration Tests

The primary experimental task was to determine the limits of ThO_2 loading in graphite spheres of various densities. Initial experiments showed that the use of succesive infiltrations was the best method of raising the ThO_2 loading. It was found that after eight infiltrations, the spheres still did not appear to be near their saturation points. However, a systematic series of runs were made using just eight infiltrations at each of the six graphite densities. The results of these runs are summarized in Figure 6-1 where the cumulative ThO_2 loading is plotted vs. the number of infiltrations for each of the six density groups. Each data point is the average of three spheres. This data is also shown in Figure 6-2 where the atom density of thorium is plotted vs. the atom density of carbon. As can be noted in Figure 6-1, loadings of 30 gms. of ThO_2 can be achieved only in the lower density graphite and that a minimum of 5 infiltrations would be required.

The uniformity of the ThO_2 dispersion in the graphite spheres was checked by sectioning several spheres and analyzing segments from the center region and the edge region. This was done on a number of spheres which had been infiltrated from 1 to 8 times. The ThO_2 distribution was quite uniform. Loadings in the outer region were 4% to 6% higher than the loadings in the center region, the higher values being associated with the greater number of infiltrations.

From this work it is concluded that graphite bodies can be loaded with ThO_2 by the thorium nitrate infiltration process but that relatively large loadings will require use of lower density graphite and many infiltration steps.

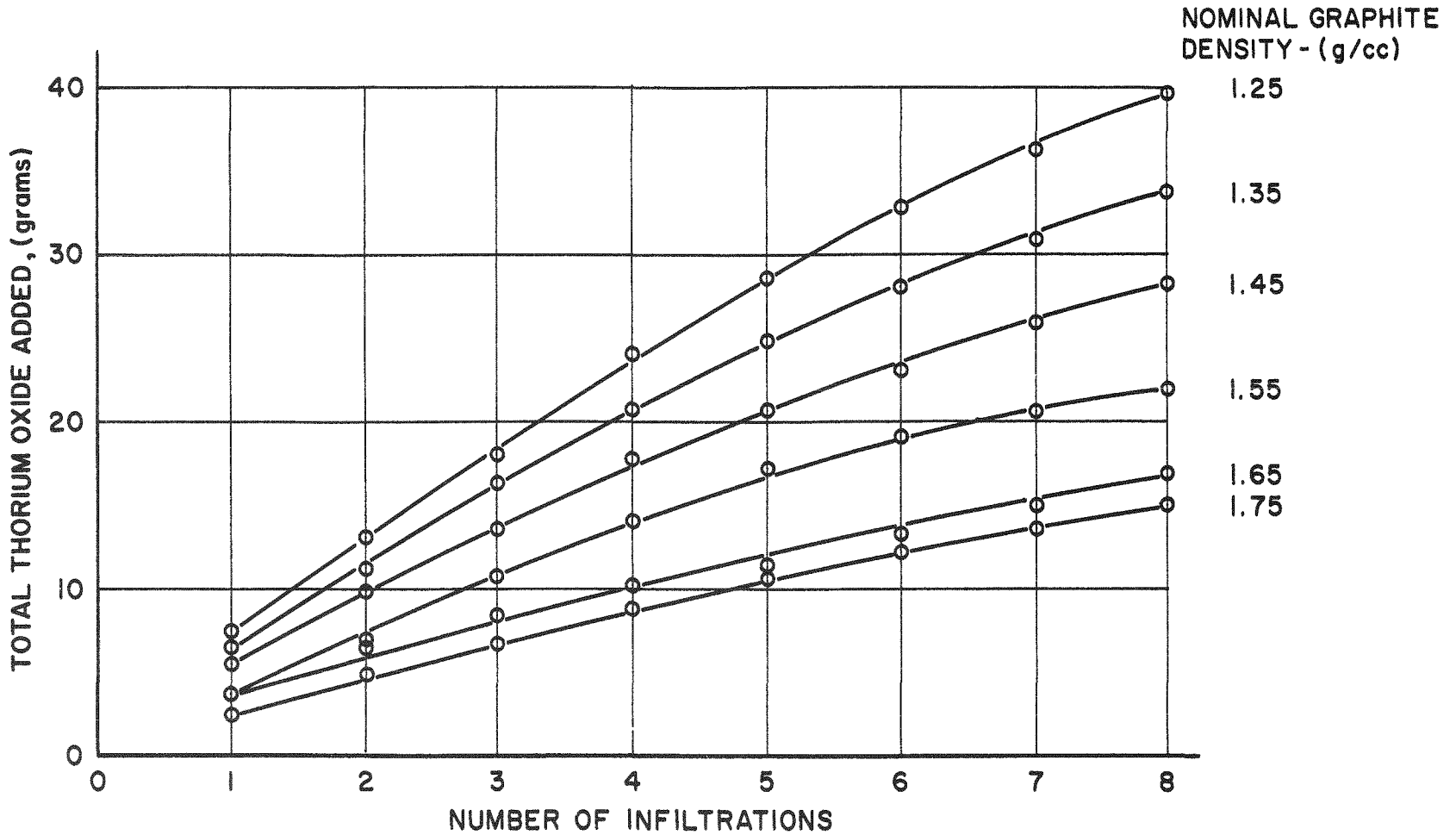

THORIUM OXIDE LOADING vs INFILTRATION FREQUENCY

FIG. 6-1

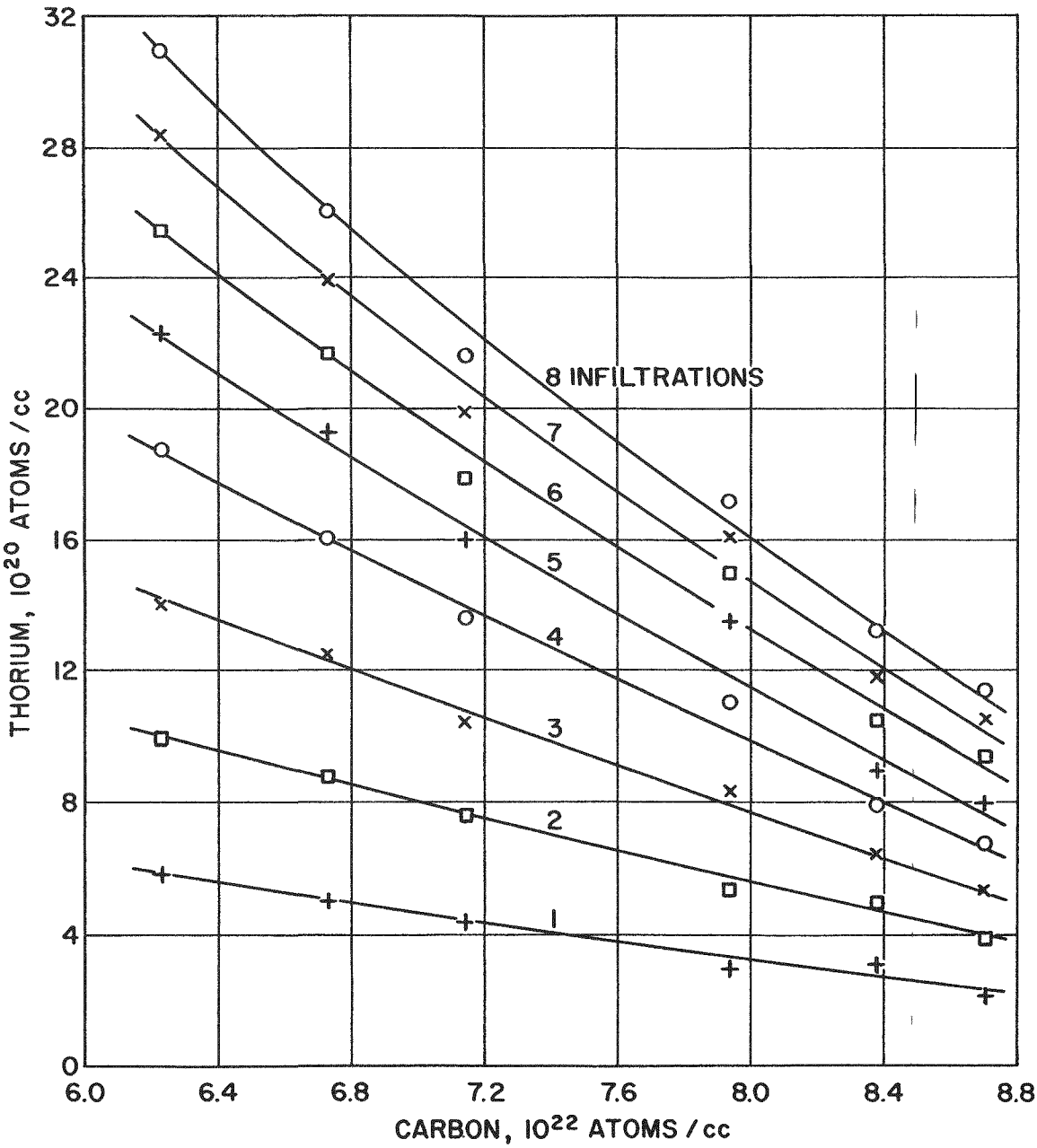

THORIUM AND CARBON DENSITIES
IN INFILTRATED GRAPHITE SPHERES

FIG. 6-2

6.2 Subsurface Coatings

The two primary methods of fission product retention which were explored in the PBR Fuel Element Development Program were coatings on the surface of the spherical fuel element and coatings on individual fuel particles. Another method, conceived by R. F. Benenati of Sanderson & Porter (8), was to locate the coating beneath the graphite surface. The coating would surround a pellet of either fissile material or fissile material dispersed in graphite. An unfueled graphite shell would in turn surround the coating. The primary advantage of locating the coating beneath the graphite surface is to protect it from the external loads imposed on PBR fuel elements, such as impact or compressive loads which normally would fracture most types of coating located directly on the fuel element surface. Another advantage of a subsurface coating is that, through suitable choice of materials, a coating operating in the plastic or molten range would tend to seal pores and fissures in the lower temperature zone of the unfueled graphite shell.

The exploratory program on subsurface coatings was performed at the Battelle Memorial Institute and consisted of (a) compatibility studies in which the compatibility of various potential coating materials with graphite in a simple shape were investigated; and (b) fabrication studies with fueled graphite spheres.

6.2.1 Materials

Two varieties of the subsurface coatings were studied. In one, materials having melting points in the range of peak PBR operating temperatures were used. In the other, materials with a higher melting point were used so that the coating could be "set" in a baking furnace prior to use. The pertinent properties of materials tested are given in Table 6-2.

TABLE 6-2

Materials Used In Subsurface Coating Studies

Material	Melting Point, °F	Absorption Cross-Section, barns
Cu	1980	3.6
4 glasses	1800 - 2500	(See Table 6-3)
Si	2600	0.13
Ni	2640	4.5
Cr	2940	2.9
Zr	3090	0.18
Ti	3270	5.6
$MoSi_2$	3690	2.7

A number of special glasses were prepared to have softening points in the range of 1800°F to 2500°F. The composition of these glasses are shown in Table 6-3.

In selecting these materials the glasses were included for the reason that they represent a ceramic that can be tailored in melting point and wettability by adjusting composition. $MoSi_2$, which was known to be compatible with graphite, was included to provide a common material in the compatibility and fabrication studies. Copper, nickel and silicon were selected as metals for possible subsurface application because of their range of melting temperatures, their reactions with graphite, and compatibility characteristics with graphite. Ti, Cr and Zr were included as high melting materials which readily formed metal carbides.

TABLE 6-3

Composition of Glasses Used in Surface Coating Studies

Material	Glass #1	Glass #2	Glass #3	Glass #4
$CaSiO_3$	27.4	19.2	19.2	35.6
Al_2O_3	8.6	6.0	6.0	18.0
SiO_2	21.2	14.8	14.8	-
BaO	42.8	60.0	55.0	-
MoO_3	-	-	5.0	-
KNO_3	-	-	-	19.6
MnO	-	-	-	9.0
TiO_2	-	-	-	4.4
CaF_2	-	-	-	13.4
σ_a, barns	0.65	0.98	0.78	3.3

6.2.2 Compatibility Tests

Materials' compatibility was studied using graphite crucibles filled with coating materials of interest. Also, a number of graphite-metal diffusion couples were tested.

The crucible studies were primarily to test wettability of potential coating materials. The materials were placed in small graphite crucibles and held at controlled temperatures for short periods of time after which they were cooled, sectioned and examined metallographically. The temperatures used were 1800°F, 2200°F and 2600°F and the time at temperature was 5 min.

The results of these tests are summarized in Table 6-4. It can be seen by examination of this table that at 1800°F there was no penetration of the graphite by any of the materials tested. There was some wetting of the surface by copper as well as silicon, as determined by metallographic examination of the interface between the crucible and the melt. At 2200°F, there was definite wetting of the graphite by copper, silicon and #3 glass and there may have been some penetration by the metals but not by the glass. At 2600°F the copper, silicon, nickel and #1 and #3 glasses all wet the surface. The copper, nickel and #1 glass all showed slight penetration while the silicon showed a greater penetration probably in the form of silicon carbide. The #2 glass showed some adherence to the graphite surface with slight penetration. The #4 glass neither wet nor penetrated the graphite, however there was some slight erosion of the crucible. The #1 glass penetrated slightly but seriously eroded the crucible. The molybdenum disilicide showed selective adhesion to the graphite.

The diffusion couples were prepared by compressing thin layers of potential coating materials between 1/4 inch thick plates of graphite and heating in argon at 2600°F for 8 hours. This test was thought to be more similar to actual conditions that would exist in a subsurface element. The materials tested were Cu, Ni, Zr, Si, $MoSi_2$ and #3 glass. The results are shown in Figures 6-3 through 6-8.

The Figure 6-3, the copper is seen to be distributed as spherical particles with no penetration of the graphite. In Figure 6-4, the nickel is seen to be well adhered to the graphite and to penetrate into the graphite pores. The dark flakes in the nickel are carbon which dissolved in the nickel and precipitated on cooling. In Figure 6-5, the zirconium was found as loose flakes of ZrC with no evident penetration of the Zr into the graphite. In Figure 6-6, the silicon was converted to small particles of SiC with penetration of the graphite. In Figure 6-7, the molybdenum disilicide is seen to have separated from the graphite except for a thin adherent layer. In Figure 6-8, the #3 glass is seen to bond well to the graphite and remain as a continuous layer. An unidentified metal phase can be noted at the graphite-glass interface.

6.2.3 Sphere Fabrication

A number of 1-1/2 inch diameter spheres were fabricated with various types of subsurface coatings surrounding fueled graphite cores. The first group of spheres was made by cold pressing. The fueled core was first molded, then the coating material was molded onto the fueled core, and

TABLE 6-4

Compatibility Tests Of Sub-Surface Coating Materials
In Graphite Crucibles

Type of Metal	Wet Graphite at Crucible Interface	Degree of Penetration into Graphite Crucible	Observations
	Heated at 1800 F for 5 minutes		
Copper	Yes	Slight	Some particles adhered to wall.
Silicon	Slight	None	
No. 1 glass	None	None	
No. 2 glass	None	None	
No. 3 glass	None	None	
No. 4 glass	None	None	
Nickel	None	None	
$MoSi_2$	None	Slight	Some particles adhered to crucible wall.
	Heated at 2200 F for 5 minutes		
Copper	Yes	Slight	Particles adhered to crucible wall.
Silicon	Yes	Very slight	
No. 1 glass	None	None	
No. 2 glass	None	None	
No. 3 glass	Slightly	None	Some adherence
No. 4 glass	None	None	Slight erosion of crucible
Nickel	None	None	
$MoSi_2$	None	Slight	
	Heated at 2600 F for 5 minutes		
Copper	Yes	Slight	Adhered to graphite
Silicon	Slightly	1/8 in. or greater	
No. 1 glass	Yes	Slight	Crucible badly eroded
No. 2 glass	None	Slight	Adhered to graphite
No. 3 glass	Yes	None	
No. 4 glass	None	None	Slight adherence
Nickel	Yes	Slight	
$MoSi_2$	None	None	

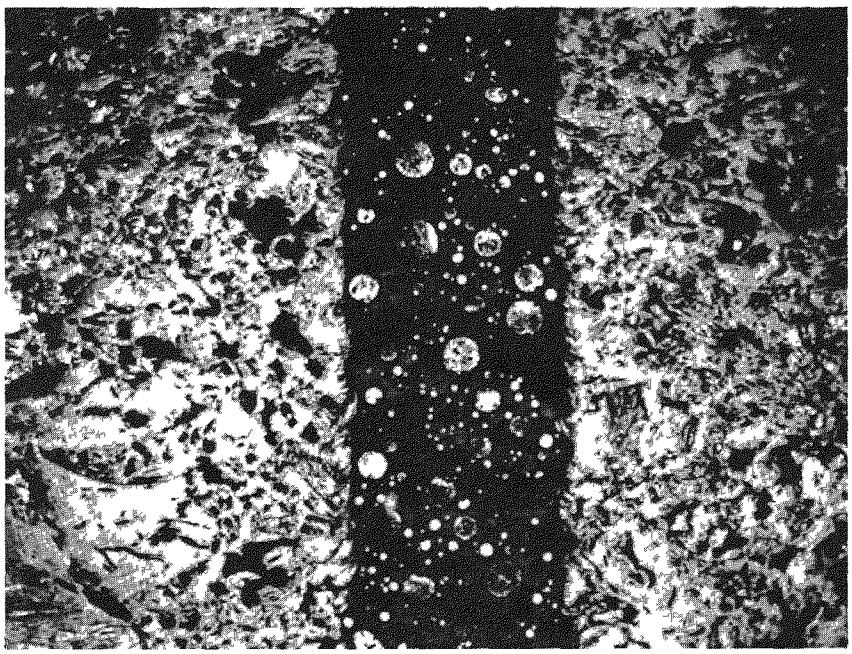

FIG. 6-3 COPPER-GRAPHITE. COPPER APPEARS AS SPHERICAL PARTICLES. (50X)

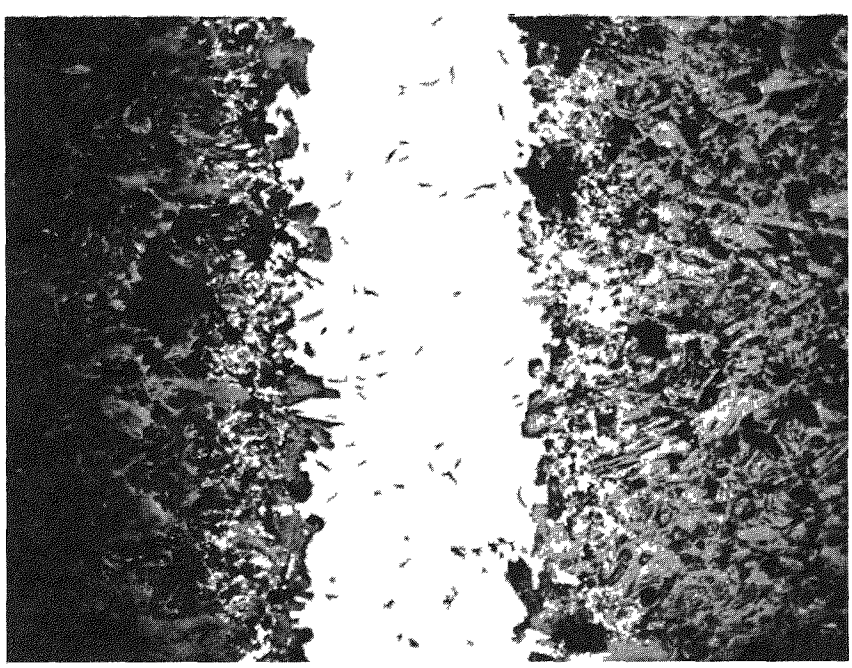

FIG. 6-4. NICKEL-GRAPHITE. DARK FLAKES IN NICKEL ARE GRAPHITE. (50X)

FIG. 6-5 ZIRCONIUM-GRAPHITE. SMALL FLAKES IN ZIRCONIUM PHASE ARE PROBABLY ZrC. (50X)

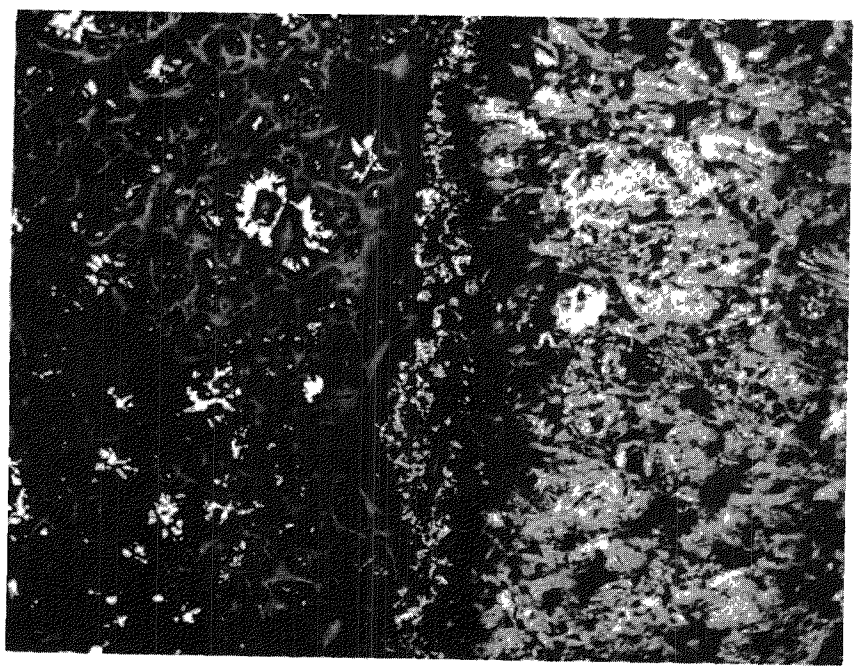

FIG. 6-6 SILICON GRAPHITE. SMALL GREY PARTICLES ARE SiC. (50X)

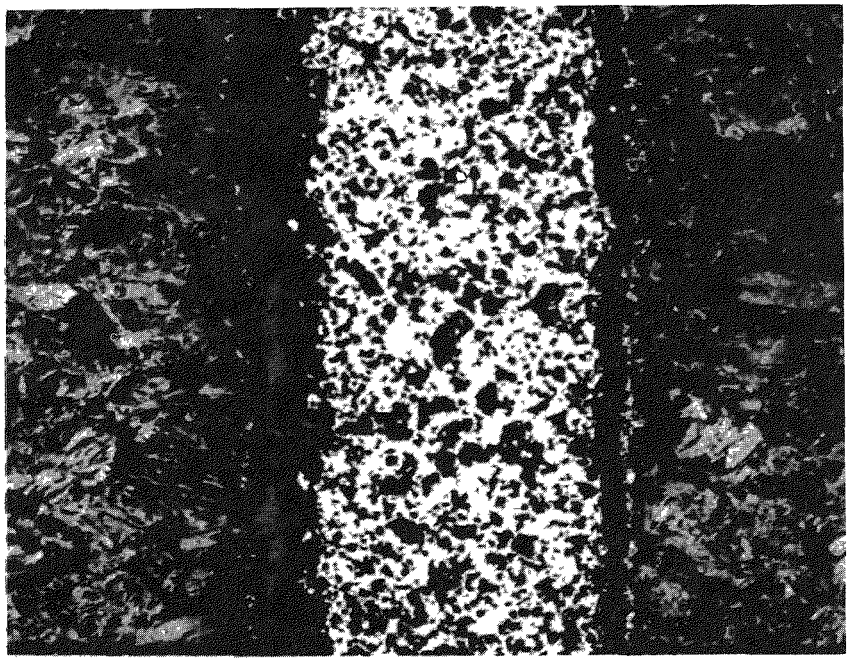

FIG. 6-7 MOLYBDENUM DISILICIDE - GRAPHITE. GAP AT INTERFACES IS FILLED WITH MOUNTING RESIN. (50X)

FIG. 6-8 No. 3 GLASS-GRAPHITE. METALLIC-LIKE PHASE AT THE INTERFACE IS UNIDENTIFIED. (50X)

finally the outer graphite shell was molded on. The spheres were first cured at 350°F to set the binder and then given a slow bake treatment at 200°F for 8 days. Degassing of all three regions occurred at the same time.

The first group of spheres contained coatings of copper, nickel and #3 glass (low-melting materials) and titanium, chromium and molybdenum disilicide (high-melting materials). These materials were generally applied to the fuel cores in a powder form mixed with carbonaceous binder. All of the spheres looked satisfactory after the 350°F cure. After the 8-day bakeout however, most of the spheres had severely cracked outer shells and some of the metal coatings had cracked as well. A high degree of metal (or metal carbide) penetration into the fueled shell was noted in most cases. The glasses did not penetrate but there was evidence of chemical reaction with the graphite. There was only slight penetration with copper but this material tended to ball up and leave gaps near the top of the sphere due to gravitational effects.

Several attempts were made to seal two thin copper hemispheres around a fueled graphite core, but outgassing and chemical reactions prevented the making of a satisfactory brazed joint.

In order to determine whether the high temperature coatings could be made to fuse into a leaktight coating, the defective graphite shells were completely removed from the Cr, Ti, and $MoSi_2$ specimens of the first group. New graphite shells were cold-pressed onto the clad fueled cores and they were all heated at 4660°F in order to melt the metal coatings. During this process, molten chromium ran out a crack which developed in the graphite shell. The titanium layer failed to penetrate the graphite shell probably due to a titanium carbide layer which had formed during the 8-day bakeout at 1500°F. The $MoSi_2$ coating, which had several cracks prior to the application of the new graphite shell, was fused together. After manually removing the shell, a hot oil test of the coated fueled core piece showed only one pinhole leak in the coating.

The next variable investigated was hot pressing. It was hoped the application of pressure while the coating layer was in its molten state would minimize coating penetration and produce a dense tight coating. A second group of spheres was prepared using this hot-pressing technique. The spheres, consisting of a fueled core, a coating and an unfueled graphite shell, were initially formed by cold pressing. The spheres were baked at 1500°F to remove volatiles in the binder and then were hot-pressed in a graphite

die under 10,000 psi pressure. Spheres containing Ni, Si, Cu and No. 3 glass were hot-pressed at the melting point of the coating material. Spheres containing $MoSi_2$, Cr and Ti were hot-pressed at only 2000°F because of limitations of the hot-pressing equipment. This latter group of spheres was subsequently heat-treated to the melting point of the seal material in a carbon resistor furnace.

Visual inspection of sectioned spheres indicated that each coating material formed a continuous layer except copper, which appeared to bead and become discontinuous. Cracking was observed in the shells of spheres containing Cr, $MoSi_2$ and Ti coatings. These spheres were not under pressure when the coating melted and the coating appeared to flow into the cracks. No cracks appeared in the specimens that were under pressure during the period when the coating was molten. Radiography indicated that the coating materials penetrated into the pores of the unfueled graphite shell.

In order to assess the coating integrity of these specimens without destroying them, the spheres were subjected to the hot oil leakage test by immersing them in silicone oil at 400°F. Bubbling by gas entrapped during fabrication was then observed. Spheres without a coating which were subjected to similar fabricating conditions exhibited bubbling for 20 to 40 minutes. In the coated elements, gas release would be expected to come from only the unfueled graphite shell outside the coating. Therefore, if a good seal were obtained, the bubbling should cease in a much shorter time. Results of the hot oil testing of the second group of spheres is given in Table 6-5.

As noted in Table 6-5, the best results were obtained with the high temperature coatings (i.e. $MoSi_2$, Cr and Ti) even though there were cracks in the outer shells of these specimens. The exploratory program was concluded with the hot oil testing of these hot pressed spheres.

TABLE 6-5

Leakage Test On Hot-Pressed Spheres With Subsurface Coatings

Coating Type	Hot Press Temp, °F	Further Heat Treatment, °F	Time Required for Bubbling to Stop, Min. (1)
#3 glass	2500	-	7
Copper	2100	-	>7
Copper	2500	-	>7
Nickel	2550	-	6
Silicon	2540	-	>7
Silicon	2540	-	6
Chromium	2000	3272	6
Chromium	2000	3272	2-1/2
Chromium	2180	3272	>7
Titanium	2000	3272	4
$MoSi_2$	2000	3600	2-1/2

(1) Testing time was 7 minutes in silicone oil (400°F).

6.2.4 Conclusions

This exploratory program on subsurface coatings has shown that several types of subsurface coatings are possible. The use of materials such as nickel or #3 glass which melt in the range of PBR operating temperatures should cause these materials to penetrate into the pores of the outermost unfueled graphite shell and also into cracks which may be present in the unfueled shell. Both of these phenomena have been observed in the uniform heating of fuel element specimens in out-of-pile furnaces. The extent of penetration must of course be limited by the amount of coating material initially added so that a continuous coating will remain around the fueled core piece.

It was found that the best specimens could be made when pressure was applied to the sphere while the coating was in a molten phase during fabrication. Limitations to the experimental equipment prevented the use of hot-pressing with the high-temperature coating materials (i.e. Cr, Ti, and $MoSi_2$) but in spite of shell cracking these latter materials appeared to form the best seals based on the limited evaluation work. It is probable that hot-pressing would have prevented shell cracking in these latter specimens.

6.3 Natural Graphite

An inherent characteristic of the Pebble Bed Reactor concept is the fixed 39% voidage in the ball bed region. One method of increasing the amount of carbon moderator in a Pebble Bed core to account for this high voidage is to replace some of the spheres with solid graphite posts. This increases the amount of carbon in the core but at the same time decreases the amount of heat transfer surface in the core. Another method of increasing the amount of carbon moderator is to increase the graphite density of the fueled spheres. For example, in the reference design for the 125 eMW-PBR (2), a graphite density of 1.68 g/cc was used and it was found necessary to replace 25% of the core volume with solid graphite posts to achieve the optimum conditions for that plant. The same effective carbon loading could have been achieved if 2.1 g/cc graphite spheres were used with no fixed graphite posts, thus increasing the thermal capacity by about 33% for the same total core size.

The general method of achieving high density graphite is by successive carbonaceous reimpregnations and regraphitizations of the graphite body. Densities up to about 1.9 g/cc have been achieved by this technique. Another method is the use of suitable starting materials which can be molded and baked to directly form a high density graphite body in only one step. One such material is natural graphite powder.

An exploratory program on the fabrication of graphite bodies using natural graphite as the filler material was conducted at the Battelle Memorial Institute. Densities in excess of 2.0 g/cc had been achieved using natural graphite powder with no binder. However, these bodies had little strength. One of the major objectives of this program was to determine whether suitable strength characteristics could be achieved by the addition of a binder without a serious decrease in density.

6.3.1 Pellet Fabrication

Three types of purified natural graphite powder were obtained from the Charles Pettinos Graphite Corp. as described in Table 6-6.

TABLE 6-6

Natural Graphite Materials

Grade No.		Impurities	Particle Size
138	Mexican, amorphous	0.9%	99%, -325 mesh
6387	Madagascar, crystalline	0.1% (B<1 ppm)	100%, -200 mesh, avg. particle size, ~10.6μ
6405	Madagascar, crystalline	0.1%	0.03%, +100 mesh 2.03%, -100, +200 mesh 17.98%, -200, +325 mesh 79.96%, -325 mesh.

A series of 1/2" x 1/2" cylindrical pellets were prepared using the three types of natural graphite shown in Table 6-6. Four types of binder were used, including two types of phenolic resin, a coal tar pitch, and furfural alcohol. Binder content ranged from 0 to 40 gms per 100 gms of natural graphite. After mixing, the pellets were cold pressed, cured at 400°F, prebaked in vacuum at 1500°F, and finally baked at 2500°F in argon. Density measurements were taken at each stage of fabrication and crushing strengths of the finished pellets were measured. A summary of the results is given in Table 6-7.

Several trends can be noted in Table 6-7. Lower densities result with a high binder content. Lowest densities resulted with coal tar pitch binder. The strengths of the resin bound pellets were generally higher than for the pitch bound pellets. For comparison purposes, two 1/2" x 1/2" cylinders were machined from AGOT graphite of 1.70 g/cc density. The compressive strengths for these pieces were found to be 3,139 psi and 3,445 psi.

The highest densities were achieved with the 6405 and 6387 graphities with the lower BV1600 binder contents. Consequently an additional series of pellets was prepared to explore this range in somewhat more detail. The use of thermax carbon black was also investigated using the same fabrication and test procedures used for the pellets in Table 6-7 . The results are shown in Table 6-8.

TABLE 6-7

Density and Strength of Natural Graphite Pellets (1st Series)

Graphite Composition [a]	Gms. binder per 100 gms of filler	Green Density, g/cc [b]	Baked Density, g/cc [c]	Compressive Strength psi [c]
6387-none	none	2.14	1.95[b]	1,000[d]
6387-BV1600	20	2.00	1.92	5,000
6387-BV1600	35	1.66	1.55	4,700
6387-BV1600	50	1.74	1.77	5,200
6387-pitch	30	1.87	1.60	3,900
6387-pitch	35	1.86	1.49	3,200
6387-pitch	40	1.81	1.45	2,700
6387-79L	20	1.91	1.85	3,800
6387-79L	30	1.78	1.67	2,500
6387-FA	40	1.72	1.68	2,600
6405-none	none	2.03[c]	2.06	1,900
6405-BV1600	20	2.02	2.02	2,900
6405-BV1600	35	1.93	1.93	3,400
6405-BV1600	50	1.89	1.88	3,400
6505-pitch	30	1.90	1.60	2,400
6405-pitch	35	1.89	1.63	3,300
6405-pitch	40	1.86	1.57	3,000
138-none	none	1.71[c]	1.72	2,400
138-BV1600	20	1.86	1.79	4,800
138-BV1600	35	1.81	1.77	5,200
138-BV1600	50	1.79	1.74	5,300
138-pitch	30	1.85	1.52	3,500
138-pitch	35	1.81	1.56	4,900
138-pitch	40	1.81	1.58	5,100
138-79L	20	1.79	1.62	1,600
138-79L	30	1.73	1.62	2,100
138-FA	40	1.65	1.55	600

(a) The first part designates the type of natural graphite described in Table 6-6. The second part designates the binder material as follows: BV1600: Bakelite phenolic resin; 79L: phenolic resin supplied by Old Ironsides Co; pitch: Barrett No. 2. medium hard pitch; FA: furfural alcohol.

(b) Average of 3 samples.

(c) Average of 2 samples.

(d) One sample tested.

TABLE 6-8

Density and Strength of Natural Graphite Pellets (2nd Series)

Graphite Compositions[a]	Gms. binder per 100 gms of filler	Green density g/ cc[b]	Baked density g/cc[b]	Compressive strength, psi[c]
6387-none	0	2.14	1.95	1,000[d]
6387-BV1600	5	2.01	1.96	1,800
6387-BV1600	10	2.00	1.95	4,800
6387-BV1600	15	1.99	1.88	3,300
6405-none	0	2.03[c]	2.06	1,900
6405-BV1600	5	2.12	2.06	3,100
6405-BV1600	10	2.09	2.01	2,700
6405-BV1600	15	2.04	2.02	3,500
6405-BV1600-10T	20	1.89	1.86	2,200
6405-BV1600-20T	35	1.79	1.70	2,700
6405-pitch-10T	40	1.82	1.51	2,500
6405-pitch-20T	35	1.84	1.56	2,200

(a) Designations are same as used in Table 6-7 except that 10T and 20T designate 10% and 20% thermax carbon black added to filler.
(b) Average of 3 samples.
(c) Average of 2 samples
(d) One specimen tested.

As can be noted in Table 6-8, there has been some decrease in strength below the values shown in Table 6-7 for the higher binder contents. Maximum strengths in the lower binder content range appear to be at 10 parts binder with the 6387 graphite and 5 parts binder with the 6405 graphite. Additions of the thermax carbon black had little effect on the strength but did decrease the final density.

6.3.2 Sphere Fabrication

The final step in the exploratory program was the fabrication and testing of spheres to determine whether they would meet PBR requirements. Madagascar Grade 6405 natural graphite filler was used in one set of spheres. For comparison, another set of spheres was prepared using a high density

synthetic graphite powder (National Carbon Grade 195) which had approximately the same particle size distribution as the 6405 material. BV1600 resin was used as the binder material in both cases. The spheres were molded in a heated (300°F) steel die at 20,000 psi. Pressure and heat were maintained on the specimens for a period of 10 minutes to cure and partially set the resin binder. The spheres were then partially baked at 1500°F in vacuum. The final bake treatment was at 2500°F in an argon atmosphere.

The test program consisted of impact tests, compression tests and density measurements. The results are summarized in Table 6-9.

TABLE 6-9

Mechanical Strength of Natural and Synthetic Graphite Spheres

Filler	Binder Content pph of filler	Green Density g/cc[a]	Baked Density g/cc[a]	Load at Failure Compressive lbs.[b]	Load at Failure Impact ft. lbs[c]
Natural (6405)	5	2.11	2.04	570	1.0
"	10	2.08	1.99	430	1.0
"	15	2.09	2.00	430	1.2
"	20	2.07	1.99	410	1.5
Synthetic (195)	20	1.91[b]	1.75[b]	580	1.9
"	40	1.84	1.68	670	3.0

(a) Average of five specimens
(b) Average of two specimens
(c) One specimen tested

As noted in Table 6-9, densities of about 2.0 g/cc were obtained with the natural graphite filler while the synthetic graphite filler definitely produced lower densities. The comprehensive strengths of 410 to 570 lbs. for the natural graphite spheres are close to the desired 500 lbs. while the impact strengths of 1.0 to 1.5 ft-lbs are below the desired 2.0 ft-lbs. Although the synthetic graphite spheres listed in Table 6-9 barely met the strength requirements, it should be recalled that commercially prepared synthetic graphite spheres such as the FA-1 and FA-22 types consistently showed compressive strengths over 2000 lbs. and impact strengths over 7 ft-lbs. This discrepancy with commercial specimens tends to cloud the present results obtained with natural graphite.

Although there were a limited number of specimens used to obtain the data in Table 6-9, there is some evidence that higher strengths but lower densities are obtained with higher binder content. During the course of testing, it was noted that the natural graphite specimens began to flake as impact loading was increased. This was not observed on the synthetic graphite specimens. A typical mode of failure for the natural graphite spheres was the separation of spherical shell segments from the outer surface of the spheres indicating poor radial bonding.

6.3.3 Conclusions

This exploratory program has shown that crystalline natural graphite, when used as the filler component, can produce bulk graphite densities in excess of 2.0 gm/cc. The coarse-grained crystalline graphite is slightly superior to the fine-grained crystalline graphite and both crystalline grades are superior to the amorphous natural graphite. It is necessary to use the resin type binders rather than conventional pitch binders in order to achieve the high densities.

However, rather poor strengths were found for the natural graphite spheres even though the compressive strengths of natural graphite pellets compared favorably with synthetic graphite pellets. The mode of failure of the natural graphite spheres indicated that poor radial bonding caused the sphere failure. In order to utilize the higher densities obtainable with natural graphite, it will be necessary to find methods of improving the strength of these spheres and preventing spalling or flaking of the sphere surface.

7.0 Graphite-UO_2 Irradiation (Capsule SP-4)

In selecting the fissile material compound in a uranium-graphite fuel element, the oxide form has a number of advantages over the carbide form, such as ease in handling during fabrication and ease of reprocessing. The greatest limitation on UO_2 is its reaction with the graphite matrix at high temperatures. Evidence of reaction at temperatures as low as 2400°F have been reported (9), however during the short baking time at 2560°F during fabrication stability is excellent. By dispersing fissile material throughout the graphite moderator, the Pebble Bed Reactor offers the best opportunity of producing high coolant outlet temperatures (1200 to 1400°F) while keeping peak fuel temperatures below 2100°F. Thus, UO_2 can be considered for PBR applications.

A capsule irradiation experiment was performed in an attempt to determine whether radiation would affect the reaction between UO_2 and graphite at temperatures approaching 2100°F. Another objective of this experiment was to assess the effect of high temperature irradiation on the strength and dimensional changes of fueled graphite. Four types of uncoated graphite spheres each fueled with a different type of UO_2 were tested. The specimen designations and the UO_2 particle sizes were: FI-1 ($1\mu UO_2$), FA-2 ($67\mu UO_2$), FA-1 (100μ) and FA-10 (400μ). A further description of these types is included in Table 2-1 and ref. (3). The specimens were irradiated in Static Capsule SP-4. The design and operation of this capsule is described in Section 8-1. The exposure conditions for the specimens are summarized in Table 7-1, where the burnup has been calculated from the thermal data and the irradiation time.

During the course of the SP-4 irradiations, there were the usual variations in the specimen operating conditions due to shifts in flux patterns, scram, etc. The values listed in Table 7-1 are typical average values for the irradiation period. The maximum and minimum recorded temperatures in the center of the FA-1 specimen were 2070°F and 1510°F respectively. The fluctuations in the temperature difference between the measured central temperature and the measured block temperature of the FA-1 specimen was too great to permit a statement that this temperature difference increased with irradiation because of deterioration of thermal conductivity of the graphite.

TABLE 7-1

Exposure Conditions For UO_2 Fueled Specimens In Capsule SP-4

Specimen Type	Measured Graphite Block Temp, °F	Ht. Gen. Rate, KW	Calculated Surface Temp, °F	Central Temp, °F	Burnup,[b] KWH/Ball
FI-1 (E8)	1400	2.3	1750	1850	7700
FA-2 (E8)	1400	2.2	1750	1900	7400
FA-1 (E82)	1300	1.9	1600	1750[a]	6400
FA-10 E5)	1300	1.7	1600	1700	5700

(a) Measured temperature. One thermocouple was imbedded in the center of this specimen. All other central temperatures were calculated.

(b) For PBR specimens, 1 KWH is equivalent to 7.2 MWD/metric ton of U, 4.4×10^{15} fissions/cc of specimen, or .0011% of the U235 atoms fissions.

In parallel with the irradiation of Capsule SP-4, four specimens identical with those in the capsule were heated in an out-of-pile furnace, duplicating the time-temperature pattern of the irradiated specimens. This step was taken in order to distinguish between radiation and temperature effects.

Special flats, approximately 1/2 inch in diameter, were machined and polished on all specimens so that "before and after" photomicrographs could be taken of specific fuel particles. These pictures are all shown in Figures 7-1(a-d) through 7-4(a-d). The a and b photos were taken before and after the out-of-pile heating test while the c and d photos were taken before and after the irradiation tests. Scribe marks were made in the graphite around selected fuel particles to permit their identification after testing.

Figures 7-1a through 7-1d are of the infiltrated specimen. The fuel particles, believed to be of the order of 1μ in size, are indistinguishable in all of the views. One grey particle, approximately 10μ in size can be noted in Figure 7-1c but appears to be missing after irradiation (Figure 7-1d). Figures 7-2a through 7-2d are of the FA-2 specimens. No clearly discernable fuel particles can be detected in the out-of-pile specimen, however, a fuel particle is clearly noted in the irradiated specimen. The particle size appears unaffected by irradiation and the

OUT-OF-PILE HEATING TEST OF INFILTRATED GRAPHITE
SPECIMEN TYPE FI-1

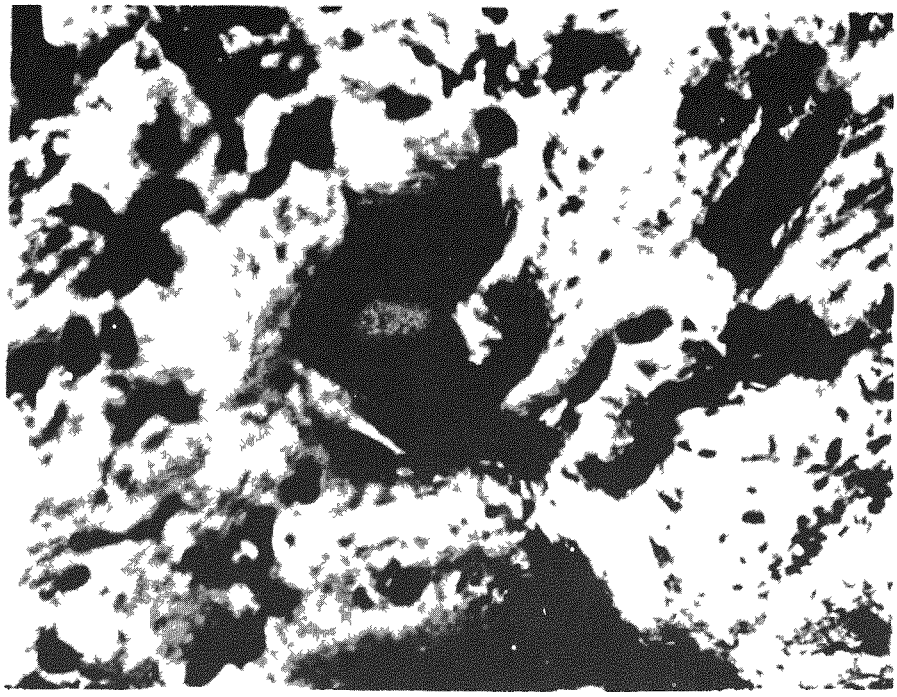

FIG. 7-1a. BEFORE HEATING. (250X)

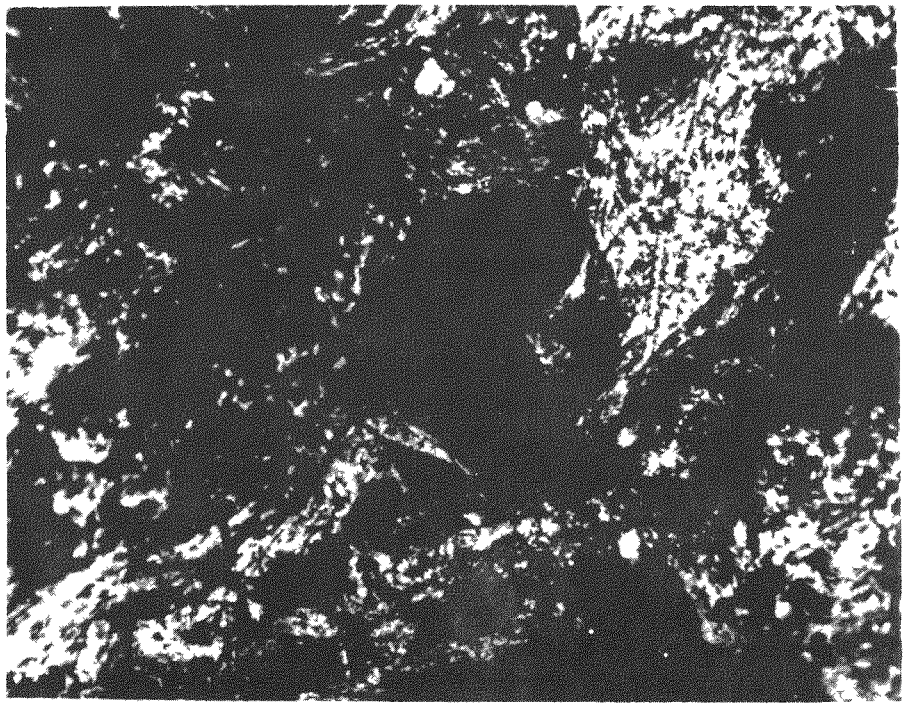

FIG. 7-1b. AFTER HEATING. (250X)

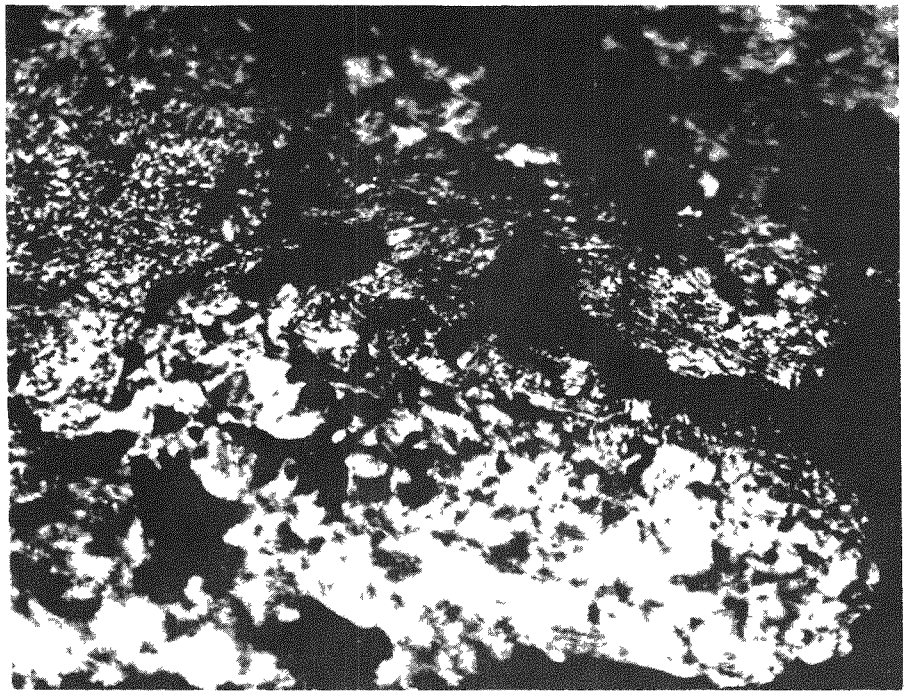

FIG. 7-1c. BEFORE IRRADIATION. (250X)

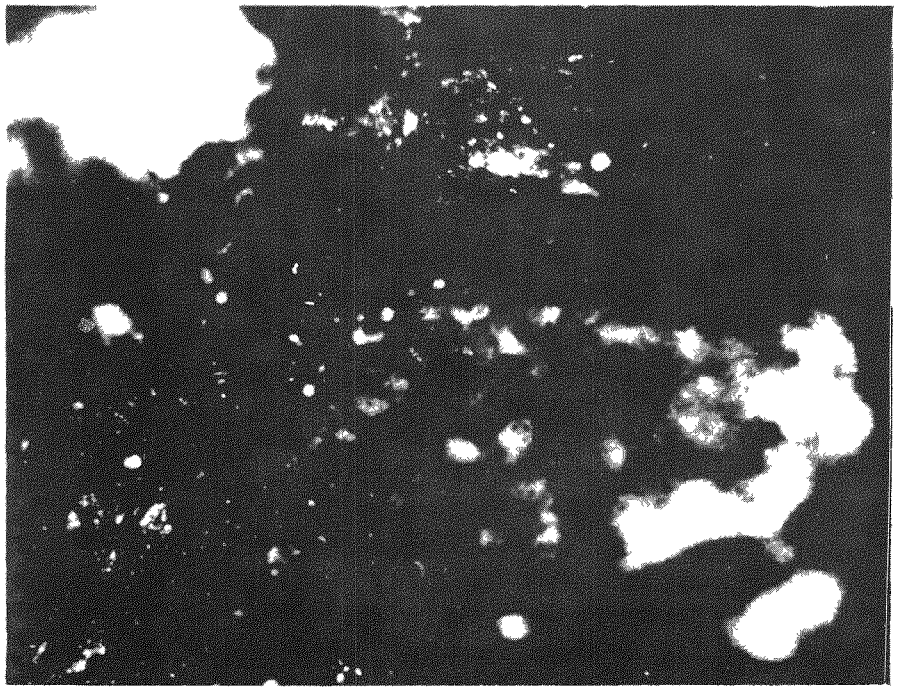

FIG. 7-1d. AFTER IRRADIATION. (250X)

OUT-OF-PILE HEATING TEST OF 67μ UO_2 IN GRAPHITE
SPECIMEN TYPE FA-2

FIG. 7-2a. BEFORE HEATING. (250X)

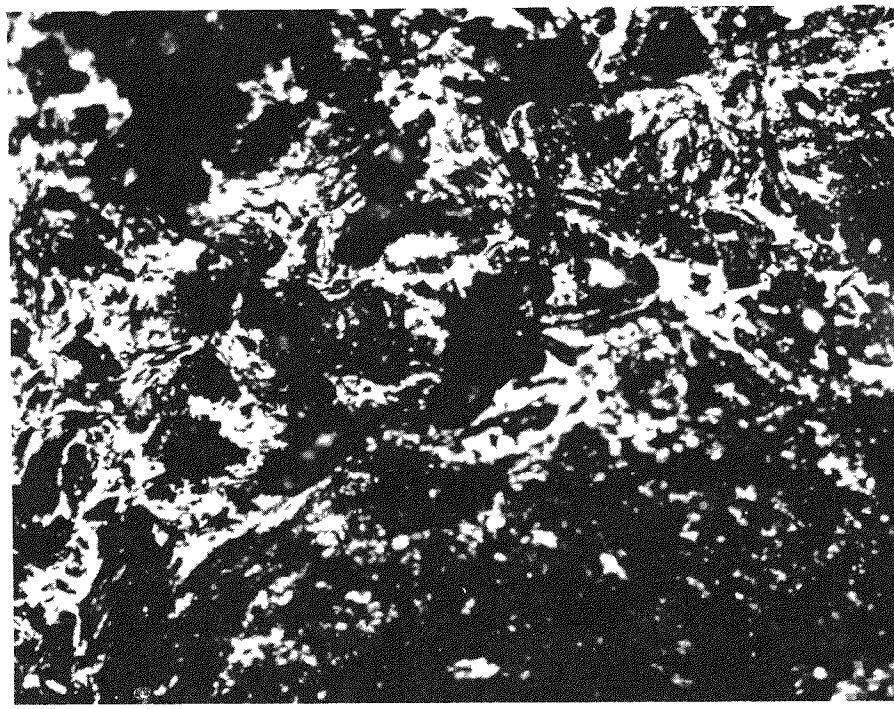

FIG. 7-2b. AFTER HEATING. (250X)

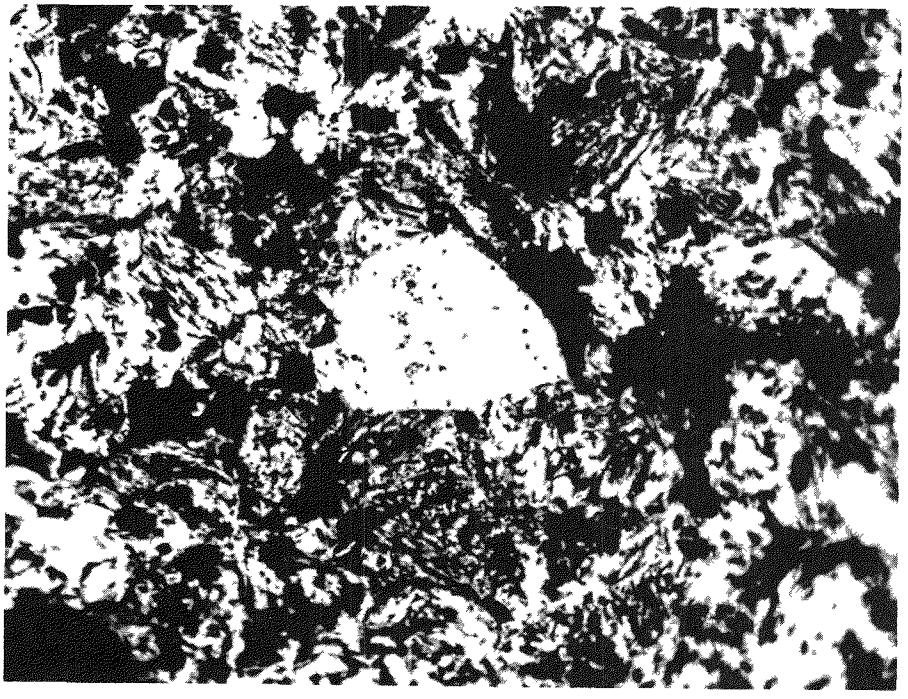

FIG. 7-2c. BEFORE IRRADIATION. (250X)

FIG. 7-2d. AFTER IRRADIATION. (250X)

OUT-OF-PILE HEATING TEST OF 105/149μ UO_2 IN GRAPHITE
SPECIMEN TYPE FA-1

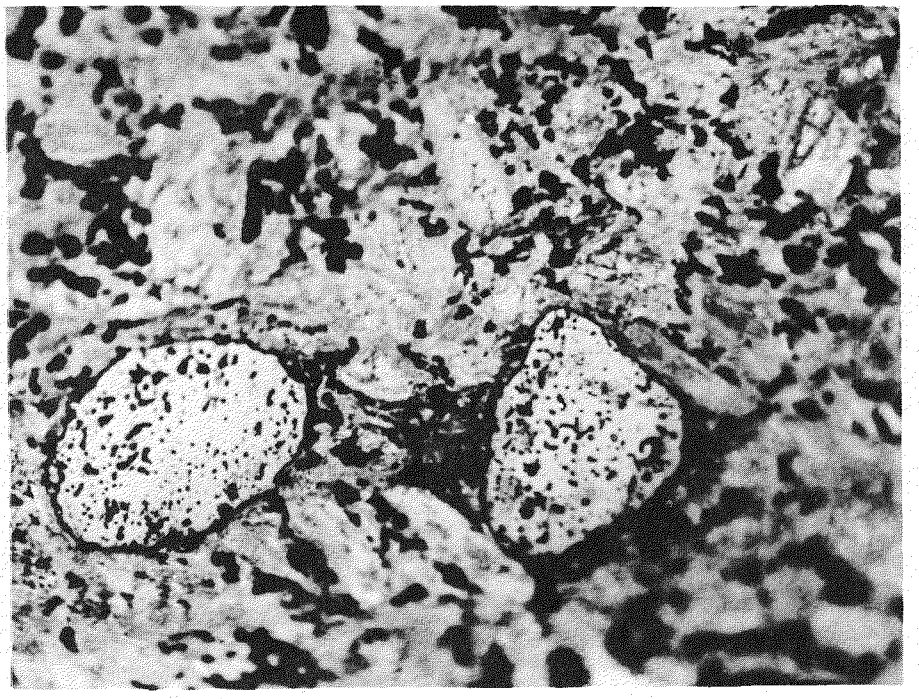

FIG. 7-3a BEFORE HEATING. (250X)

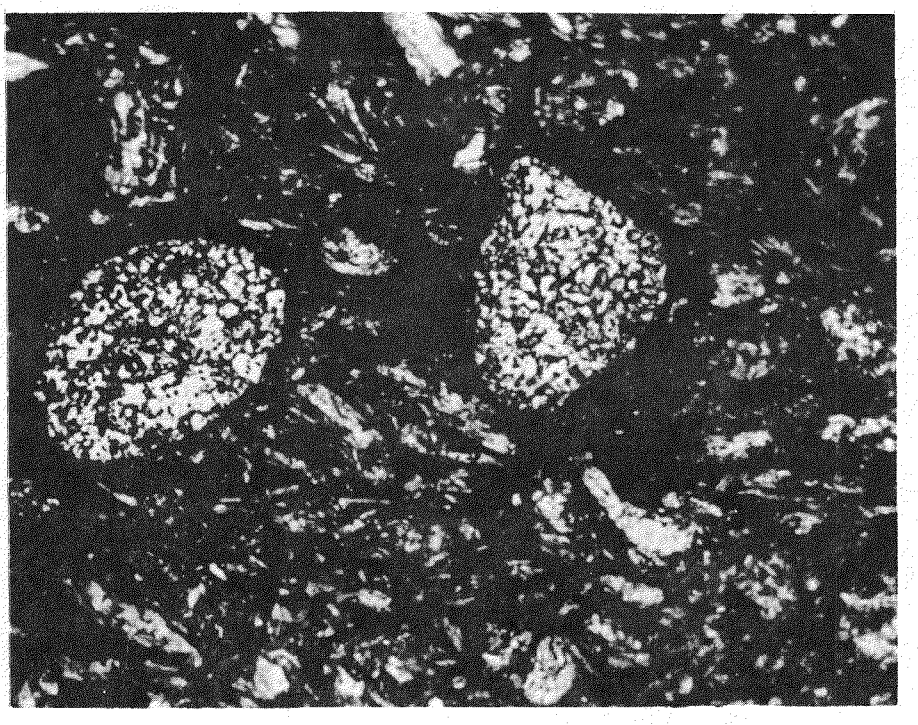

FIG. 7-3b AFTER HEATING. (250X)

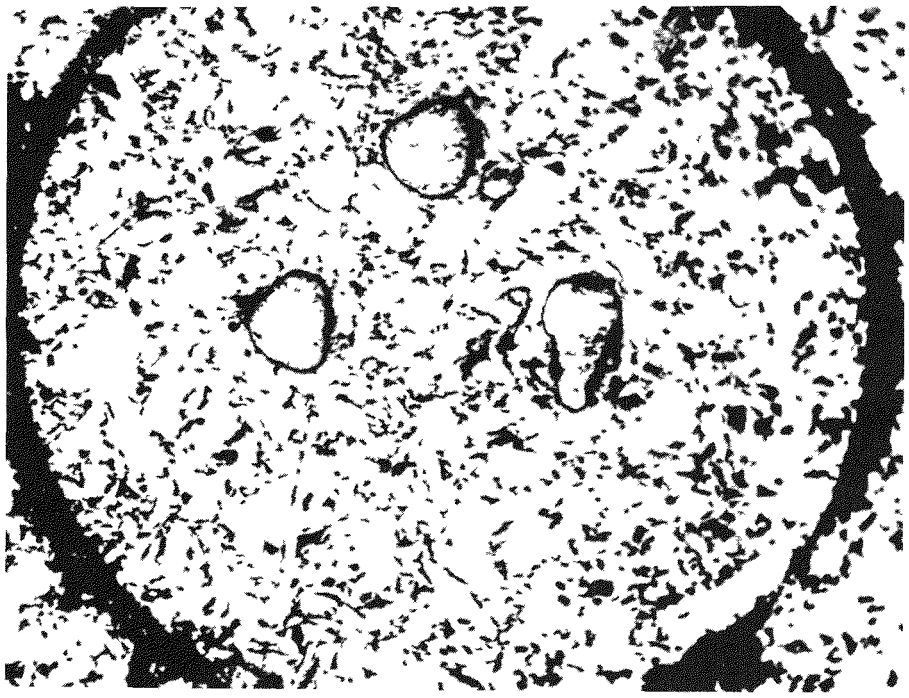

FIG. 7-3c BEFORE IRRADIATION. (100X)

FIG. 7-3d AFTER IRRADIATION, (100X). NOTE VOID SPACE AROUND PARTICLES.

OUT-OF-PILE TEST OF 350/420μ UO_2 IN GRAPHITE
SPECIMEN TYPE FA-10

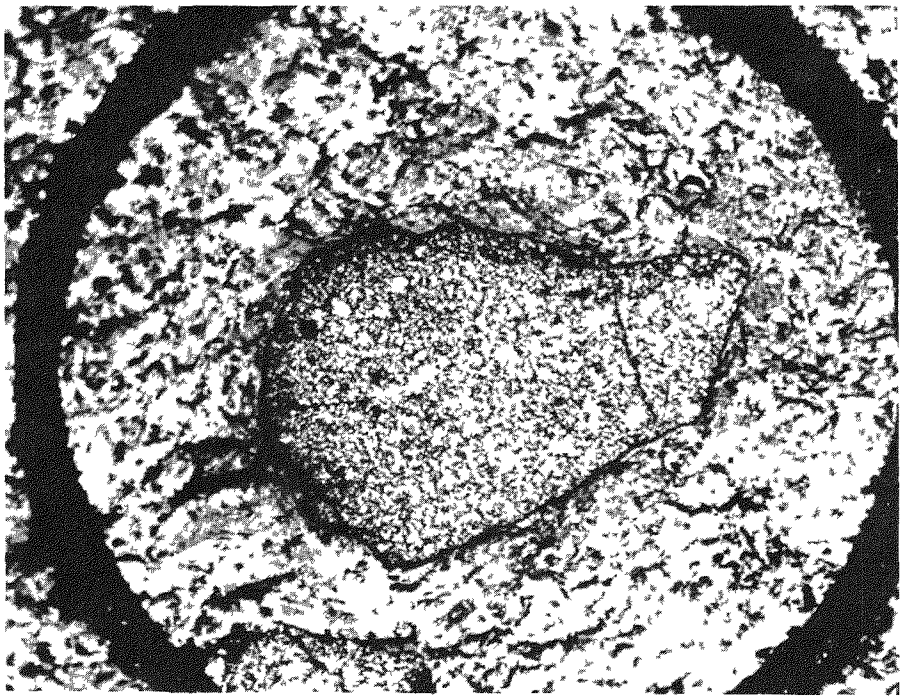

FIG. 7-4a BEFORE HEATING. (100X)

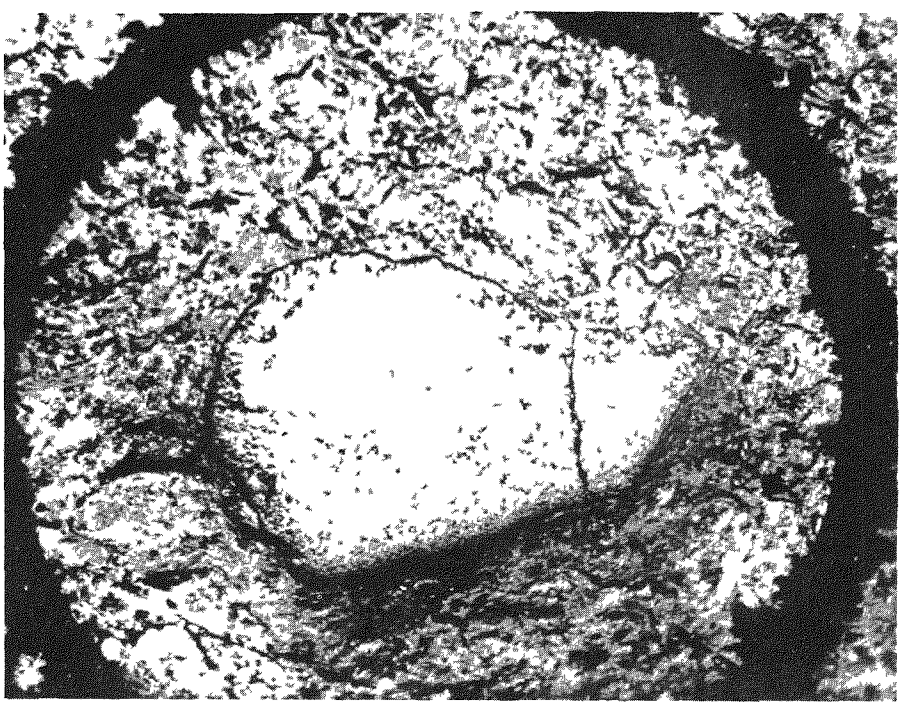

FIG. 7-4b AFTER HEATING. (100X)

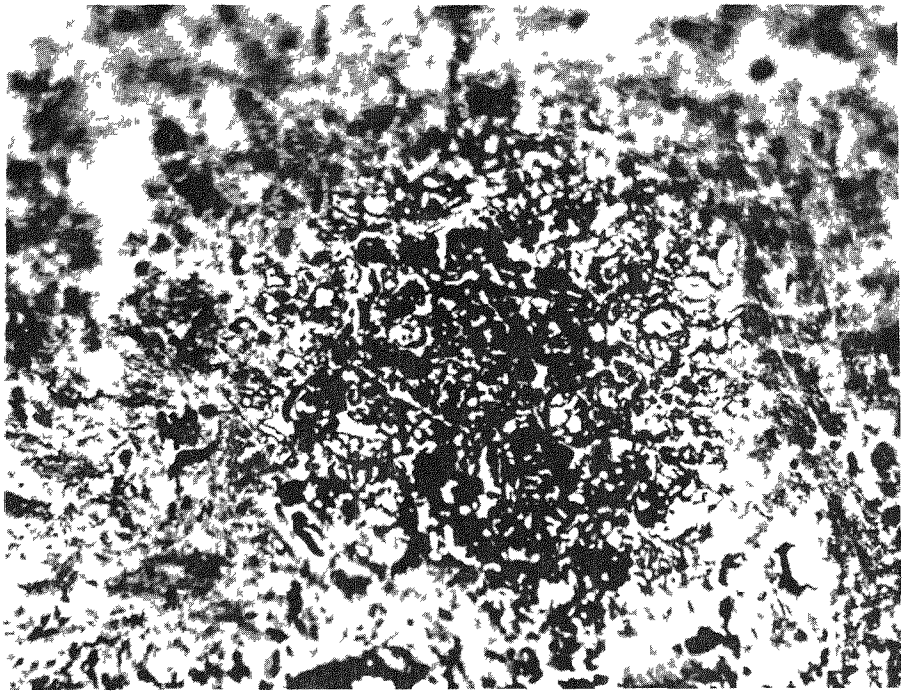

FIG. 7-4c BEFORE IRRADIATION. (250X)

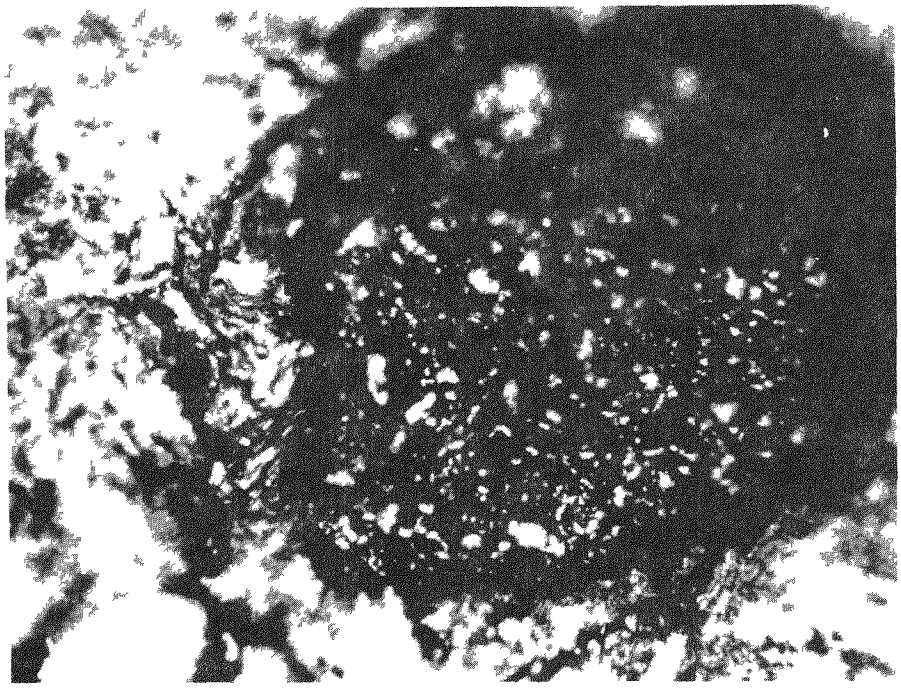

FIG. 7-4d AFTER IRRADIATION. (250X)

characteristic appearance of uranium carbide is not evident.

Excellent views of the fuel particles in the FA-1 specimens were obtained as noted in Figures 7-3a through 7-3d. No change in particle dimension or appearance can be noted in the out-of-pile test. Although there is no apparent carbide formation in the in-pile test there is a noticeable increase in the void region aroung the particle (Fig. 7-3d). The increase in radius of the graphite void is approximately 20μ. Since fission fragment recoil range in graphite is also about 20μ, this result strongly suggests that the local graphite region directly affected by fission fragment recoil has become hardened and brittle and most probably came out during polishing of the specimen. Deterioration of the fuel particle itself is also noted, the decrease in radius being about 10 microns. Figures 7-4a through 7-4d are of the FA-10 specimens. No affect on the UO_2 particles can be noted in the out-of-pile test. Although the original fuel particle in the irradiation test appears badly fragmented, no significant affect to the particle or the graphite matrix can be noted in the post-irradiation view.

Other measurements made on the in-pile and out-of-pile specimens were macroscopic examination, weight change, dimensional change, and impact strength. The weights and dimensions of all specimens prior to testing are given in Table 7-2.

These specimens had additional flats machined on their surfaces to permit accurate measurement of their diameters. The dimensional shrinkages noted in Table 7-2 are predominantly due to irradiation effects since insignificant shrinkages were found for the out-of-pile specimens except in the case of the FI-1 type. The irradiation-induced shrinkages do not decrease with increasing UO_2 particle size (i.e. decreasing recoil fission fragment exposure to the matrix) as might be expected which implies that properties of the graphite matrix and/or neutron damage are the significant factors rather than damage by fission fragment recoil. The FI-1 specimen has a fully graphitized matrix (Type AGOT). The low shrinkage of the FA-2 specimen could be related to the low degree of graphitization and low density (1.50 g/cc) of this specimen which was made with a coke filler and baked at only 2000°F. Both the FA-1 specimen and the FA-10 specimen have a graphite filler but the pitch binders were not graphitized, again due to the relatively low bake temperature. The FA-10 specimen was reimpregnated several times to raise its graphite density to 1.80 gm/cc. The graphite density for the FA-1 specimen was 1.62 gm/cc. It would appear that the high

TABLE 7-2

WEIGHTS AND DIMENSIONS OF UNCOATED UO_2 FUEL SPECIMENS IN OUT-OF-PILE AND IN-PILE TESTS

Specimen Type and No.	Test	Weight Change		Dimensional Change			
				Polar (a)		Equatorial (b)	
		Initial, gms.	Change, %	Initial, in.	Change, %	Initial, in.	Change, %
FI-1(E8)	In-Pile	52.3128	-0.40	1.477	-0.76	1.476	-0.67
FA-2(E8)	"	45.1378	-0.55	1.447	-0.03	1.452	-0.08
FA-1(E82)	"	51.8004	-0.11	1.478	-0.47	1.490	-0.52
FA-10(E5)	"	56.0927	-0.06	1.469	-0.69	1.469	-0.81
FI-1(E2)	Out-of-Pile	52.621	-0.77	1.487	-0.07	1.479	-0.10
FA-2(E7)	"	45.351	-2.55	1.447	0.0	1.449	-0.07
FA-1(E76)	"	51.892	-0.45	1.476	0.0	1.476	0.0
FA-10(E6)	"	55.727	-0.09	1.474	0.0	1.471	0.0

(a) Molding or extrusion axis

(b) Perpendicular to molding or extrusion axis

shrinkage of the FA-10 specimen, in spite of the minimum fission fragment exposure due to its large 400μ fuel particles, is associated with its large number of reimpregnations.

Identical specimens from the same production batches as the FA-1 and FI-1 type had also been irradiated in a previous capsule, SP-1. This irradiation was described in ref (2). The dimensional changes from Capsule SP-1 are compared with those observed in Capsule SP-4 in Table 7-3. The infiltrated specimen (FI-1) showed a smaller shrinkage at the longer exposure which indicates that the lower temperature of the SP-1 irradiation may have been the dominant factor. This effect is not borne out in the case of the admixture specimen (FA-1), although the shrinkage increase with the higher temperature irradiation is only 50% of the exposure increase. Due to the lower fission fragment recoil exposure (i.e. larger fuel particle size) in the admixture specimen, the effect of fast neutron damage could be relatively more significant in the admixture element than in the infiltrated element.

TABLE 7-3

Comparison of Dimensional Changes Observed in Capsule SP-1 and SP-4 for FA-1 and FI-1 Specimens

	Type FI-1			Type FA-1		
Capsule	Temp. °F.	Exposure KWH/Ball	Dimensional Change, %	Temp. °F	Exposure KWH/Ball	Dimensional Change, %
SP-1	1350	1500	-0.93	1350	1400	-0.22
SP-4	1800	7700	-0.71	1700	6400	-0.50

The weight loss data shown in Table 7-2 clearly indicates that temperature effects are most significant since the weight losses are all larger for the out-of-pile specimens. It is interesting to note that the relative order of weight losses are the same for both the out-of-pile and the in-pile specimens. The major factor in these weight losses is probably further devolatilization of adsorbed gases.

Impact tests were performed on these specimens by dropping a steel weight onto the specimen from successively increasing heights to the point of failure. Since previous tests (ref 2) had shown that PBR specimens actually increase in compressive strength with irradiation, this test was not selected for the SP-4 specimens. The impact test results for the out-of-pile and the in-pile specimens are summarized in Table 7-4.

TABLE 7-4

Impact Data on Uncoated Spheres

Specimen Type	As-Received Failure, Ft-lbs.	As-Received No. Impacts	After Out-of-Pile Heating Failure, Ft-lbs.	After Out-of-Pile Heating No. Impacts	After SP-1 Irradiation Failure, Ft-lbs.	After SP-1 Irradiation No. Impacts	After SP-4 Irradiation Failure, Ft-lbs.	After SP-4 Irradiation No. Impacts
FI-1	12.5	12	9.4	22	10.4	12	11.7	35
"	11.5	11						
"	13.6	11						
FA-1	11.5	11	6.8	16	8.4	10	9.4	28
"	11.5	11						
"	7.3	5						
FA-2	7.5	15	6.8	16			3	9
FA-10	10.4	10	10.6	23			12.5	37

For purposes of comparison, the impact data on as-received specimens, and the admixtured and infiltrated specimens after irradiation in Capsule SP-1 are also included.

Although there is random scatter in this impact data, all values are significantly above the design objective of 2.0 ft. lbs for PBR specimens except the FA-2 type. No significant effect of irradiation on impact strength can be noted, although there is a slight drop in impact strength for several of the specimens.

The Capsule SP-4 irradiation has demonstrated that more than one type of uranium-graphite material has adequate structural properties to meet the reference design conditions of a large Pebble Bed Reactor. Some further work will be required to establish the cause and nature of the weight losses observed, but nonetheless, our initial selection of graphite as a high temperature ceramic structural material for use in PBR fuel element appears fully justified.

8.0 Capsule Design and Performance

One incidential advantage of the PBR fuel element concept is the ease of testing full scale fuel elements under conditions closely approaching those of a large power reactor. By replacing the thorium in the reference fuel element with additional enriched uranium, a relatively low powered research reactor such as the 2 MW Battelle Research Reactor can produce power densities in test specimens up to 75% of the desired maximum power density. In addition, fission product leakage can be monitored by adding helium inlet and outlet lines to the capsule. Two capsules were under irradiation in the BRR during Phase II: Capsule SP-4 which was a static capsule, and capsule SP-5, which contained two sweep compartments in addition to a static compartment.

8.1 Static Capsule SP-4

The primary purpose of this irradiation was to investigate the stability of UO_2 fueled graphite under high temperature irradiation. Four 1 1/2" diameter uncoated graphite spheres fueled with different types of UO_2 were included. These specimens and the experimental results on them are described in Section 7.0. Two additional coated specimens were included. These were coated with Si-SiC and pyrolytic carbon and are described in Sections 3.1.1 and 3.2.1 respectively.

The design features of Capsule SP-4 are shown in Fig. 8-1. Since this experiment was concerned solely with the effects of irradiation on physical properties of the specimens, no helium lines were included for detecting fission product leakage. The capsule was designed without auxiliary electrical heaters, depending solely on nuclear heat generation and thermal resistances in the capsule to achieve the desired specimen temperature. Each specimen is mounted in a split graphite cylinder. A 30 mil annulus is provided around each specimen. This annulus is filled with a free flowing graphite powder which minimizes the thermal resistance of the gap while permitting the specimen to expand or contract without restraint. An inconel inner capsule is fitted over the six graphite cylinders. Fins are provided on the outside of the inner capsule. The number of fins and fin thickness were selected to achieve a specimen surface temperature of 1900°F which would result in specimen central temperatures of 2000 to 2100°F. A stainless steel outer capsule is fitted over the fins. Heat is rejected from this outer capsule wall directly to the

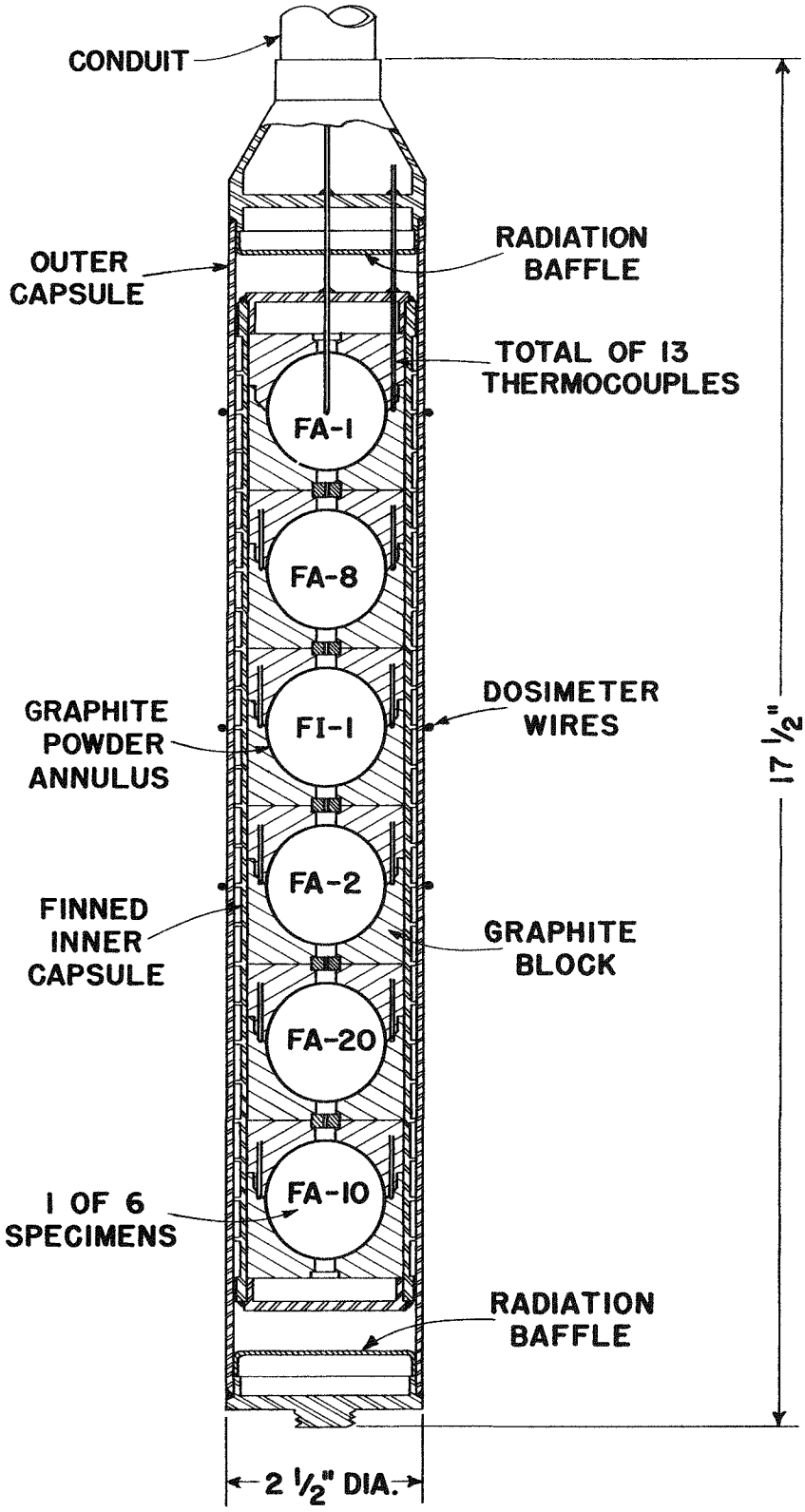

FIG. 8-1 STATIC CAPSULE SP-4

BRR pool water. A total of 13 thermocouples were installed in the capsule. Two thermocouples are located in the graphite cylinder just outside the equator of each specimen. In addition, a hole was drilled to the center of the uppermost specimen (Type FA-1) and a thermocouple installed therein. The specimen power level actually obtained can be calculated from the measured temperatures in the graphite cylinder, the pool water temperature, and the effective thermal conductivity of the capsule parts. Using this power level, the specimen temperatures can then be calculated, again starting from the measured graphite cylinder temperature.

Capsule SP-4 was inserted into the BRR on August 25, 1959. Typical operating conditions are summarized in Table 8-1.

TABLE 8-1

Operating Conditions for Capsule SP-4

Specimen	Measured Graphite Block Temp. °F	Ht. Gen. Rate, KW	Calculated Surface Temp.	Central Temp., °F
FA-1(E82)	1300	1.9	1600	1750[a]
FA-8(E6)	1400	2.2	1750	1850
FI-1(E8)	1400	2.3	1750	1850
FA-2(E8)	1400	2.2	1750	1900
FA-20(336E)	1250	2.0	1550	1750
FA-10(E5)	1300	1.7	1600	1700

(a) Measured temperature. One thermocouple is imbedded in the center of this specimen only. All other central temperatures are calculated.

As can be noted, the target temperature of 1900°F surface temperature was not achieved. Several factors were investigated in an attempt to explain or improve the situation. Since no auxiliary electrical heaters were included, the target temperature was to have been achieved by proper selection of the thickness and material of the various thermal barriers with respect to the anticipated flux levels. One factor was uncovered when laboratory measurements of the thermal conductivity of the Inconel-X used for the inner capsule showed that the literature value used in design was 20% low. An attempt was made to increase the neutron flux by rearranging fuel elements in the BRR core. However, there was no significant increase.

Several plans were studied to apply an external thermal barrier to the capsule to increase the temperature. However, the close tolerance required at the capsule-barrier interface appeared impractical to achieve with remote handling devices under 23 ft. of pool water.

The irradiation of Capsule SP-4 was terminated on March 7, 1960. The accumulated full power operating time was 139.5 days. During the course of the irradiation, 6 thermocouples failed, 2 each for the FA-10 and FA-20 specimens, and 1 each for the FA-2 and FI-1 specimen. However, there was sufficient operating time with all thermocouples working so that temperatures where thermocouples had failed could be estimated with confidence based on thermocouple readings at other locations.

The estimated irradiation exposures for the specimens given in Section 7.0, 3.1.1, and 3.2.1 were based on the calculated power levels listed in Table 8-1 and the equivalent full power operating time of 139.5 days. Analysis of the cobalt-nickel dosimeter wires for several of the specimens gave somewhat lower values A comparison of these values is given in Table 8-2.

TABLE 8-2

Comparison Of Estimated Exposures To Specimens In Capsule SP-4 By Two Methods

Specimen	Estimated Exposure, KWH/sphere From Thermal Data	From Dosimetry
FA-1	6400	3700
FI-1	7700	4400
FA-2	7400	4400

Based on previous experience, burnups calculated from thermal data are usually within $\pm$ 30% of the dosimetry data. As noted in Fig. 8-1, the dosimeter wires are located on the outside wall of Capsule SP-4. The unperturbed thermal neutron flux in the experimental hole was about 3.5×10^{13} and a perturbed flux at the capsule wall should have been about 2×10^{13}. The flux level corresponding to the dosimetry data was only 1×10^{13}. Thus, it is felt that the dosimetry data is probably low but the source of the discrepancy is unexplained.

8.2 Sweep Capsule SP-5

The primary purpose of this irradiation was to investigate the fission product retention characteristics of promising fuel element specimens under high level irradiation. The two most promising specimens selected fro Capsule SP-5 were the Si-SiC coated specimen (FA-23) and a specimen fueled with vapor-deposited Al_2O_3 coated UO_2 (FA-22).

The design features of Capsule SP-5 are shown in Figure 8-2. The general method of mounting each specimen in a graphite cylinder and using a doubly contained capsule with fins on the inner capsule is the same as for Capsule SP-4 described in the previous section. However, the outer capsule of SP-5 is divided into two independent compartments. The upper compartment, called the sweep compartment, conatins two separate inner capsules. Separate helium inlet and outlet lines are brought to each inner capsule. Gas flow, which is upwards through the graphite powder annulus surrounding each specimen, scavenges any fission products which leak from the specimens and carries them to trapping apparatus outside the capsule. An FA-22 and an FA-23 specimen are located in the two inner capsules of the sweep compartment.

A separate static compartment is located below the sweep compartment. No helium lines are connected to the static compartment. An additional FA-22 specimen, an additional FA-23 specimen, and two FA-20 specimens are included in the static compartment. A simple threaded connection joins the sweep compartment and the static compartment so that if it becomes desirable to examine the sweep compartment specimens (i.e. if large increases in fission product release rates indicate failure of both specimens), the upper compartment can be disengaged and the lower compartment left in the reactor for further irradiation. No thermocouples are included in the static compartment because of this disconnect feature. Temperatures and power levels for these specimens are estimated from temperature data in the sweep compartment and the axial flux profile in the experimental hole.

Irradiation of Capsule SP-5 was started on April 6, 1960 and continued through the end of Phase II (October 31, 1960). Typical operating conditions during the irradiation are listed in Table 8-3.

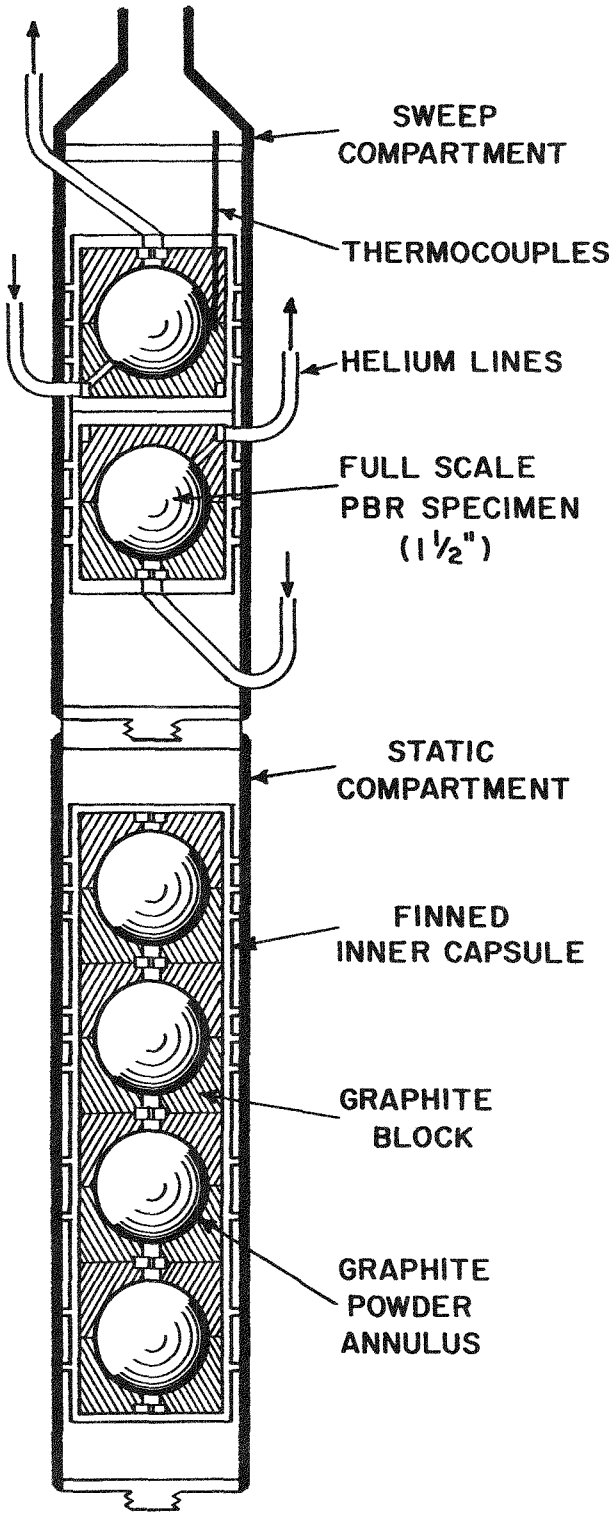

FIG. 8-2 SWEEP CAPSULE SP-5

TABLE 8-3

Typical Operating Conditions For Specimens In Capsule SP-5

Specimen No.	Measured Block Temp, °F	Ht. Gen. Rate, KW	Calc. Surface Temp, °F	Calc. Central Temp, °F
Sweep:				
FA-22(471E)	1090	1.5	1360	1550
FA-23(E8-7)	1010	1.6	1300	1440
Static:				
FA-22(470E)	-	1.4	1360	1540
FA-20(338E)	-	1.3	1360	1460
FA-23(E8-12)	-	1.0	1300	1390
FA-20(345E)	-	0.8	1360	1420

A schematic diagram of the off-gas train used to measure fission product leakage rates is shown in Figure 8-3. Two independent gas trains are included. Sweep helium flow is maintained continuously throughout the irradiation. The flow is normally through a doubly-contained bypass line directly to the final activity removal traps. Fission product concentrations in this helium stream are measured by diverting a portion of the flow through the analytical train for a period of about 2 hours.

Special under water traps for the non-volatile daughter products of the short-lived noble fission product gases were installed as shown in Fig. 8-3. These traps consists of a stainless steel container 2 1/2 " OD by 36" long filled with layers of stainless steel mesh. The sweep helium flow normally bypasses these traps. A sample is taken by actuating the underwater valves and diverting the full flow through the trap. Segments of the stainless steel mesh can be removed from the trap and radiochemically analyzed for such isotopes as Sr 89, Ba 140, Ce 141, and I 131.

Data obtained for the long-lived volatile fission product release and from the non-volatiles trap is given in Section 3.1.2 for the FA-23 specimen and in Section 4.4 for the FA-22 specimen.

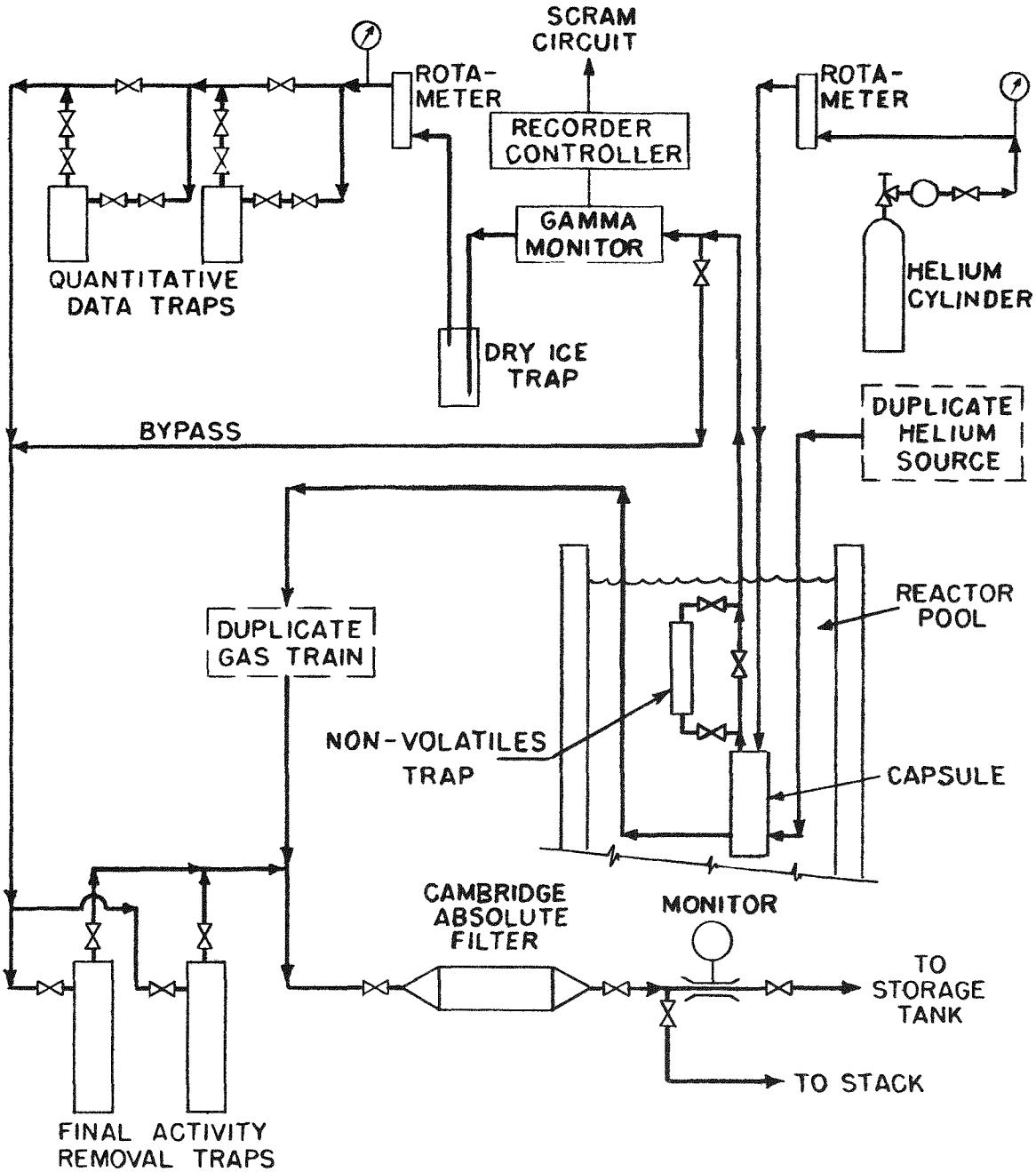

FIG. 8-3 GAS TRAIN FOR MEASURING
VOLATILE FISSION PRODUCT RELEASE
FROM SWEEP CAPSULE SPECIMENS

9.0 In-Pile Loop

The design, construction and operation of an in-pile loop to study the behaviour of fission products escaping from a PBR fuel element is being performed under a subcontract to the Nuclear Science and Engineering Corp. The purposes of this loop are to study the equilibrium activity levels in a recycle helium stream; methods of lowering gas stream activity level; the amount, location, and nature of deposited fission products; and methods of decontaminating equipment surfaces. In addition to testing low-release PBR fuel element specimens, an uncoated uranium-graphite specimen will be tested to simulate problems of a "dirty" primary loop.

The in-pile portion of the loop will be inserted in experimental hole W-11 of the Brookhaven Graphite Reactor with the blowers, heat exchangers, sampling stations, etc. located on the adjacent floor space. Design characteristics of the loop are as follows:

Circulating Fluid	Helium
Operating Pressure	14 psia
Flow Rate	8 scfm
Max. Helium Temp.	1250°F
Min. Helium Temp.	250°F
Max. Specimen Temp.	1800°F
Max. Specimen Power	0.25 KW

Two major variables, the system pressure and the specimen power, have been selected with a view to minimizing the cost of the loop. The use of sub-atmospheric pressure eliminates the need for double containment while the modest power level in the specimen will provide measurable activity yet minimize the gas flow requirements and shielding costs.

Figure 9-1 is a schematic diagram of the in-pile loop. Gas leaves the in-pile section at 1250°F and enters the shell side of a coiled tube heat exchanger where it is cooled to 550°F. The exchanger is designed for easy replacement of the tube coil so that deposition on the tube surface as a function of temperature can be studied. An intermediate Dowtherm loop, which transports heat from this exchanger to a water-cooled sink, has been included to permit adequate control of the helium outlet temperature. The helium next passes through a removable 550°F test

FIG. 9-1 SCHEMATIC DIAGRAM OF IN-PILE LOOP

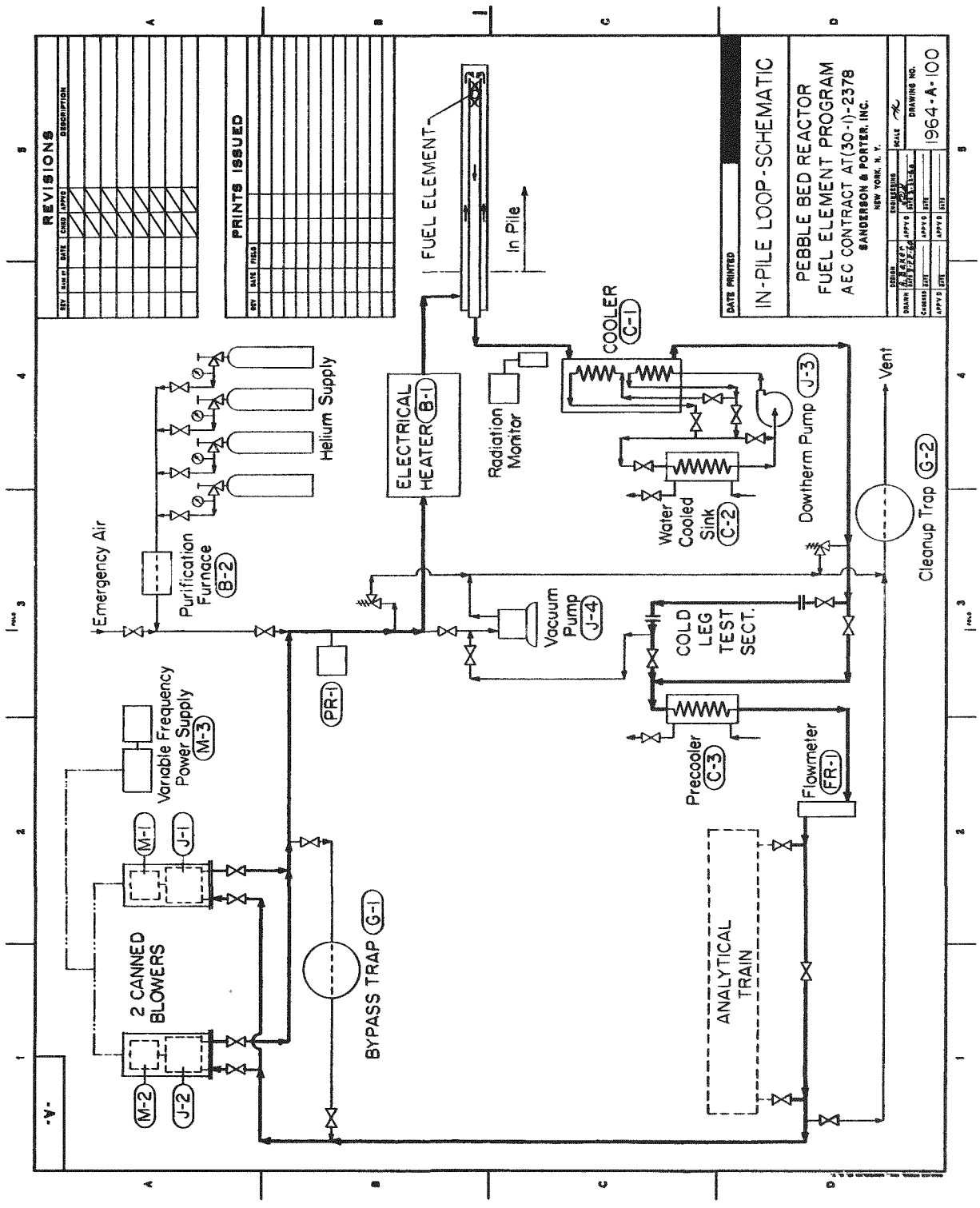

section containing deposition coupons and a precooler to lower the temperature to 250°F which enables the use of an economical low temperature blower. Before entering the blower, provision is made for in-line or bypass operation of an analytical train which will gather data on fission product release rate and activity levels in the gas stream.

Two Dexter-Conde positive displacement blowers are provided, although only one is required for normal operation. Each blower and its drive motor are mounted in a canned enclosure so that leaktightness will not depend on a rotating seal. Flow variation is achieved by powering the drive motors from a variable frequency motor generator set. A bypass charcoal trap is provided from the blower discharge back to the blower inlet so that the effect of continuous gas decontamination can be studied. After leaving the blower, the helium temperature is raised to 1200°F by an electrical resistance heater and then enters the in-pile section.

A drawing of the in-pile section is shown in Figure 9-2. Inlet helium flows through the annulus of the co-axial pipe section, through the test specimen holder located at the innermost end of the center pipe, and returns through the center pipe. Separate offset inlet and outlet lines are used through the fixed shield plug. The specimen holder and hot leg coupons are replaceable through a flanged connection on the front end of the center pipe and a removable shield plug. A vacuum jacket containing two stainless steel foil radiation shields are provided to prevent overheating of the reactor graphite.

A mockup of the test specimen holder is shown in Figure 9-3. Portions of unfueled graphite spheres are mounted in each half of a split graphite cylinder and all graphite surfaces are coated with siliconized silicon carbide. The fueled specimen is mounted between the unfueled graphite spheres to simulate a packed bed arrangement. Two thermocouples are imbedded in the surface of the fueled specimen to permit accurate temperature measurement.

Subassemblies of the loop components were prepared and tested for leaktightness prior to shipment to BNL. The final assembly including the auxiliary water, air and Dowtherm systems was completed at BNL. A photograph of the assembled loop on the floor adjacent to hole W-11 at the BNL Graphite Reactor is shown in Figure 9-4. The in-pile section is seen facing away from the pile face in order that shakedown tests could be performed prior to irradiation. During these out-of-pile tests, an unfueled graphite sphere containing a miniature 0.25 KW electrical heating

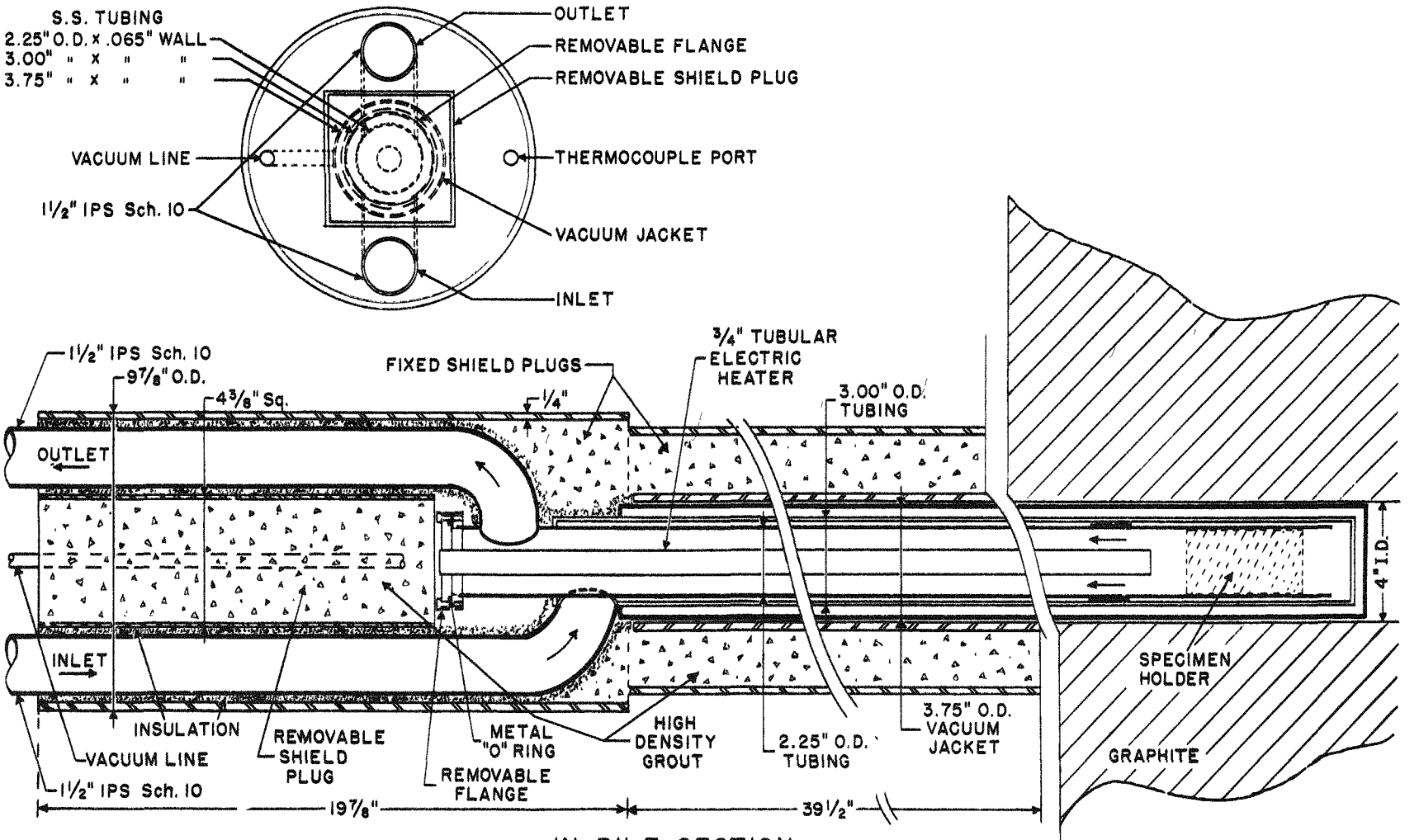

IN-PILE SECTION

FIG. 9-2

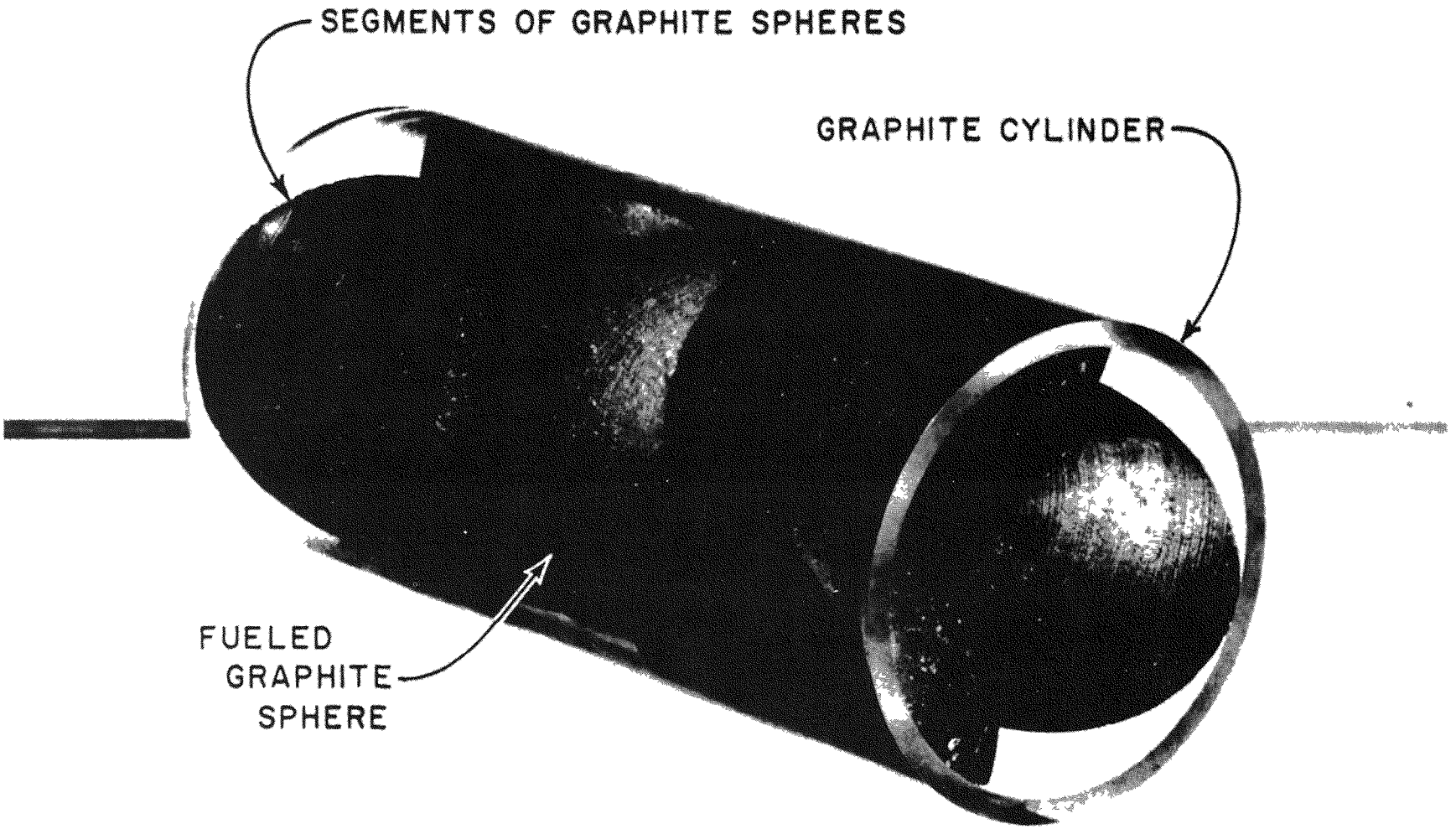

Fig. 9-3 MOCKUP OF TEST SPECIMEN HOLDER
FOR IN-PILE LOOP

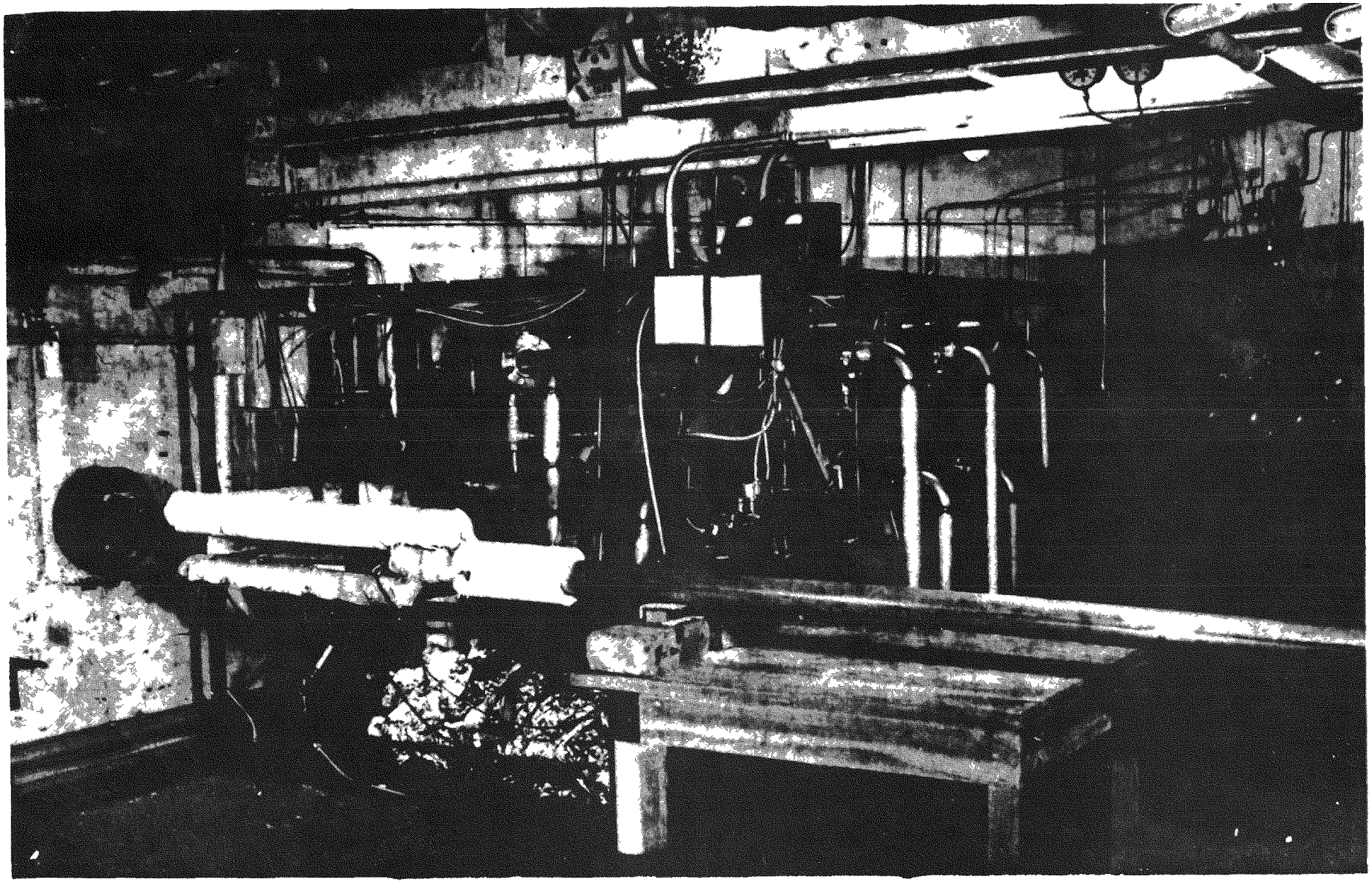

Fig. 9-4. In-Pile Loop Assembly Shown at the BNL Reactor with In-Pile Section Arranged for Pre-Irradiation Shakedown Tests

element was used in place of the fueled specimen in order to simulate nuclear heating.

During the course of the shakedown tests, several problems arose. Excessive float bounce in the primary helium flowmeter was corrected by the addition of a damping orifice at the meter outlet. An accumulation of a greasy substance in the blower casings, due either to excessive lubrication or faulty cleaning, caused the graphite vanes in the blower to seize and break during the startup of one of the blowers. After replacing the vanes and a thorough degreasing, the blower performance improved noticeably and smooth operation was achieved over the range of 2 to 24 scfm at 14 psia discharge pressure. One series of tests was run to measure the temperature difference between the specimen and the helium stream as a function of helium flow rate. At 0.2 KW input to the dummy specimen, temperature difference varied from 140°F at 21.4 scfm to 325°F at 5.5 scfm. A temperature difference of 550°F had been estimated at 8 scfm and 0.25 KW using heat transfer correlations from packed bed data. The lower temperature differences actually obtained are attributed to additional conduction losses to the adjacent unheated support spheres. It is planned to achieve the design temperature difference by operating the specimen at 0.4 KW (i.e. in the maximum thermal flux obtainable in Hole W-11) and using reduced helium flow rates of 5 scfm or lower.

A serious deficiency in the thermal capacity of the system was also uncovered during the shakedown tests. At low helium flowrates, the heat capacity of the circulating helium was insufficient to maintain gas temperatures throughout the hot leg piping and the in-pile section. This required the addition of auxiliary heaters to make up heat losses from the system. Flexible heating cable consisting of nichrome wire insulated with fiberglass, asbestos and stainless steel braid was wrapped on high temperature sections of the out-of-pile piping. A 3/4 in. diameter stainless steel sheathed electrical heater was installed in the in-pile section. With these modifications, uniform pipe temperatures were achieved in the out-of-pile section and helium temperatures of 1100°F to 1150°F were achieved at the specimen holder in the in-pile section which was slightly below the design helium temperature of 1200°F.

At the end of Phase II, the in-pile section was dismantled for insertion into the reactor. Initial in-pile operation will be with an unfueled electrically heated sphere to provide a final checkout prior to operation with a fueled specimen.

The first fuel element to be irradiated in the loop will be an FA-22(E) specimen fueled with alumina coated UO_2 from batch 6H (see Table 2-1). This specimen will be otherwise similar to the FA-22 specimens being irradiated in Capsule SP-5 except for the provision of two thermocouple holes in the in-pile loop specimen. During fabrication of these specimens, small graphite plugs were molded into the sphere. After baking, thermocouple holes were drilled in the plugs so that none of the alumina coatings on the fuel particles would be damaged. The results of a neutron activation screening test on this specimen are given in Table 4-11 in Section 4.4. Data on fission product leakage rates and volatile fission product concentration in the helium stream during loop operation will be obtained. It is probable that the low release rates from the FA-22 specimen will make it difficult to obtain meaningful data on fission product deposition.

The second fuel element to be irradiated in the in-pile loop will be an FA-1(E) specimen fueled with uncoated UO_2 shot. Leakage factors of the order of 10^{-2} are expected from this type of specimen so it should be possible to obtain data on the efficiency of the bypass clean-up trap and fission product deposition in addition to measuring leakage rates and volatile fission product activity levels.

10.0 Further Development

Based on the encouraging results with coated fuel particles, the reference fuel element adopted for the Pebble Bed Reactor is a graphite sphere fueled with a dispersion of coated fuel particles. Further development of this fuel element could proceed along two parallel paths - coated particle development and graphite sphere development.

Coated Particle Development. There are numerous aspects of particle coatings which should be investigated irrespective of the type of coating material under consideration:

1. A thorough evaluation of the fabrication process variables should be made. These variables include the type and size of equipment used, the degree of agitation, the deposition temperature, and gas composition. The objective here is to achieve the minimum production costs (i.e. maximum deposition rate and/or maximum particle throughput) while meeting specifications on coating integrity.

2. A detailed investigation of the characteristics of molecularly deposited coating material should be made. These characteristics should include density, crystal structure, pore structure, strength, thermal conductivity, and expansion coefficient and they should, of course, be correlated with performance tests. The objective here is to determine which of these properties are most significant in predicting coating performance.

3. Although the reactor designer will impose certain requirements on particle diameter and coating thickness, the limitations imposed by the fabrication process should be explored.

4. The location and causes of uranium contamination of the coating material should be better understood so that it can be controlled to acceptable levels.

5. High-fired shot has been used as the fuel particle in most of the work to date. The use of less expensive, possibly more porous, and out-of-round particles should be explored.

6. Further work should be done on the incorporation of a porous inner layer in the coating which could act as a reservoir for fission product gases.

7. The vapor deposition process readily permits the incorporation of additives to the coating material. A wide range of variables (i.e. additive material and quantity) is possible. The effect of additives on basic characteristics of the coating material should be explored so that coating performance can be improved where required.

8. The migration rates of uranium and thorium as a function of temperatures should be explored.

9. The effect of neutron and fission fragment exposure as a function of temperature on properties of the coating should be understood. A wide variety of coated particle types can be economically irradiated by using a small quantity of each particle type. Since rather promising irradiation data has already been obtained on Al_2O_3 coatings, this work should be continued and an early irradiation test on pyrolytic carbon coatings should be undertaken.

Graphite Sphere Development. This area involves the incorporation of coated fuel particles into a spherical graphite matrix and the evaluation of the fuel element as a whole. Specific areas which require further work are as follows:

1. Sources of uranium contamination can arise from damage to the particle coatings during the graphite sphere fabrication procedure (i.e. mixing, molding, and baking). Processing conditions should be selected to give the best graphite characteristics while minimizing uranium contamination.

2. The presence of coated fuel particles at the surface of a graphite sphere could lead to the loss of fuel particles from the element during reactor operation and damage to the particle coatings by external forces acting on the fuel element. An unfueled layer such as a surface coating or an unfueled graphite shell should be developed for this type of fuel element.

3. Chemical reaction between metal oxide coatings and the graphite matrix limits the maximum operating temperature for this type of fuel element. A better understanding should be obtained of the factors which could accelerate the reaction rate, such as choice of raw materials, bake-out cycle, and graphite impurity levels.

4. All high temperature graphite reactors can be subject to two types of corrosive attack: sudden oxidation by the admission of air in the event

of a rupture in the primary loop and the mass transfer of carbon by reaction with trace impurities of CO_2 or H_2O in the helium coolant. If gas blanketing techniques to prevent combustion in the case of sudden oxidation are not feasible, then a protective coating such as silicon carbide or possibly pyrolytic carbon will be required. Except for the possible effects of pinholes or cracks, a silicon carbide coating would also prevent carbon transfer. A better understanding of carbon transport phenomenon is needed with regards the relationship of reaction rates to circuit transit time, the use of inhibitors, and the use of a low specific surface area coating like pyrolytic carbon.

5. The thermal characteristics of graphite spheres fueled with coated particles should be studied. The greatest uncertainty in setting the thermal stress limits on a spherical graphite fuel element is in the effect of irradiation on thermal conductivity.

6. Promising versions of PBR fuel elements should be subjected to Sweep Capsule irradiations covering a range of temperatures and burnups to produce a final evaluation of the effects of irradiation on fission product retention and important physical characteristics such as impact, compression, abrasion, etc.

7. Batches of fuel elements should be manufactured in quantities of at least 1000 so that properties of mass produced spheres could be checked, inspection procedures developed, and production experience obtained which would form a basis for realistic fuel cost estimates.

LIST OF REFERENCES

1. NYO 8753; Vol. I; Design and Feasibility Study of a Pebble Bed Reactor-Steam Power Plant; Sanderson & Porter; May 1, 1958.

2. NYO 2373; Progress Report on the Pebble Bed Reactor Program; Sanderson & Porter; June 1, 1958 to May 31, 1959.

3. NYO 2706; Phase I Progress Report on the Fuel Element Development Program for the Pebble Bed Reactor; Sanderson & Porter; May 1 to October 31, 1959.

4. S&P 1964-14; Quarterly Progress Report on the Fuel Element Development Program for the Pebble Bed Reactor; Sanderson & Porter; November 1, 1959 to January 31, 1960.

5. NYO 9058; Quarterly Progress Report on the Fuel Element Development Program for the Pebble Bed Reactor; Sanderson & Porter; February 1 to April 30, 1960.

6. NYO 9061; Quarterly Progress Report on the Fuel Element Development Program for the Pebble Bed Reactor; Sanderson & Porter; May 1, 1960 to July 31, 1960.

7. NYO 9059; Thorium Oxide Infiltration of Graphite Spheres; W. E. Parker and F. Rusinko, Jr; Speer Carbon Co.; June 15, 1960.

8. Internal Memorandum; R. F. Benenati; Sanderson & Porter; September 15, 1958.

9. Summary Report on Phase I of AT(40-1)-2560; Graphite Matrix Nuclear Fuel Elements, Vol.I; National Carbon Company; December 22, 1959.

10. BMI-1471; Alumina Coating of UO_2 Shot by Hydrolysis of Aluminum Chloride Vapor; M. F. Browning, N. D. Veigel, T. E. Cook, W. S. Diethorn and J. M. Blocher, Jr; Battelle Memorial Institute; October 25, 1960.

List of References continued

11. AECU 4480; Symposium on High Temperature Technology; pp 108-133; W. D. Kingery.

12. NYO 9069; Pebble Bed Friction Factor and Thermal Expansion Tests; C. A. Leeman; Babcock & Wilcox Co; August 31, 1960.